Numerical Modeling of Highly Saline Wastewater Disposal in Northeast British Columbia

by

Matthew Stuart Simons

B.Sc., McGill University, 2014

Thesis Submitted in Partial Fulfillment of the
Requirements for the Degree of
Master of Science

in the
Department of Earth Sciences
Faculty of Science

SIMON FRASER UNIVERSITY
Spring 2018

Approval

Name:	**Matthew Simons**
Degree:	**Master of Science (Earth Sciences)**
Title:	**Numerical Modeling of Highly Saline Wastewater Disposal in Northeast British Columbia**
Examining Committee:	**Chair: Gwenn Flowers** Professor
	Dr. Diana Allen Senior Supervisor Professor
	Dr. Dirk Kirste Supervisor Associate Professor
	Dr. Laurie Welch Supervisor Hydrogeologist BC Oil and Gas Commission
	Dr. Carl Mendoza External Examiner Professor Emeritus Earth and Atmospheric Sciences University of Alberta
Date Defended/Approved:	April 26, 2018

Abstract

Dense, saline wastewater generated during oil and gas activities (hydraulic fracturing and production) is commonly disposed of in deep formations, but the migration of this wastewater after entering the subsurface is poorly understood. This study uses numerical models to simulate wastewater disposal in the Paddy-Cadotte of Northeast British Columbia using both single-well axisymmetric box models and a regional model of the formation in which multiple disposal and water source wells operate. A sensitivity analysis performed on the box models reveals that dispersivity and permeability exert the strongest control on overall wastewater distribution. Models show that wastewater migrates further than predicted using a simple volumetric calculation, and extends further along the base of the formation than the top due to variations in fluid density. Interference between disposal and source wells is observed to influence wastewater migration, while formation dip and regional groundwater flow have no discernible impact.

Keywords: density-dependent flow; wastewater disposal; regional groundwater flow, numerical model

Acknowledgements

This project would not have been possible without my senior supervisor, Dr. Diana Allen, whose support has meant so much to me. I would like to thank both her and my other committee members, Laurie Welch and Dirk Kirste, for their guidance and insights. I would also like to thank the knowledgeable reservoir engineers and geologists at both the British Columbia Oil and Gas Commission and Encana Corporation for their valuable information on disposal well operation/regulation and the geology of the Paddy-Cadotte. This research was funded by the Pacific Institute for Climate Solutions. Additional funding was provided by the Contaminated Sites Approved Professionals Society, Geoscience BC, and Simon Fraser University.

I would like to thank my friends and family, both near and far, for their constant outpouring of support and kind words. I owe a great deal to my office mates, who were always willing to offer their services as living thesauri, help me pick the right color for a figure, and provide distractions when I probably should have been working.

Table of Contents

List of Tables

List of Figures

List of Variables

$\bar{\alpha}$	Density Difference Ratio
A_{Max}, A_{Min}	Maximum and Minimum Plume Axis Length
b	Formation Thickness
C, C_0	Solute Concentration, Reference Concentration
c^f, c^s	Specific Heat Capacity of Fluid and Solid Phases, respectively
D_{ij}	Tensor of Hydrodynamic Dispersion
e_j	Components of the Gravitational Unit Vector
f_μ	Constitutive Viscosity Relation Function
g	Gravitational Acceleration
h, h_f	Hydraulic Head and Equivalent Freshwater Head, respectively
K	Hydraulic Conductivity Constant
k_i	Intrinsic Permeability
K_{ij}	Tensor of Hydraulic Conductivity
n	Porosity
p, p_0	Pressure, Reference Pressure
P_A	Plume Asymmetry Coefficient
P_{F90}	90% of the Formation Fracture Pressure
$P_{Friction}$	Frictional Pressure Loss during Disposal
p_g	Freshwater Pressure Gradient
P_{Hydro}	Pressure Exerted by Water Column
$P_{Wellhead}$	Maximum Allowable Wellhead Pressure
Q	Fluid Source/Sink
q	Darcy Flux
Q_C	Mass Source/Sink
Q_T	Heat Source/Sink
r	Radial Extent of Wastewater
R, R_d	Retardation Factor and its Time Derivative, respectively
S_s	Specific Storage Coefficient
t	Time
T, T_0	Temperature, Reference Temperature

T_E	Thermal Expansion Coefficient
V	Injected Volume of Wastewater
Z	Elevation of Pressure Recorder
μ	Fluid Viscosity
α	Solutal Expansion Coefficient
α_L, α_T	Longitudinal and Transverse Dispersivity, respectively
β	Fluid Compressibility
θ	Chemical Decay Rate
λ_{ij}	Tensor of Hydrodynamic Thermodispersion
λ^f, λ^s	Thermal Conductivity of Fluid and Solid Phases, respectively
ρ, ρ_0	Fluid Density, Reference Fluid Density
ρ_C	Fluid Density at User-Defined Concentration
ρ_s	Solid Density

Chapter 1.

Introduction

The drilling and hydraulic fracturing of wells and subsequent gas production can generate highly saline wastewater (Goss et al., 2015), with total dissolved solids (TDS) in excess of the typical value for seawater of 35,000 mg/L The cumulative amount of wastewater produced from hydraulic fracturing is increasing rapidly with the steady drilling of new wells and a trend toward more water use per well (Alessi et al., 2017). In Northeast British Columbia (NEBC), an average of 75 m^3 of wastewater is generated for every million m^3 of gas produced from the Montney (IHS Energy, 2016), the most productive gas play in the province. This results in large quantities of wastewater that must be disposed of; the most viable method of disposal is injection into deep, permeable geologic formations, which will be referred to throughout this thesis as disposal formations/units[1].

Disposal formations in areas of oil and gas development are targeted for wastewater disposal as they are inferred to provide long term geological containment or "hydraulic isolation" of disposed fluids. The disposal formation may be a depleted hydrocarbon reservoir (or pool) or any deep water-saturated formation that has sufficiently high porosity and permeability and is confined by low permeability "cap rock" (e.g., shale). It is assumed that because groundwater flow velocities in the deep subsurface are low (Bachu, 1988), the wastewater will be permanently trapped and its movement will be limited both vertically and laterally by geological controls and/or pressure/head gradients. However, the potential response of the hydrogeological system to the injection

[1] The terminology used when referencing these disposal formations is often inconsistent, with both industry and the British Columbia Oil and Gas Commission using the terms "aquifer", "reservoir", and "disposal formation". The BC Environmental Protection and Management Regulation (EPMR; under the Oil and Gas Activities Act) defines an aquifer as a geologic formation, a portion of a formation, or group of formations "that contains water with up to 4 000 milligrams per liter of total dissolved solids (TDS) and is capable of storing, transmitting and yielding that water". The disposal formations that exist in BC are targeted specifically because they exist below the base of usable groundwater (defined below), and contain water that is in excess of 4,000 mg/L TDS, thereby eliminating them from being classified as aquifers under the EPMR definition. Industry still occasionally refers to these disposal formations as aquifers, but this thesis specifically avoids using that term as it gives the impression that wastewater is being injected into formations containing potable groundwater, when this is not the case.

of large quantities of saline wastewater is unknown (Ferguson, 2015). Little effort has been made in characterizing deep groundwater flow systems, as well as tracking this disposed saline wastewater and predicting its migration (Alley et al., 2014). Understanding and predicting the migration of disposed wastewater, however, is key to supporting effective management of deep disposal reservoirs with respect to both disposal of wastewater and sourcing of deep groundwater, particularly in light of increasing oil and gas development and associated potential increases in wastewater disposal.

Conceptually, the presence of low permeability cap rock confining the higher permeability and higher porosity disposal formation creates hydrogeological conditions whereby injected wastewater is contained within the disposal formation and preferentially migrates laterally within the disposal unit. The lateral migration of a wastewater plume, however, will be affected by numerous factors including injection rate, geological heterogeneities, pressure variability within the disposal unit, disposal or production at nearby wells, and fluid density differences between formation water and injected wastewater. Disposed wastewater can reach TDS values of over 300,000 mg/L (IHS Energy, 2016), and typically has a greater density and viscosity compared to the disposal unit formation water. This may lead to concentration gradients and associated density differences between the plume and the formation water, complicating the prediction of plume migration. Standard groundwater modeling codes, in which the groundwater flow equation is solely solved, are not capable of accurately simulating the injection and migration of dense, viscous fluids. Instead, specialized codes such as FEFLOW (Diersch, 2002), a finite-element modeling program capable of solving the density-dependent flow and solute transport equations, are necessary.

This research aims to characterize the migration of saline wastewater plumes within geological formations used for disposal of wastewater. This will be accomplished using the finite-element modeling code FEFLOW (Diersch, 2002) to simulate the disposal of wastewater on both the single-well and study area scale. Single-well migration is investigated through the use of box models representing simplified disposal formations on which a sensitivity analysis is performed to assess the relative contribution of formation and fluid characteristics to overall plume shape and extent. The study area scale migration of wastewater is investigated by simulating a disposal formation in which

both wastewater disposal and source water extraction occurs in order to investigate the potential for well interference.

1.1. Background

1.1.1. Generation of Wastewater

Hydraulic fracturing, commonly known as fracking, is the process of injecting fluid into a hydrocarbon bearing rock at high pressure in order to create fractures that act as conduits for releasing the oil and/or gas that is contained within (BC Oil and Gas Commission (BCOGC), 2011; Hubbert and Willis, 1957). In unconventional "tight" reservoirs, hydraulic fracturing is typically carried out in horizontal wells. The wells are first drilled vertically down to the formation of interest, and then gradually turned 90º to enable the drill to pass horizontally along the target formation. Horizontal drilling significantly increases the contact area of the borehole with the hydrocarbon producing zone. Following drilling, the casing is perforated and hydraulic fracturing fluid is pumped into the well at high pressure, fracturing the rock in multiple stages of injection over the horizontal length of the borehole. The result of hydraulic fracturing is a significant increase in the hydrocarbon yield in the low porosity medium (Figure 1.1). In most cases, the fluid used for hydraulic fracturing is dominantly (~99.5% by volume) water and sand (Gregory et al., 2011). The sand acts as a proppant to keep the fractures open and allow the hydrocarbon to flow freely to the well. The remaining 0.5% volume is made up of chemical additives such as friction reducers and biocides that help to increase the efficiency of the fracking process (Gregory et al., 2011).

The act of drilling and fracking a well is water intensive, using anywhere from 800 m^3 (Johnson and Johnson, 2012) to over 75,000 m^3 (Precht and Dempster, 2012) of fracturing fluid per well. This quantity depends on local geology, the number of fracture stages, and the length of the borehole. A certain amount of this fluid is recovered at the surface and is known as flowback water. The amount of fracking fluid that returns as flowback varies greatly based on geology and can range from 15-100% of the initially injected volume (Rivard et al., 2014), while the rest of the fluid remains in the formation. The chemicals in the flowback necessitate either treatment or safe disposal of the fluid. The low salinity of the flowback water generally reduces the cost of treatment, allowing it to be recycled and used to drill and frack other wells (Henderson et al., 2011). If

flowback water cannot be treated or recycled for re-use, it must be disposed via disposal wells.

As the oil or gas is extracted from the well, so too are naturally occurring, highly saline formation waters, referred to as produced water, which is generated throughout the lifetime of a well. The chemical composition of the formation water is largely the result of the initial conditions of deposition (typically evaporative hypersaline environments) and the subsequent water/rock interactions that occurred over millions of years (Lee and DeBlois, 2011). The TDS values of formation water generally increase with depth, and can range from 4,000 to 350,000 mg/L (Bachu and Underschultz, 1993; Hayes, 2009). A range of techniques exist to treat this wastewater product (Fakhru'l-Razi et al., 2009; Hallock et al., 2013; Burnett, 2004), yet the techniques remain time-intensive and costly, resulting in the bulk of wastewater being managed through the use of disposal wells (Clark and Veil, 2009; Figure 1.1).

Some regulators make no distinction between fracturing fluids that return to the surface and formation waters that are extracted along with hydrocarbons (BCOGC, 2016a), grouping them together and calling them produced water, while others refer to both flowback and produced water as wastewater. This thesis follows the latter terminology.

1.1.2. Wastewater Disposal and General Regulations

Wastewater disposal wells are either drilled explicitly for the purpose of disposing wastewater, or they may be wells that were previously drilled for hydrocarbon production which reached the end of their production lifecycle and were repurposed (IHS Energy, 2016). Commonly, disposal wells are vertical, although some attempts have been made to use horizontal wells for wastewater disposal (Ron Stefik, BCOGC, personal communication). In BC, disposal wells are differentiated from injection wells in that the former are used exclusively to dispose of wastewater, while the latter is an umbrella term that includes disposal wells, fracking wells, and wells used to inject fluid into a hydrocarbon-producing formation in order to increase pore pressure and increase hydrocarbon yield. This scope of this thesis solely encompasses disposal wells.

The formations targeted for wastewater disposal are either "deep aquifers" (BCOGC, 2016c) or depleted hydrocarbon pools; both of which have high permeability relative to

the confining cap rock and base formations (BCOGC, 2016c; Warner et al., 1986). In theory, the confined nature of these formations reduces the likelihood of contamination of shallower groundwater that may be accessed by domestic wells. In BC, disposal formations are restricted to units that contain “deep groundwater”[2] as defined in the BC Water Sustainability Regulation under the BC Water Sustainability Act (BCOGC, 2016c). This reduces the risk of highly saline wastewater contaminating relatively shallow and potentially potable groundwater. Close proximity of the disposal formation to the area of wastewater production is desirable, as it reduces the cost and time required to transport wastewater to disposal wells.

[2] In British Columbia, “deep groundwater” exists below the base of usable groundwater, which is low salinity, potable water that could be used for domestic purposes. This base of usable groundwater begins between 300-600 m below ground surface, depending on the presence of a regional geologic marker known as the base of fish scales that marks the boundary between the Upper and Lower Cretaceous in the Western Canada Sedimentary Basin (BCOGC, 2016d).

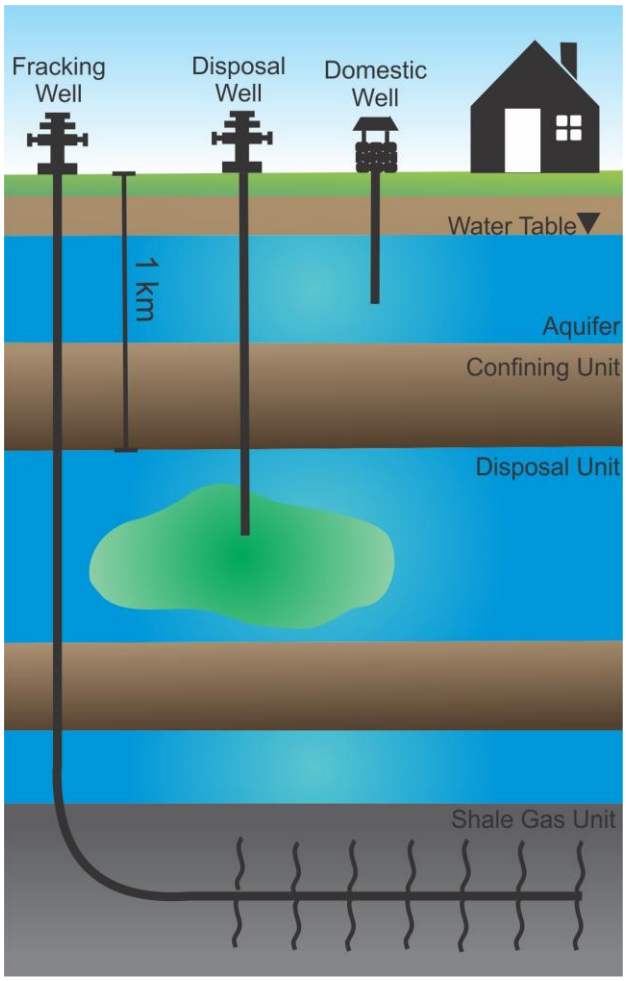

Figure 1.1. Relative depths of a hydraulically fractured well (left), a wastwater disposal well (middle), and a domestic groundwater well (right). Not to scale.

The regulations concerning the approval and operation of disposal wells vary by province and state, but are generally similar (BCOGC, 2016a; Alberta Energy Regulator (AER), 1994; Oklahoma Corporation Commission, 2014; Ontario Oil, Gas and Salt Resources, 2002). Companies intending to dispose of wastewater in the subsurface must issue reports to the provincial or state regulator proving that the formation is hydraulically isolated from overlying units. This includes fracture mapping within the bounding low permeability units and providing records indicating that the borehole has been properly cemented through these units. Companies are also required to submit monthly disposal volumes (BCOGC, 2016c; Mississippi Oil and Gas Board, 2012), with these data being available through commercial data vendors such as Accumap (IHS Energy, 2016).

1.1.3. Pressure Regulations

In BC, a variety of regulations also exist concerning the permissible pressures related to wastewater disposal, all of which are presented in the Water Service Wells Summary Information (BCOGC, 2016c). These regulations contain two main parts that are important to this thesis: pressures generated in the formation during disposal and background formation pressures measured in an annual test during which disposal is temporarily suspended.

The first of these regulations states that bottom hole pressures during disposal cannot exceed 90% of the formation fracture pressure. This pressure is typically determined by either intentionally fracturing the disposal formation, derived from a step-rate injection test, or is interpolated from other known fracture pressures measured nearby. Bottom hole pressures during disposal are typically not monitored, and so the known formation fracture pressure (taken from disposal approval letters from the BCOGC specific to each well) must be converted into a wellhead injection pressure which can easily be monitored on the surface by disposal well operators. This conversion is performed by accounting for the hydrostatic pressure of the fluid column in the disposal well and any frictional pressure loss that may occur in the well. For the purposes of this thesis, the formation fracture pressure at the bottom of the well is more important than the wellhead injection pressure, since the model simulates pressures in the formation and not at ground surface. However, the fracture pressure data available for each disposal well discussed in this thesis are only available in terms of wellhead injection pressure, and must be converted to formation fracture pressure. This process is presented in greater detail in Chapter 2.

Background pressures within the formation are regulated as well, being limited to a maximum value of 120% of the initial virgin reservoir pressure (IVRP), which is the pressure in the disposal formation measured in the middle of the perforated interval of the well prior to any production or injection in the disposal formation. It is noted that, during disposal, pressures will likely greatly exceed this 120% IVRP limit (up to 90% of the formation fracture pressure as discussed above); it is only the background formation pressure that is subject to this limitation. This background pressure is measured in an annual pressure test, during which the well is temporarily shut down and the bottom hole pressures are measured. If pressures in the well drop below 120% IVRP within 60 days

then the well can continue operating, though the well does not need to remain shut down for the full 60 days. Formation pressures at the 60 day mark can be extrapolated from initial pressure fall-off and used to gauge whether the 120% limit is met. If it exceeds this limit, the well must be shut down until pressures fall to lower levels, at which point disposal can begin again.

1.1.4. Volumetric Calculation for Estimating Plume Extent

A common method used by industry and regulators to estimate the lateral extent of wastewater disposed of in formation for gauging potential interference with other disposal or source wells is based solely on porosity estimates, formation thickness, and total volume of waste injected (Ron Stefik, BCOGC, personal communication).

$$r = \sqrt{\frac{V}{\pi b n}} \tag{1.1}$$

where

r = radial extent of wastewater [m]
V = volume of waste injected [m^3]
n = formation porosity [-]
b = formation thickness [m]

This equation assumes total displacement of water in pore spaces in the disposal formation. It neglects mass transport processes such as advection, dispersion, and diffusion, all of which cause the longitudinal and lateral extent of the wastewater plume to be larger than that due to pore fluid displacement alone. It also fails to account for buoyancy related effects that may arise due to density differences between fluid types in the subsurface as a result of variations in temperature and salinity.

1.1.5. Thesis Motivation

Despite the recent surge in unconventional gas production throughout Canada and the United States (US) within the past 10-15 years (Wang et. al, 2012), little work has been done to predict the migration of wastewater in the deep subsurface, an area where

groundwater is poorly understood (Alley, 2013). Ferguson (2015) states “There has been little monitoring of formation pressures . . . and almost no effort dedicated to tracking injected brine in the subsurface.” In BC, wastewater disposal is poised to increase given the recent increase in shale gas development in NEBC (Johnson and Johnson, 2012). Formations suitable for wastewater disposal may be targeted by multiple operators. Estimates of storage capacity, which along with other data are used to inform aspects of deep reservoir management, are carried out on a well by well basis based on estimates of porosity, formation thickness and total injection volume (Ron Stefik, BCOGC, personal communication; Equation 1.1). Moreover, some formations currently used for wastewater disposal are also being used as a source of “deep groundwater” (defined in the BC Water Sustainability Regulation under the Water Sustainability Act). At present, the primary source of water for hydraulic fracturing is surface water with some shallow (fresh) groundwater use (BCOGC, 2016b), but deep groundwater is also used and usage has the potential to increase as a viable alternative to shallow fresh groundwater (Encana Corporation, 2014). However, little is known about the potential for interference among disposal wells and between disposal and source wells that are completed in the same formation.

1.2. Purpose and Objectives

The aim of this thesis is to characterize the migration of saline plumes in the subsurface created by the disposal of wastewater. The specific objectives of this thesis are:

1) To understand how formation characteristics (permeability, specific storage, thickness, horizontal gradient, etc.) influence plume movement on the local and regional scale;

2) To evaluate the validity of using a porosity-based calculation for determining the extent of disposed wastewater in a formation, and;

3) To investigate the potential for interference among disposal wells and between disposal wells and source wells that are completed in the same formation.

The study region chosen for this research is Northeast British Columbia. Production of wastewater associated with oil and gas exploitation in this region has been increasing since the onset of hydraulic fracturing in approximately 2005 due to advancements in horizontal drilling technology (IHS Energy, 2016). The volumes of wastewater that

cannot be recycled are disposed of in deep formations (BCOGC, 2016c). One formation that is currently being used for disposal, the Paddy-Cadotte, is the focus of the research. This particular formation was recommended for focus through consultation with the BCOGC and is currently being used conjunctively for disposal and deep water source operations.

1.3. Scope of Work

The proposed scope of work for meeting the objectives involves three main components:

1) Developing a conceptual hydrogeological model of the Paddy-Cadotte by compiling geologic, hydrogeologic, and oil and gas data (e.g., borehole and geophysical logs, formation fluid pressure and chemistry, and wastewater disposal/source water extraction rates).

2) Conducting a sensitivity analysis to evaluate how different formation and fluid characteristics influence wastewater plume migration and structure. This is accomplished by simulating density-dependent flow and heat and mass transport for single well injection using a series of generic box models with varying parameter values.

3) Simulating groundwater flow and plume movement under variable injection histories and source water extraction scenarios in a regional model of the Paddy-Cadotte to provide insights regarding how wastewater has migrated to date, and where it may travel in the future.

1.4. Thesis Organization

Chapter 1 provides an introduction to the thesis, including a background on hydraulic fracturing and wastewater disposal. The purpose and objectives of the research are presented.

Chapter 2 gives an overview of the study area in Northeast BC. Details concerning the disposal wells and source wells, the geology of the different formations, particularly the Paddy and Cadotte, and the hydrogeology of the area (hydrostratigraphy, regional groundwater flow and groundwater chemistry) are discussed.

In Chapter 3, an overview of the development of the generic density-dependent flow and heat and mass transport numerical models is given. This chapter is an extended version of a conference proceedings paper “Numerical modelling of highly saline wastewater

disposal in Northeast British Columbia" presented at GeoOttawa 2017 (Simons et al., 2017).

Chapter 4 describes the results of the study area wastewater disposal and source water extraction simulations. The influence of formation dip, regional hydraulic gradient, and interference between wells on the overall extent of wastewater plumes is investigated and compared to plume sizes calculated using Equation 1.1.

Chapter 5 offers conclusions and proposals for future work stemming from this research.

Chapter 2.

Study Area

This chapter summarizes the well information for disposal wells and water source wells within the study area that target the Paddy-Cadotte (i.e. their location, depth, pumping/injection rate, etc.). The geological and hydrogeological characteristics are then discussed for the Paddy-Cadotte in and around the study area through inferences based on the regional geological and hydrogeological context and available regional oil and gas well data. These data are used to provide a basis for defining model domain and parameterization in Chapters 3 and 4. It should be noted that the data used to support the hydrogeological characterization in this chapter were collected for purposes specific to the regulation of oil and gas activities in British Columbia, and some limitations exist regarding the extension of the data toward hydrogeological interpretation, including spatial coverage, data collection procedures designed for specific purposes (e.g., drill stem tests (DSTs)), and general uncertainties regarding representative hydrogeological data. While the focus of this research is on a single disposal formation, the methods used to characterize and model this formation could potentially be applied to other disposal formations.

The study area for this thesis is located approximately 20 km west of the City of Dawson Creek, BC within the Montney gas play of Northeast, BC (NEBC) (Figure 2.1), which has been host to oil and gas related activities for decades. The study area is defined by a group of active disposal wells and water source wells that target a porous geological reservoir composed of the Paddy and Cadotte Members of the Peace River Formation, hereafter referred to as the Paddy-Cadotte (Figure 2.2).The Paddy-Cadotte has a relatively recent and less complex disposal history (initiated within the past 5 years) compared to other disposal formations within the Montney gas play that may have received wastewater for multiple decades (e.g. Cadomin, Gething, Baldonnel, and Halfway). Due to this, the Paddy-Cadotte is ideally suited for this research as it will be more straightforward to model from a disposal history perspective (see Chapter 4).

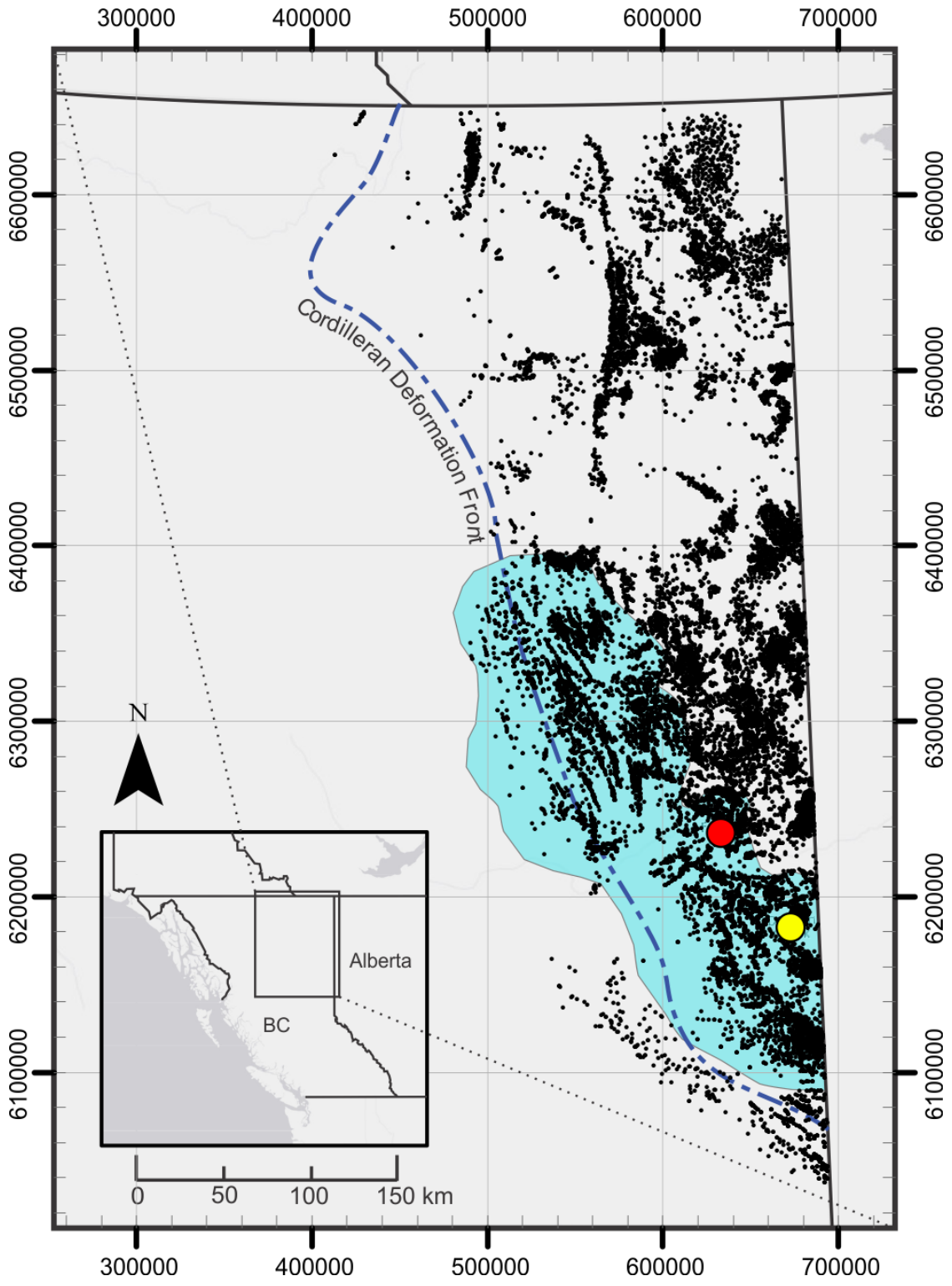

Figure 2.1. **Map of Northeast BC showing surface hole locations of oil and gas wells (black dots; IHS Energy, 2016), extent of the Montney play trend (blue; BCOGC, 2012)), and locations of Fort St. John (red dot) and Dawson Creek (yellow dot). Grid markings are in UTM coordinates.**

2.1. Disposal and Source Wells

The wells of interest in this study are the 11 disposal and water source wells that target the Paddy-Cadotte clustered together approximately 20 km to the west of the City of Dawson Creek (Figure 2.2). As of October 2017, this cluster included five disposal wells and six water source wells, although there are plans to install up to 14 additional dual-purpose horizontal wells by 2019 in this area (see section 2.1.2) (Encana Corporation, 2014). The disposal volume and source water extraction volume histories for the wells are shown in Table A1 in Appendix A and were compiled using both Accumap (IHS Energy, 2016) and the BCOGC's online database (BCOGC, 2017a). Fluid volumes are shown for up to October 2017, as these are the most current values at the time of writing (December 2017). These volumes will be used in the regional model of the area discussed in Chapter 4. It should be noted that there are two additional disposal wells which target the Paddy-Cadotte, WA 26920 and WA 27084, located slightly to the north of Dawson Creek (Figure 2.2). These wells have been used to dispose of significant volumes of wastewater (390,000 and 914,000 m^3, respectively), but are located far (~20 km) from the area of interest and so will not be considered in this study.

Industry wells are referred to by their Unique Well Identifier (UWI), a 16-character code specifying the well's bottom hole location in the Dominion Land Survey System or National Topographic System, or by their Well Authorization (WA) number, a five digit code assigned to a well based on the order in which the license was assigned. This thesis refers to wells using their WA (e.g. 'WA 10677' or just 'well 10677').

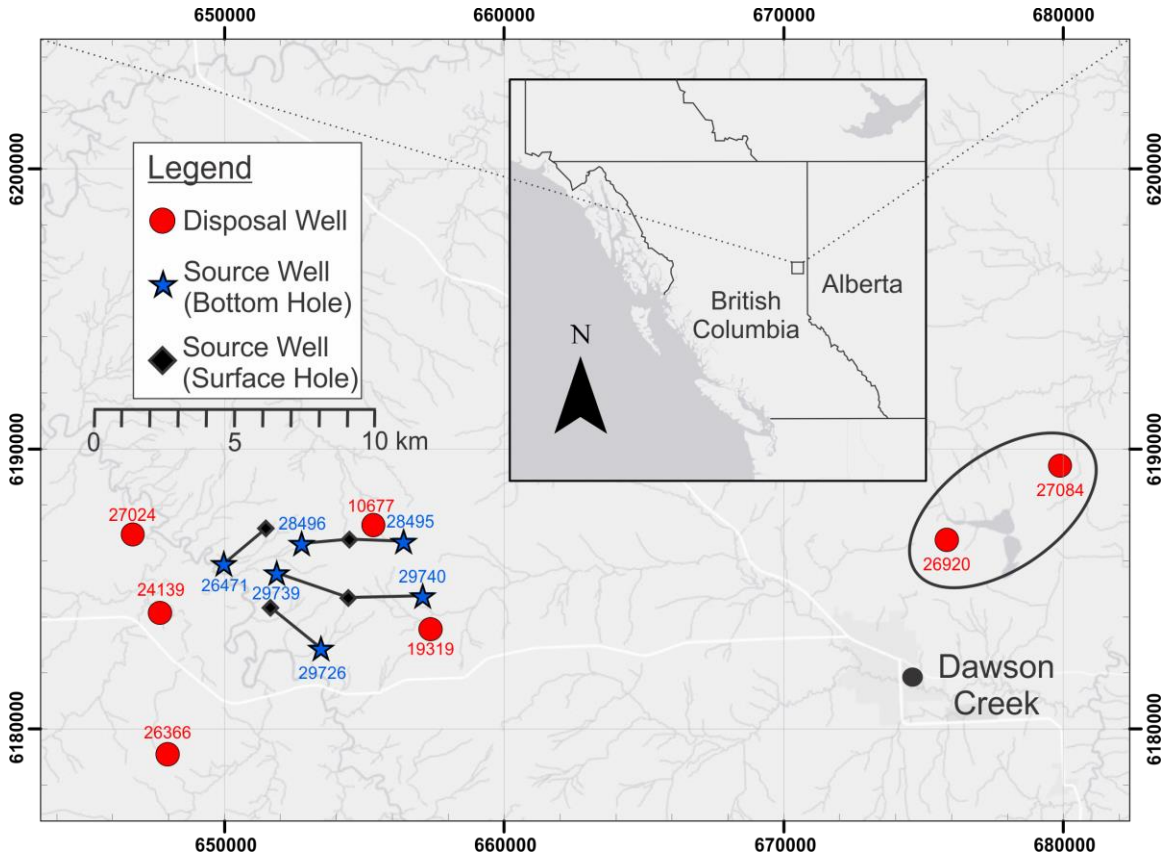

Figure 2.2. **Map showing the locations of disposal wells (red dots), source well bottom locations (blue stars) and source well surface locations (black diamonds) targeting the Paddy-Cadotte. Because the source wells are horizontal, the location of both the surface hole and bottom hole locations are marked, with the surface hole being the location where drilling was initiated and bottom hole being the end of the well. Wells are labelled according to their WA numbers. Note that some source wells share well pads. Disposal wells 26920 and 27084 (circled) are actively injecting, but are not considered in this study.**

2.1.1. Disposal Wells

Depth and disposal volumes for the disposal wells targeting the Paddy-Cadotte are provided in Table 2.1, with additional information presented in Table A2 in Appendix A. The five disposal wells that target the Paddy-Cadotte were constructed between 1997 and 2011, though disposal operations only began slowly in late 2014 at WA 19319. Operation of all five disposal wells was underway by late 2015 (Appendix A, Table A1). Two of the wells (WA 19319 and WA 26366) were drilled with a true vertical depth (TVD)

within or just below the Paddy-Cadotte, roughly 1000 m below kelly bushing (mKB)[3]. The other three wells reach vertical depths of >2700 mKB, and are inferred to have been originally drilled to target a deeper formation, being more recently repurposed and perforated at shallower depths for use as disposal wells. The cumulative volume of wastewater disposed of in each individual well ranges from 105,000-153,000 m^3, with the exception of WA 27024, which has only disposed of 8,100 m^3, and WA 10677, which has disposed of over 873,000 m^3 (Appendix A, Table A1). This translates to injection rates of roughly 140-190 m^3/day for WA 19319, WA 26366, and WA 24139, 14 m^3/day for WA, and 1090 m^3/day for WA 10677. These rates are variable (temporally and from well to well), as well use is dependent on supply of wastewater to be disposed, and wells can shut down for months at a time (Appendix 1, Table A1). It is noted that, as of March 2017, WA 19319 had surpassed the 120% IVRP limit (Petro Management Group Ltd., 2017; see Chapter 1) and is currently shut down until pressures drop sufficiently (BCOGC, 2017b).

Table 2.1. General information for the disposal wells targeting the Paddy-Cadotte. Cumulative disposed water volumes are current up to October 2017. Months of operation are between October 2014 and October 2017.

Well Authorization Number	19319	10677	26366	24139	27024
True Vertical Depth (mKB)	1029.0	2720.0	1144.9	2708.6	2811.8
Cum. Disposed Water (m^3)	152147	873833	105545	153715	8123
Mean Disposal Rate (m^3/d)	188	1092	137	185	14
Months of Operation	29	29	25	27	20

The perforated intervals of these disposal wells are shown in Figure 2.3. They predominantly target a high permeability horizon within the Cadotte (see Sections 2.2 and 2.3.2), with the exception of WA 19319, which is perforated over the entire length of the Paddy and Cadotte, and WA 26366, which is perforated over the lower half of the Paddy. Depositional environments during the time of Paddy sediment deposition were spatially variable (see Section 2.2), and so could have led to localised areas of higher permeability, making them suitable locations for disposal wells such as WA 19319 and 26366. In order to increase the permeability of the formation in the area surrounding the

[3] The kelly bushing is a part of the drilling rig that is typically several meters above ground surface and is commonly used as a datum in the oil and gas industry

perforated interval, each well was stimulated in a manner similar to that outlined in Chapter 1; fluid was injected into the well at high pressure in order to create fractures in the surrounding rock. The resulting increase in formation permeability is discussed further in Chapter 4.

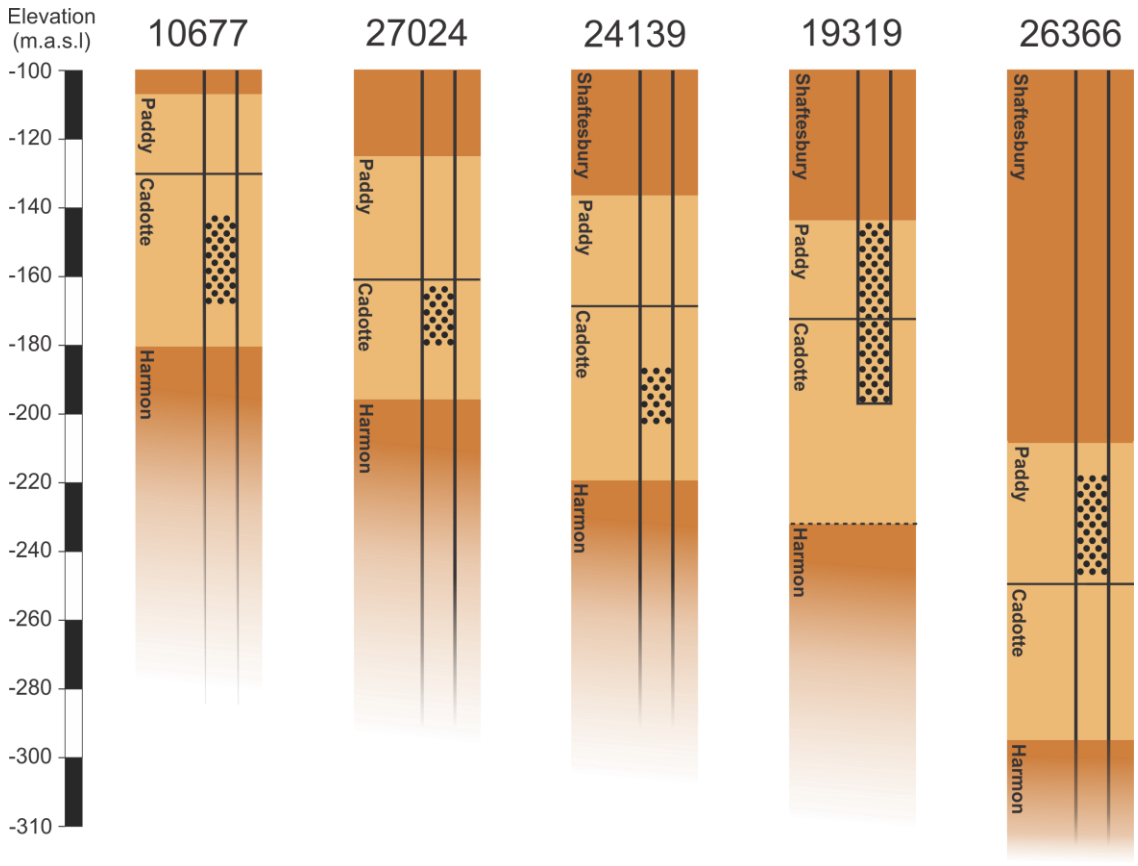

Figure 2.3. Wellbore schematics showing intervals in the Paddy and/or Cadotte over which the wells are perforated (dotted section of well).

As mentioned in Chapter 1, disposal pressures must not exceed 90% of the formation fracture pressure, a value which varies from well to well. This pressure, in a converted form of maximum wellhead pressure (i.e. pressure measured at the surface and not in the well), is specifically stated in a given well's approval letter (see Appendix B for each study area disposal well's approval letter). For the purposes of this thesis, however, it is the formation fracture pressure that is more useful, and so the wellhead pressures for each disposal well in the study must be backwards converted as the measured formation fracture pressures for each well are not readily available. This can be done using the equation:

$$P_{F_{90}} = P_{Wellhead} + P_{Hydro} - P_{Friction} \quad (2.1)$$

where

$P_{F_{90}}$ = 90% of the formation fracture pressure [kPa]

$P_{Wellhead}$ = maximum allowable pressure measured at the wellhead [kPa]

P_{Hydro} = pressure exerted by the height of the water column in the well [kPa]

$P_{Friction}$ = frictional pressure losses in the well during disposal [kPa]

In this equation, P_{Hydro} can be determined by multiplying the depth of the middle of the perforated interval of a disposal well below ground surface by an assumed pressure gradient of 10.5 kPa/m, though in cases where very saline wastewater is being disposed a larger pressure gradient may be necessary. Frictional losses ($P_{Friction}$) are usually conservatively estimated as 200 kPa. Table 2.2 shows the maximum allowable bottom hole pressures ($P_{F_{90}}$) of each disposal well in the study area as determined using Equation 2.1.

Table 2.2 Values used to determine the allowable bottom hole pressures for each disposal well in the study area. Wellhead injection pressures for each well are presented in Appendix B, and frictional pressure losses during disposal are assumed to be 200 kPa.

Well Authorization Number	10677	19319	24139	26366	27024
Wellhead Injection Pressure (kPa)	14400	9050	13400	12300	13070
Depth below ground surface (m)	983.25	962.20	918.10	1020.85	884.10
Water column pressure (kPa)	10324.13	10103.1	9640.05	10718.93	9283.05
90% Fracture Pressure (kPa)	24524.13	18953.1	22840.05	22818.93	22153.05

2.1.2. Source Wells

The water source wells operating in the Paddy-Cadotte are outlined in Table 2.3, with greater detail given in Table A3 in Appendix A. All water source wells are owned by the Encana Corporation and are dual-purpose wells, meaning that they are capable of operating as both disposal wells and source wells. They are all currently being used for source water and have not yet been used for disposal, but Encana plans to convert them to disposal wells at some point in the future (Encana Corporation, 2014), potentially re-pressurizing the formation back to at least its initial reservoir pressure. It should be noted that these wells are “water source wells” as defined in the Petroleum and Natural Gas

Act. The wells (WA 29726, 29740, 29739, 26471, 28496, and 28495) require a status on record as “active gas production” as they all produce natural gas at levels that require conservation. The natural gas, while not in gas phase at the formation depth, is exsolved upon water extraction due to pressure changes (BCOGC, 2016c).

The water source wells are horizontal, increasing the contact area with the Paddy-Cadotte and allowing for water to be extracted more quickly from the formation. The length and direction of the horizontal sections of these wells are shown in Figure 2.2, with the blue stars representing the bottom hole location and the lines leading away terminating at the location of the well pad (black diamonds). Similar to the operation of disposal wells, the rate of source water extraction is dependent on the need for water, and so can be highly variable over time and from well to well. A notable period of inactivity is June-October 2016, during which time all six source wells were inactive (Appendix A1). When operational, these wells typically pump at average rates of 120-200 m^3/day.

Table 2.3. General information for the source wells targeting the Paddy-Cadotte. Cumulative extracted water volumes are current up to October 2017.

Well Authorization Number	29726	29740	29739	26471	28496	28495
True Vertical Depth (mKB)	952	1013	1006	914	1017	997
Cum. Extracted Water (m3)	54853	80765	97270	56401	103610	104322
Mean Extraction Rate (m^3/d)	122	148	165	121	166	193
Horizontal Perforated Length (m)	1909	2085	2198	1680	1280	1486

2.2. Regional Geology

The Western Canada Sedimentary Basin (WCSB) is a large wedge of sedimentary rock overlying Precambrian basement. The basin spans from British Columbia, where it is ~6 km thick, to Manitoba, where it pinches out. It is host to significant quantities of hydrocarbons, making Canada the third largest country in terms of hydrocarbon reserves (Alberta Energy Regulator (AER), 2016). In NEBC, the majority of these hydrocarbons are found in unconventional reservoirs, such that they require additional stimulation (i.e. hydraulic fracturing) before they can be produced (BCOGCa, 2016). Notable unconventional gas reservoirs include the Horn River Basin, the Liard Basin, and the Cordova Embayment, though the largest and most active is the Montney gas play

(BCOGC, 2014). This reservoir is of greatest relevance to this thesis as it is the primary source of wastewater that is disposed of in the Paddy-Cadotte.

The geologic units of greatest interest to this thesis are, from deepest to shallowest, the Lower Cretaceous Harmon shale, Cadotte sandstone, Paddy sandstone, and Shaftesbury shale (Figure 2.4), which represent a major regressive-transgressive cycle (Leckie and Reinson, 1993). The sandstones act as reservoirs from which source water can be extracted and into which wastewater can be injected, while the shales act as confining units that are considered to restrict wastewater to the disposal formation. The relative depth of the Paddy-Cadotte in the area of Dawson Creek is shown in Figure 2.5, which also characterizes each formation from ground surface down to the Montney as either a permeable or confining unit. Details on formations relevant to this thesis are provided in the following sections.

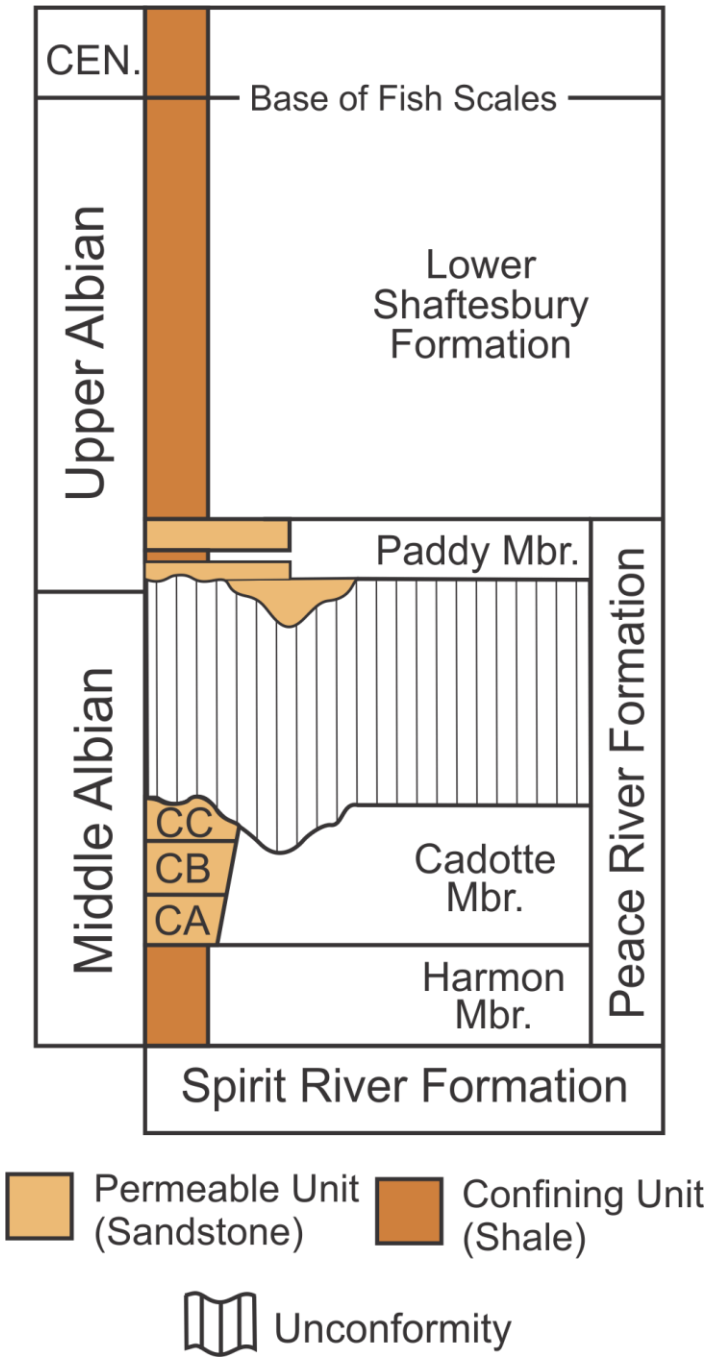

Figure 2.4. **Stratigraphy of the middle to upper Albian in the plains area of NEBC showing the positions and lithologies of the Harmon, Cadotte, Paddy, and Shaftesbury units. Modified from Leckie and Reinson (1993) and incorporating Cadotte allomembers from Buckley and Plint (2013).**

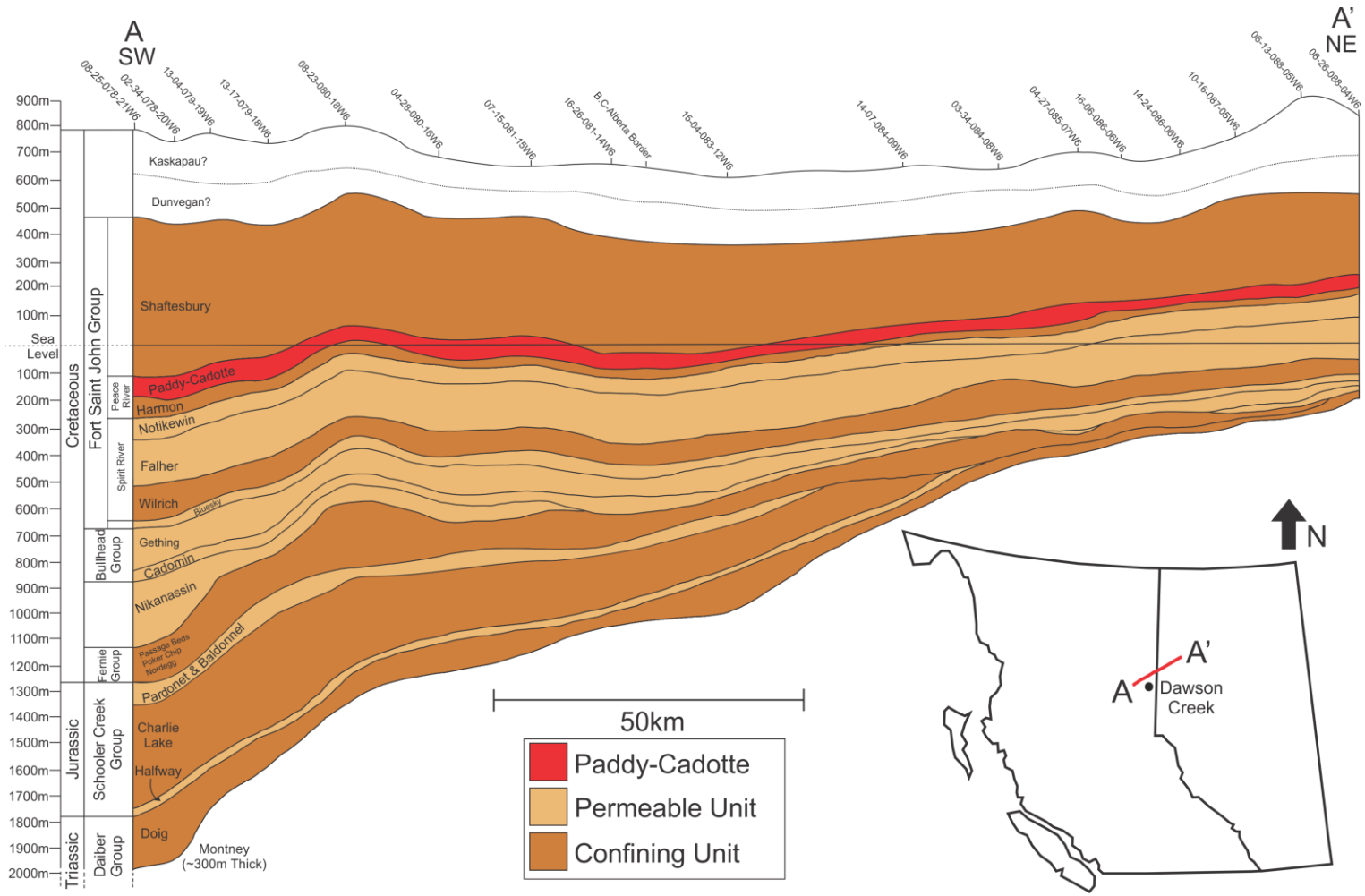

Figure 2.5. **Geologic units of the Western Canadian Sedimentary Basin (WCSB) in the area of Dawson Creek down to the Montney Formation. Units are colored according to their potential to store and transmit water, with more permeable units in light brown and less permeable, confining units in dark brown. The Paddy-Cadotte is shown in red. Figure based in part on classification scheme from Riddell et al. (2012).**

2.2.1. Harmon Shale

The Harmon shale was deposited during the middle Albian in the southern part of the Harmon/Hulcross sea, an embayment of the Boreal Ocean (Figure 2.6; Buckley and Plint, 2013), and, regionally, ranges in thickness from 120 m in the west to less than 10 m in the east, demonstrating a regional wedge-like structure (Leckie et al., 1990).

2.2.2. Cadotte Sandstone

A drop in sea level initiated the deposition of quartz-rich Cadotte sediments in a wave-dominated shoreface environment (Figure 2.6; Buckley and Plint, 2013), which were likely sourced from the orogeny to the west (Hyde and Leckie, 1994). The Cadotte coarsens upwards from fine-grained lower shoreface sands and muds to upper shoreface conglomerate or medium grained sands. The top 1-4 m of the Cadotte are either granulestones or coarse sandstones, interpreted to represent foreshore deposits (Leckie et al. 1990). Buckley and Plint (2013) identified three allomembers within the Cadotte (Figure 2.4), each approximately one third of the total thickness of the unit. The lowest allomember, CA, consists of sandstone interbedded with mudstone units. CB overlies CA and lacks the mud typical of CA, making it blockier. The topmost allomember, CC, is similar to CB, but shows a greater range of grain size. Both CB and CC are typically targeted for wastewater disposal (Figure 2.3; Section 2.3.2), as they lack the mudstone that is present in CA, imparting a greater porosity and permeability.

The Cadotte is relatively tabular in shape (in contrast to the Paddy and Harmon which have a much more pronounced wedge-shape), though it does thin slightly from 60 m in the west to 20-30 m near the BC-Alberta border (Figure 2.7). This more gradual thinning is attributed to reduced crustal flexural subsidence during sediment deposition (Plint et al., 2012). The Cadotte is unconformably overlain by the Paddy, having been locally incised, and hosts what have been interpreted to be buried paleovalleys (Hayes, 1988).

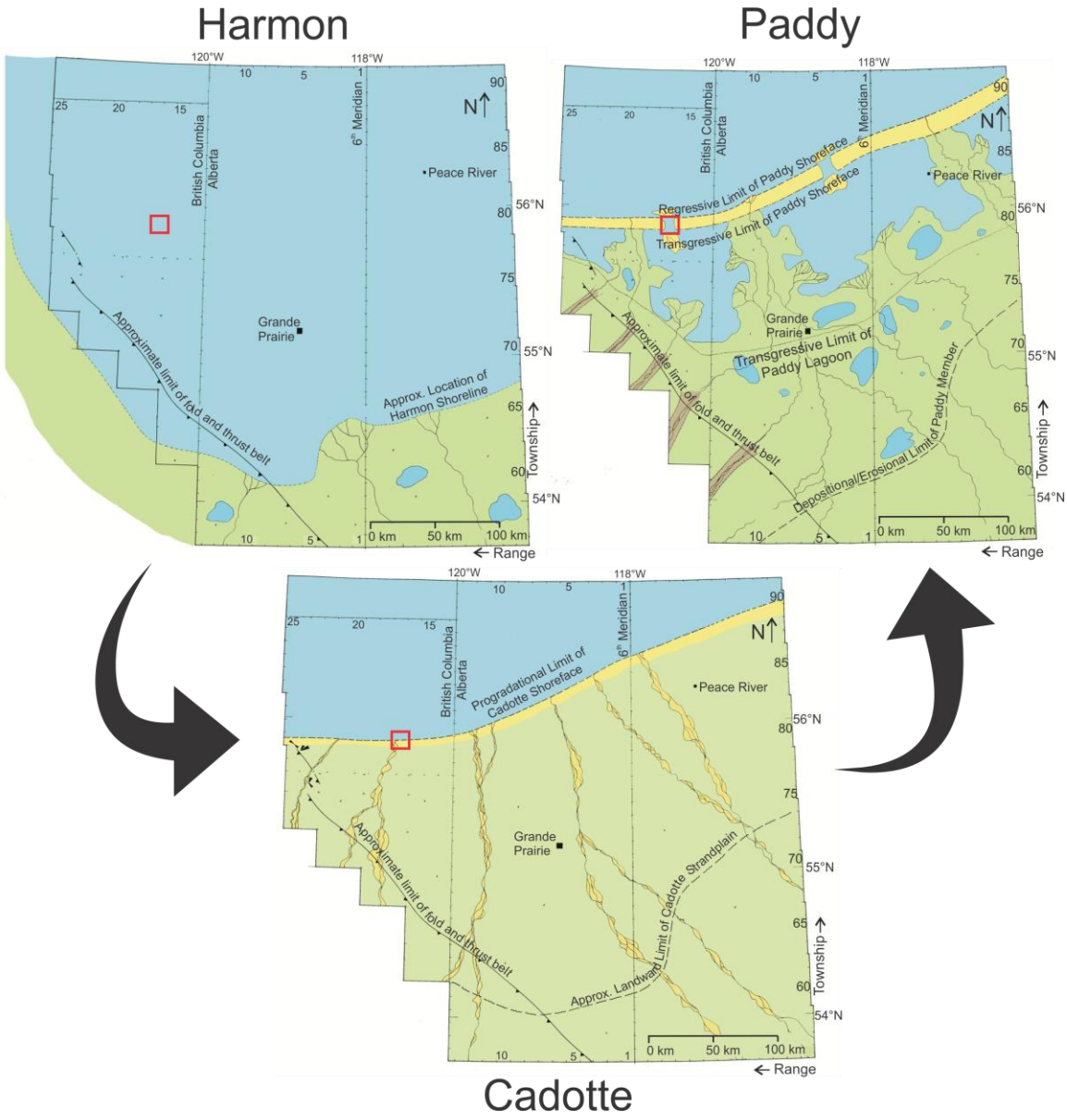

Figure 2.6. Regional paleogeography during the deposition of Harmon, Cadotte, and Paddy sediments in the middle to late Albian (Buckley and Plint, 2011). Red squares show location of the study area .

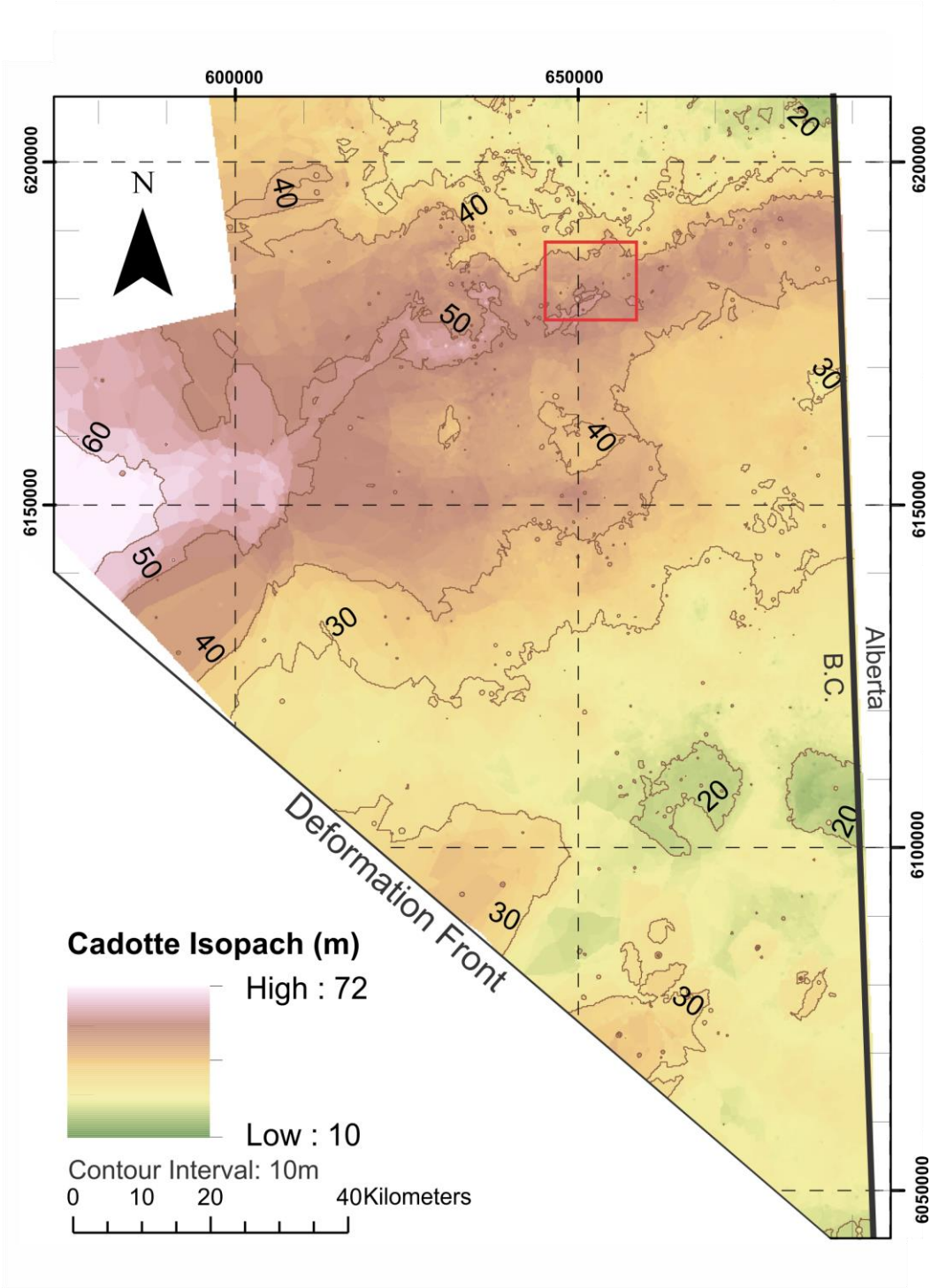

Figure 2.7. **Isopach map of the Cadotte unit in NEBC. Red square shows location of study area. Map was created using formation thickness data from Accumap (IHS Energy, 2016; n= 4662, 103 of which are in the study area) that were then kriged in ArcMap using a linear semivariogram model, a nugget of 30, major range of 70000, and partial sill of 120.**

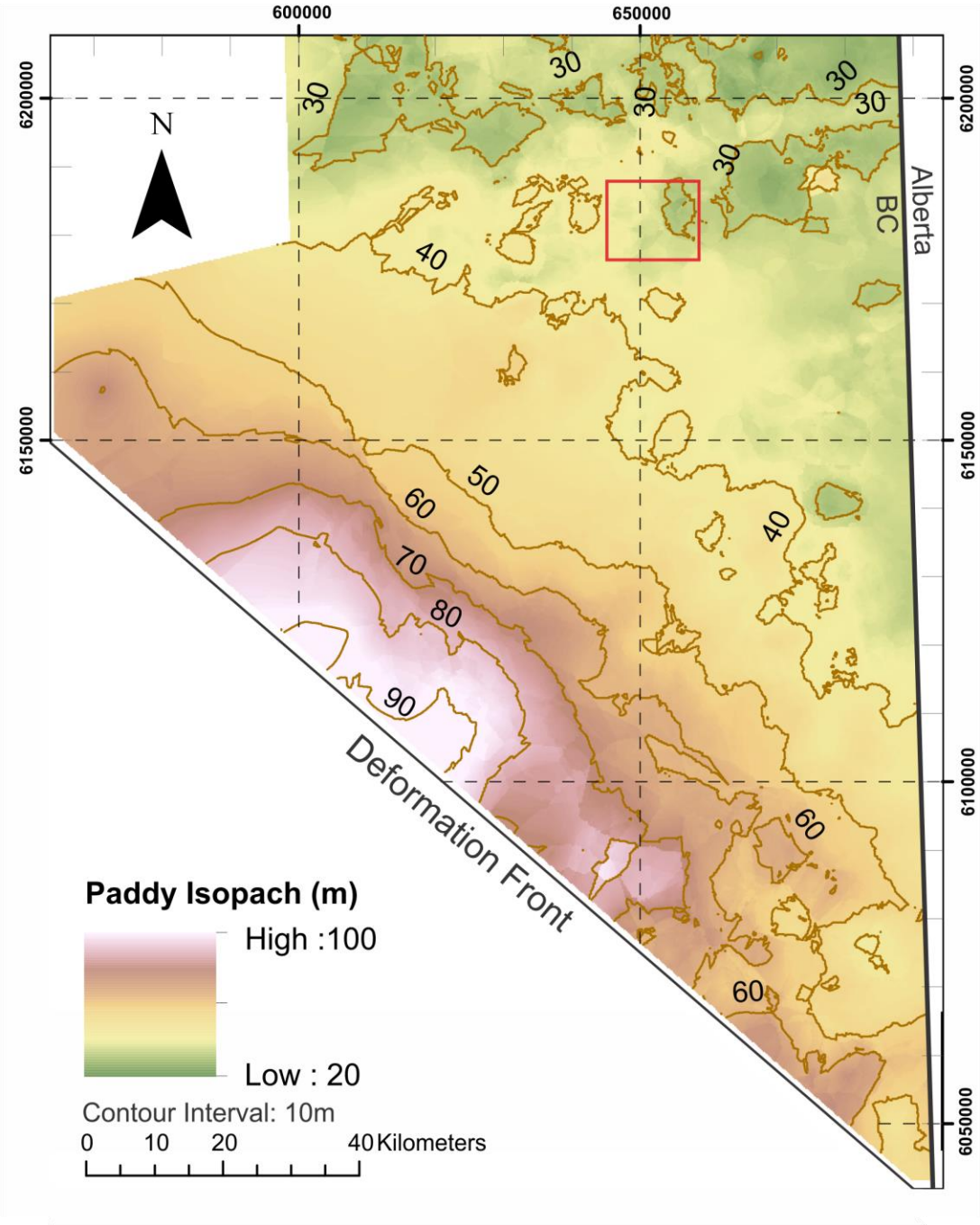

Figure 2.8. **Isopach map of the Paddy unit in NEBC. Red square shows location of wells of study area. Map was created using formation thickness data from Accumap (IHS Energy, 2016; n = 4662, 103 of which are in the study area) that were then kriged in ArcMap using a linear semivariogram model, a nugget of 32, major range of 25000, and partial sill of 38.**

2.2.3. Paddy Sandstone

As noted above, the base of the Paddy represents a subaerial unconformity created during a major retreat of the Harmon/Hulcross Sea (Leckie and Reinson, 1993). Paddy sediments are interpreted to have been deposited in varying environments, ranging from lakes and lagoons to river-dominated deltas (Figure 2.6; Buckley and Plint, 2013). This generated a more diverse range of facies than observed in the Cadotte, resulting in spatial variability of lithologies and making correlation of sub-members difficult. The Paddy is generally dominated by alluvial and lagoonal deposits to the south, nearshore sandstone units across middle latitudes, and marine deposits to the north (Buckley and Plint, 2013). This spatial lithological variability could lead to similar variability in porosity and permeability, making the Paddy more suitable for wastewater injection or water sourcing in some areas than others (see Figure 2.3, WA 26366 and 19319) This unit shows a marked wedge shape, thinning from a maximum thickness of approximately 100 m in the west (near the Rocky Mountains) to less than 30 m in the northeast (Figure 2.7). Plint et al. (2012) interpreted this geometry to be a result of a high degree of flexural subsidence due to tectonic loading in the orogeny to the west.

2.2.4. Shaftesbury Shale

The Shaftesbury shale is a dark marine mudstone that overlies the Paddy and is interpreted to have been deposited during a major transgressive event when the Western Interior Seaway was flooded, connecting the Gulf of Mexico and Arctic Ocean (Williams and Stelck, 1975). This unit is over 400 m thick in NEBC (IHS Energy, 2016) and is host to the Fish Scales Zone, a distinct basin-wide marker of the transition from Lower Cretaceous to Upper Cretaceous bedrock and is identified by its copious fish fossils (Leckie, 1988). In NEBC, this marker is used to help define the depth below which saline wastewater can be disposed (BCOGCb, 2016).

2.3. Hydrogeology

The bulk of the hydrogeological understanding of the Paddy-Cadotte derives from a report by Petrel Robertson and Canadian Discovery (2011) completed for Geoscience BC. Their report characterizes what it refers to as deep aquifers in the area of the Montney play in order to support unconventional gas development.

2.3.1. Regional Groundwater Flow

Formation pressures for the Paddy and Cadotte are publically available through Accumap (IHS Energy, 2016), and were determined using drill stem tests (DSTs). DSTs are used by industry to test the permeability, productive capacity, and pressure of a hydrocarbon reservoir, but can also be used to measure pressure in disposal formations such as the Paddy-Cadotte (Dahlberg, 1994). During a DST, a specialized tool is lowered into the borehole and packers are inflated in order to isolate the formation of interest. A valve in the tool opens and closes in order to allow fluid to flow out of the formation and for pressure to be measured. Pressures measured during a DST can potentially be inaccurate and not representative of formation pressures for a number of different reasons, such as equipment failure during the test, improper analysis of measurements, or lower pressure in the well due to production at other nearby wells.

Petrel Robertson and Canadian Discovery (2011) reviewed available DST data for the Paddy-Cadotte and each test was assigned a quality code ranging from A to G based on the confidence in the accuracy of the measurements, with A being the greatest confidence and G being the lowest. When using these data to interpret the pressure regime within the Paddy-Cadotte, greater emphasis was placed on the high quality data, except when a particular area was data sparse, in which case lower quality data may have been used. These pressures were converted to equivalent freshwater hydraulic head using the equation:

$$h_f = \frac{p}{p_g} + Z \quad (2.2)$$

where:

h_f = equivalent freshwater hydraulic head [m],

p = pressure measured in the DST [kPa],

p_g = freshwater pressure gradient (9.81 kPa/m, assuming freshwater to have a density of 1000 kg/m^3), and

Z = elevation of the pressure recorder [metres above sea level; m.a.s.l.].

Interpreted regional equivalent freshwater head contours are shown on maps for the Paddy and Cadotte on Figure 2.9. It is noted that defining a flow system using solely equivalent freshwater heads can introduce error, as it does not account for variations in pressure, temperature, and salinity and the corresponding potential forces induced by these variations (Bachu, 1995; Bachu and Michael, 2002). Additionally, equivalent freshwater heads can only be used to provide an indication of horizontal groundwater flow, not vertical (Bachu, 1995). To better define regional flow in deep formations, high density of data related to pressure, temperature, and salinity are required. However, these data do not exist in the Paddy-Cadotte in high enough resolution, and so the head contours presented in Figure 2.9 represent the best available representation of flow in the formation, though the potential error of using solely equivalent freshwater heads is acknowledged.

Although there are limitations in the spatial coverage of data points for areas across both maps, similarities are apparent in equivalent freshwater head contours for the Paddy and Cadotte (Figure 2.9). The equivalent freshwater heads towards the southwest reach values of 600 m, and decrease to 300 m in the northeast, resulting in an inferred horizontal groundwater flow direction towards the northeast. In the general location of the study area, equivalent freshwater head is interpreted based on the available data to range from 400 to 500 m, which is equivalent to pressures of between 4000-8000 kPa. Encana (2014) estimated the Darcy velocity in the Cadotte to be ~1 m/year. Based on the interpreted equivalent freshwater head contours, groundwater flow may be directed into a regional corridor that runs east-west near the study area at the upgradient side, extending toward the Alberta border on the downgradient side (Figure 2.9). The flow

corridor also appears to have the smallest hydraulic gradient in both units, and is roughly coincident with a high porosity zone (indicated on Figure 2.9 and discussed below). Petrel Robertson and Canadian Discovery (2011) noted that this area of the Paddy-Cadotte is furthest from the orogen to the west and has undergone less burial diagenesis, preserving reservoir quality and making it a good location for wastewater disposal.

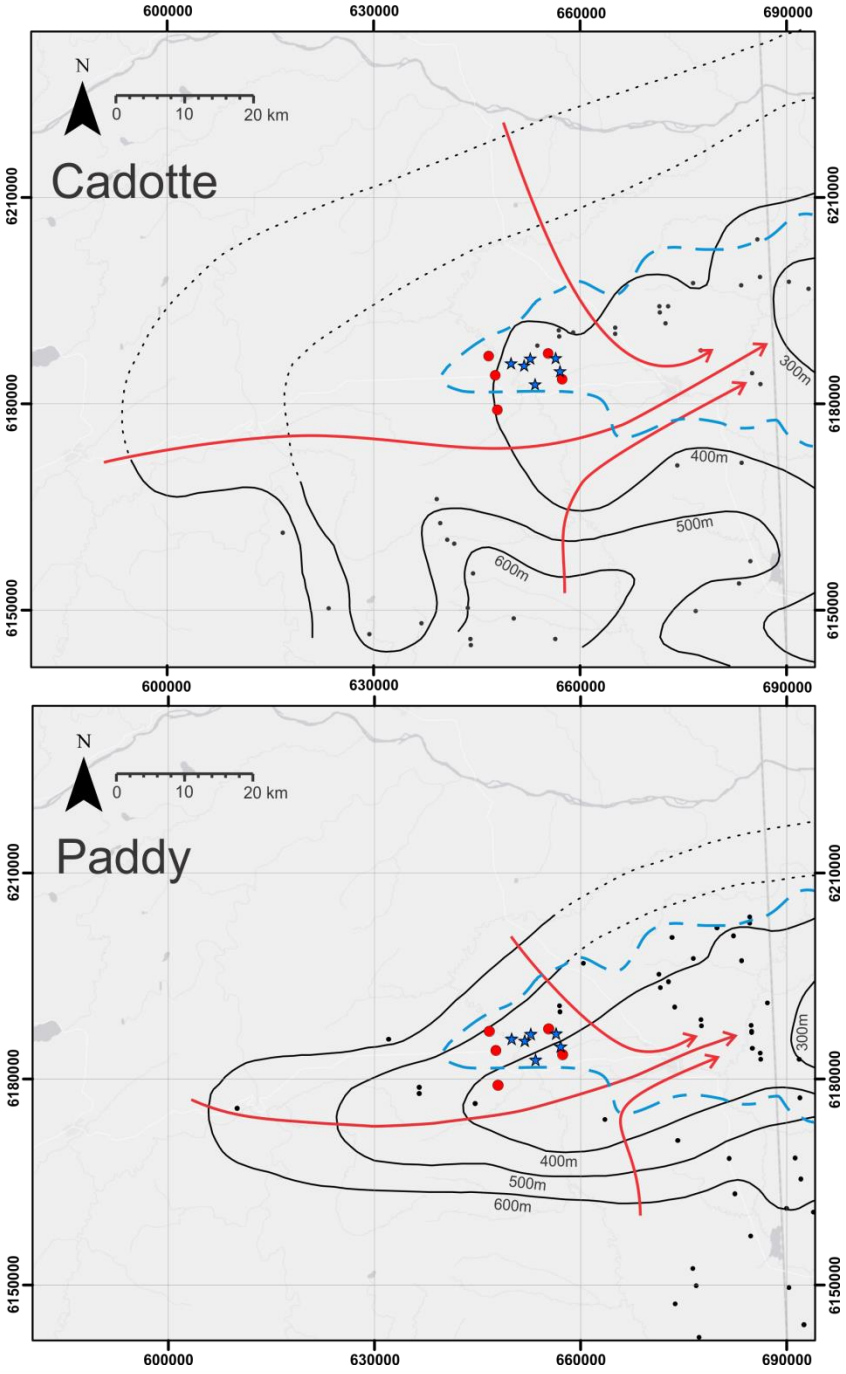

Figure 2.9. **Interpreted equivalent freshwater hydraulic head contours in the Cadotte (above) and Paddy (below) (from Petrel Robertson and Canadian Discovery, 2012). Black dots show locations of available equivalent freshwater head data derived from DSTs, red circles show locations of disposal wells, blue stars show locations of source wells, red arrows show interpreted direction of groundwater flow, and blue dashed lines show the extent of a high porosity zone (see Section 2.3.2). Modified from Petrel Robertson and Canadian Discovery (2011).**

2.3.2. Study Area Hydrostratigraphy

The hydrostratigraphy in the study area is interpreted based on available data from geophysical logs for 385 wells within and around the study area, as well as permeability measurements taken from a single core (WA 00019) located near the study area. Hydrostratigraphy of the Paddy-Cadotte is defined on the basis of variations in porosity identified in the aforementioned geophysical logs and permeability and porosity values are assigned to those units based on measurements taken from the core.

Density porosity logs measure the electron density of a formation by bombarding it with gamma rays (Alberty, 1992). The gamma rays are scattered after colliding with the formation and the number of returning rays is measured by a detector on the logging tool, providing a measure of the bulk formation density. Density can be converted to porosity using:

$$n = \frac{\rho_{ma} - \rho_b}{\rho_{ma} - \rho_f} \quad (2.3)$$

where:

n = porosity [-]
ρ_{ma} = matrix density [g/cm^3]
ρ_b = formation bulk density [g/cm^3]
ρ_f = density of fluid saturating the formation [g/cm^3]

Formation density is measured shortly after the well is completed, and so the fluid saturating the rock is typically mud filtrate. The matrix density is a literature value determined on the basis of lithology. For example, if a density log were completed for a sandstone unit, the matrix density would be 2.65 g/cm^3, whereas in a limestone unit it would be 2.71 g/cm^3. The Paddy-Cadotte is dominantly sandstone, and so the former value is used in Equation 2.3.

Neutron logs are a measure of the hydrogen concentration in a unit (Alberty, 1992), and are obtained by bombarding the formation with neutrons. A detector on the logging tool measures the energy of returning neutrons, which lose energy after colliding with the

formation. The greatest amount of energy is lost when the neutrons collide with hydrogen atoms in water molecules, as the two have similar masses. The energy loss of the returning neutrons can be translated into a measure of the water filled porosity of the formation. Error can be introduced if the formation is not fully saturated or contains gas, both of which can cause porosity to be underestimated. The Paddy-Cadotte is fully saturated and contains no reported gas phase at depth in the area of the disposal and source well field (Petrel Robertson and Canadian Discovery, 2011), and so an underestimation of porosity due to either of these factors is unlikely. As noted in Section 2.1.2, some natural gas is produced at the water source wells. However, this is due to dissolved gas exsolving as the water is depressurised on its way up to the surface.

Neutron and density logs can be used to interpret geology and formation fluid properties. Typically, both logs will show similar values for porosity, but differences between the two can be indicative of gas in the formation and/or a greater amount of shale/clay than otherwise expected (Alberny, 1992). An example of a neutron and density log is shown in Figure 2.10 for disposal well WA 10677 in the study area. The density log (solid line) generally shows good alignment with the neutron log (dashed line), though the neutron log is consistently 3-6% greater in terms of porosity than the density log. This is likely due to a small amount of clay present in the formation, resulting in the matrix density being slightly different than that of pure sandstone (2.65 g/cm^3). When a small amount of variation is present between the neutron and density logs, porosity can be calculated by taking an average of the two (Alberny, 1992).

Three different porosity zones can be identified in Figure 2.10: the Paddy and upper Cadotte, the middle Cadotte, and the lower Cadotte. The Paddy and upper Cadotte show low porosity and a generally jagged line, which transitions into a high porosity zone in the middle Cadotte that has a smoother profile. In the lower Cadotte, the porosity decreases once again and a greater difference can be observed between the neutron and density logs. These porosity zones can roughly be correlated with the allomembers discussed in Section 2.2.2. The lower Cadotte is likely representative of allomember CA, which is known to have a greater amount of shale than the rest of the Cadotte, and is likely the reason for the deviation between the neutron and density logs over this interval. The highest porosity zone, in the middle Cadotte, relates to allomember CB, which is a blockier, more uniform sandstone. It is this portion of the Cadotte that is targeted for wastewater disposal. The green bar in Figure 2.10 shows the length of the

perforated portion of WA 10677, which aligns well with the high porosity zone. High porosity zones are targeted for wastewater disposal because they are also typically of higher permeability, allowing for greater quantities of waste to be injected at a higher rate. The correlation between porosity and permeability[4] is not always consistent (Figure 2.11), but in general a high porosity is typically indicative of a high permeability.

[4] Permeability is measured in core; either full diameter core or plugs. Kmax is the maximum permeability, which is generally aligned with bedding.

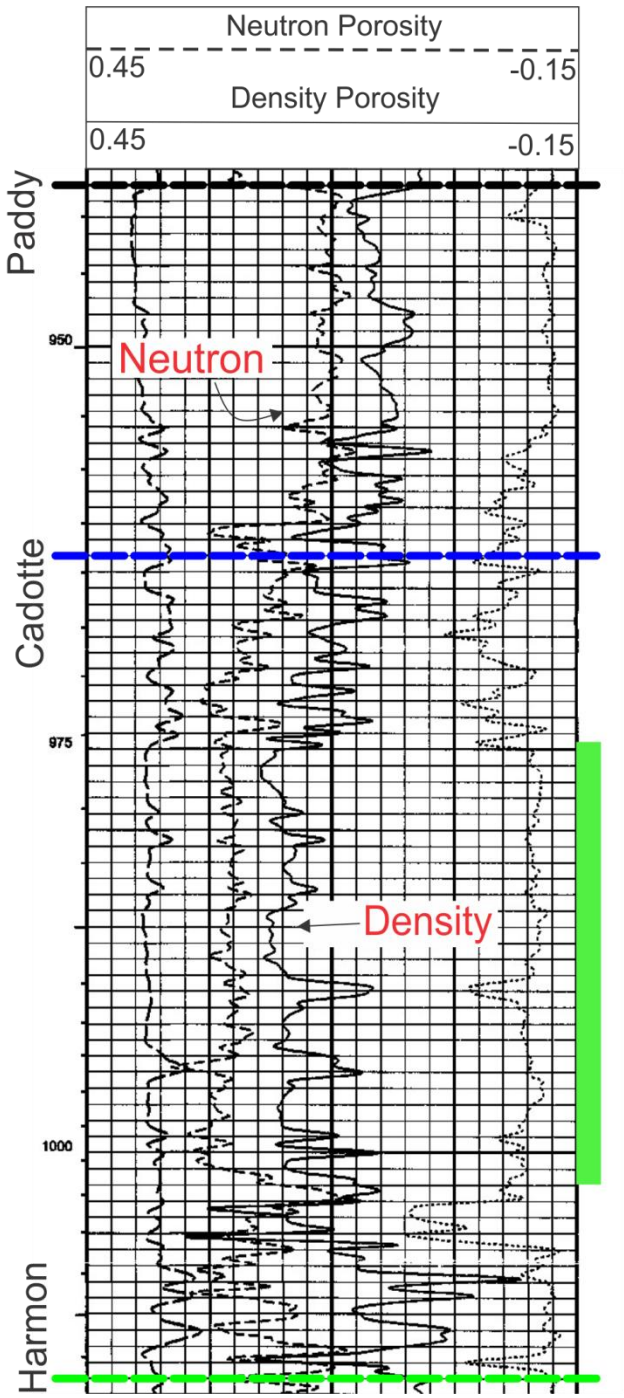

Figure 2.10. **Neutron (dashed line) and density (solid line) logs for WA 10677 in the Paddy-Cadotte (IHS Energy, 2016). Porosity increases from right to left, with each grid square representing an increase of 0.03. The vertical green bar indicates the length of the perforated interval in the well, note how it targets the high porosity zone.**

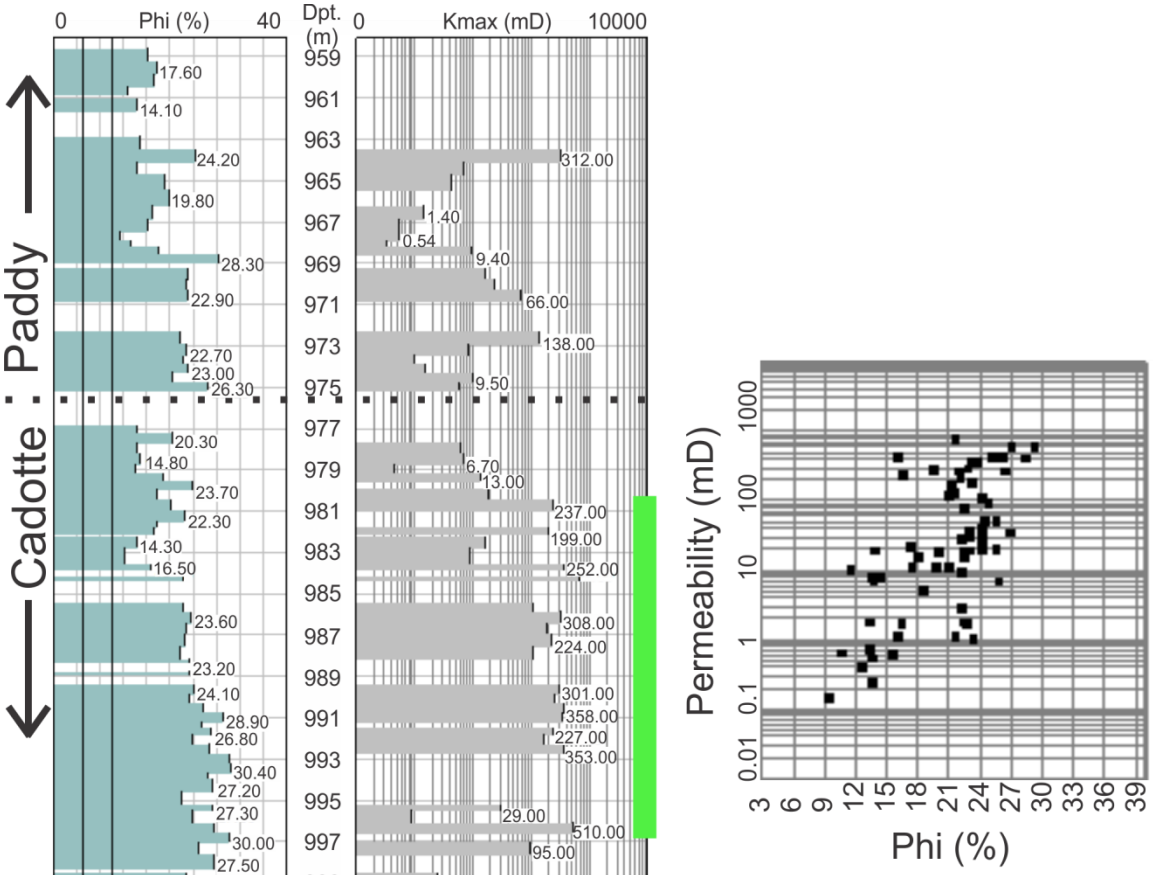

Figure 2.11. Porosity (Phi in %; left) and permeability (as Kmax; middle) values for core from WA 00019 (IHS Energy, 2016), as well as a cross plot of the relationship between the two (right). The green bar indicates the high porosity/permeability zone within the Cadotte.

Determining permeability values for the various porosity zones in the Paddy-Cadotte within the study area is complicated by a lack of core logs and associated permeability/porosity measurements. Core for the Paddy-Cadotte exists to the south and west of the study area, but upon review of the core data it was felt that those core do not reflect the porosity intervals observed in the neutron and density logs from the study area[5], namely the high porosity zone within the Cadotte. This high porosity zone is

[5] Petrel Robertson and Canadian Discovery (2011) argue that, since the Paddy-Cadotte dips to the southwest, reservoir quality is degraded in that direction due to increased burial diagenesis

interpreted to only be present in (and slightly around, see Chapter 4) the area delineated by the dashed blue line in Figure 2.9. A single core log exists for this area, WA 00019, with its associated porosity and permeability measurements shown in Figure 2.11. This log spans the upper half of the Cadotte and lower half of the Paddy, and provides values for permeability that can be related to the porosity zones observed in the neutron and density logs throughout the area. The higher porosity zone targeted for disposal shows porosity values of 20-30% and permeability values of 200-500 mD[6], while the lower porosity zones in the Paddy and lower Cadotte have porosity values of 14-19% and permeability values ranging from 1-100 mD. There is roughly an order of magnitude difference in permeability between the higher and lower permeability zones.

Three hydrostratigraphic units were defined based on the trend observed in the porosity logs (HSUs 1, 2, and 3; Figure 2.12). HSU 1 and 3 have similar porosity and permeability values. HSU 1 represents the Paddy and part of the upper Cadotte (inferred to correlate with allomember CC previously interpreted by Buckley and Plint (2013) as discussed in Section 2.2.2), while HSU 3 represents the lower, more shale-rich portion of the Cadotte (inferred to correlate with allomember CA). HSU 2 is of greater permeability and porosity than HSUs 1 and 3, and is inferred to represent the blocky sandstone portion of the Cadotte, referred to as allomember CB by Buckley and Plint (2013).

reducing the porosity of the formation. The only location in which reservoir quality (i.e. porosity) is relatively high is in the northeast (the location of the disposal/source well cluster), which is represented by the dashed blue line in Figure 2.9.

[6] The Darcy is a measure of the intrinsic permeability of a medium, most commonly used in the oil and gas industry where the presence of multiple fluids (gas, fresh water, brine, etc.) of varying density and viscosity make the use of hydraulic conductivity difficult. 1 Darcy = 9.869×10^{-13} m^2.

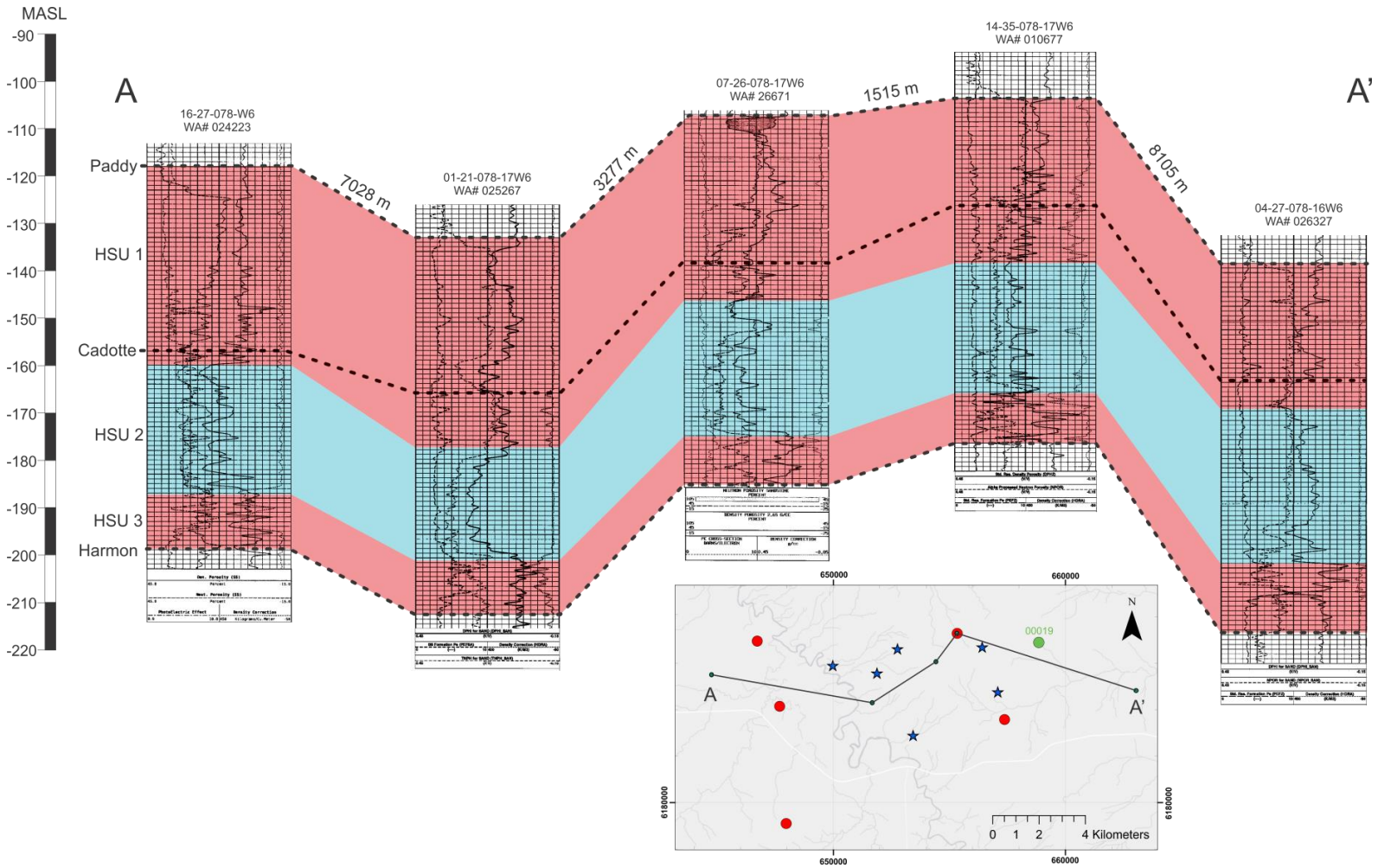

Figure 2.12. Interpreted hydrostratigraphy of the Paddy-Cadotte shown using neutron and density porosity logs from wells aligned W-E across the study area. Green dot shows the location of WA 00019, for which core with permeability measurements are available. Geophysical logs and formation top picks from Accumap (IHS Energy, 2016)

2.3.3. Aqueous Geochemistry

This section discusses the chemistry of the two main fluid types considered in this study: Paddy-Cadotte formation water and wastewater. The dissolved solids present in both of these fluids are simplified to be entirely Na-Cl (for reasons detailed below), making salinity and TDS equivalent in this case. Both terms are used interchangeably throughout this thesis.

Wastewater Chemistry

The wastewater managed by disposal wells in the study area is a mixture of flowback water and produced water. Unfortunately, major data gaps exist concerning the ultimate fate and composition of wastewater, as industry is not required to track and/or provide this information (Goss et al., 2015). The reasoning below is provided to infer the chemistry of disposed wastewater.

Flowback water is hydraulic fracturing fluid that returns to the surface after a well has been completed (i.e., hydraulically fractured). It is dominantly water and sand (99.5% by volume) with minor amounts of chemical additives, such as friction reducers and biocides, that serve to increase the efficiency of the fracturing process (Gregory et al., 2011). On average across Northeast BC, the water used as the base for the fracturing fluid is dominantly sourced from surface water (BCOGC, 2015) and has a very low TDS (essentially fresh water) in comparison to waters typically found in deep geologic formations. The source of water used for hydraulic fracturing fluid, however, can vary locally and may include deep groundwater or recycled produced water (defined below) of higher TDS.

Produced waters are those naturally occurring in hydrocarbon-bearing formations that are extracted along with oil/gas throughout the lifetime of a producing well. The chemistry of these waters varies based on the producing formation. This study only considers produced waters from the Montney Formation, the chemistry of which is discussed below.

The relative proportion of produced water to flowback in wastewater associated with any given well varies over time (Kondash et al., 2017). Immediately after fracturing operations are complete, the wastewater returning to the surface is almost entirely

flowback water (low TDS), and the relative proportion of produced water to flowback water increases over time. As an example, within less than 10 days, the proportion of produced water to flowback may become close to 50/50, and after 100 days the wastewater may be almost entirely representative of formation water (Kondash et al., 2017). Throughout the lifetime of a producing hydraulic fractured well, the total volume of produced water is greater than the total volume of flowback water. Kondash et al. (2017) suggest approximately 5% of the wastewater generated is flowback, while the remaining 95% is produced water.

It is assumed that wastewater requiring disposal is predominantly comprised of produced water. Therefore, the chemical composition of wastewater dominantly reflects the composition of the waters in the formation targeted for hydrocarbon extraction, which in this case is the Montney.

Montney Formation Water Chemistry

Montney Formation water analyses (BCOGC Formation Code 5000) were accessed through the BCOGC online data portal (BCOGC, 2017a). Wastewater is typically not tracked prior to disposal (Alessi et al., 2017), and so could potentially travel long distances if a suitable disposal well is not located close to the gas well from which it was produced. Because of this, the formation water analyses presented here are from the entire Montney Play and are not restricted to wells close to the study area. Potentially inaccurate analyses, due to contamination by drilling fluids or data entry error, were identified and removed using culling criteria from Kirste (2000). Data were eliminated if they:

- Reported a charge balance error of >5%. This indicates that either errors were made when analyzing the sample, or that a major cation or anion was not accounted for.
- Had densities lower than 1 g/cm^3, likely due to contamination by alcohols from the drilling process.
- Reported abnormal ion concentrations due to contamination by other drilling additives. These were identified by plotting major cations and anions against Cl and manually removing any samples that deviated significantly from major identified trends.
- Had TDS values less than 40 g/L, potentially due to dilution by low salinity drilling fluids. A previous analysis of Triassic formation waters in the area, which includes the Montney, Charlie Lake, and Halfway Formations, reported

salinity values ranging from 40 to >200 g/L, and so were used to constrain the lower bound of this culling criterion (Kirste et al., 1997).

Data could also have been culled based on pH, with samples reporting pH greater than 10 or less than 4 being eliminated, but the analyses available did not include this information. Originally, 1240 Montney Formation water analyses were downloaded from the BCOGC data portal, and after culling only 908 remained.

The remaining water analyses ranged in TDS from 40 to ~300 g/L (Figure 2.13), with the mean and median of the sample distribution being ~150 g/L. The chemistry of these samples is presented in a Piper plot (Figure 2.14). Montney waters are shown to be strongly Na-Cl type, though some samples tend towards slightly higher Ca. The samples are dominantly Na-Cl type, and so an assumption that Montney Formation water salinity is entirely due to Na and Cl is made. This simplifies the process of determining wastewater density due to varying salinity, pressure, and temperature (Chapter 3).

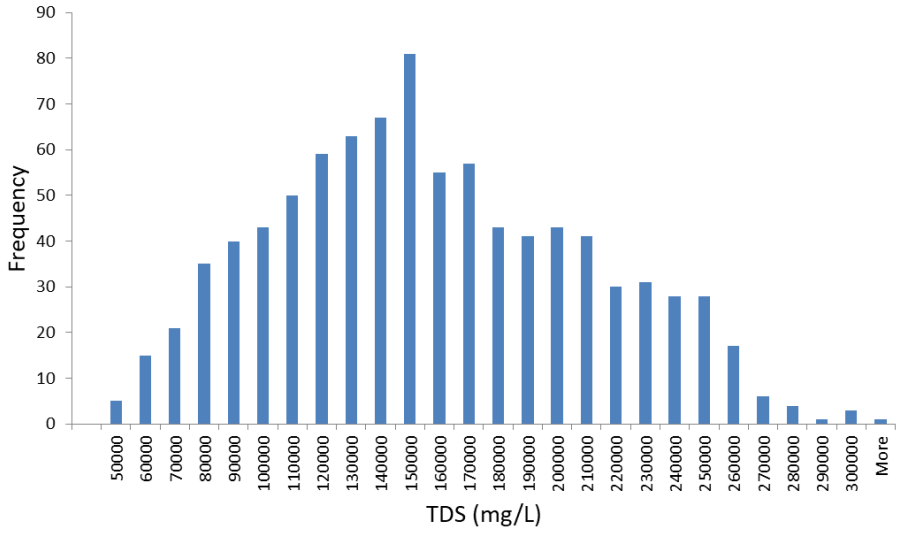

Figure 2.13. Salinity distribution for culled Montney Formation water samples (n = 908) taken from the BCOGC online data portal (BCOGC, 2017a).

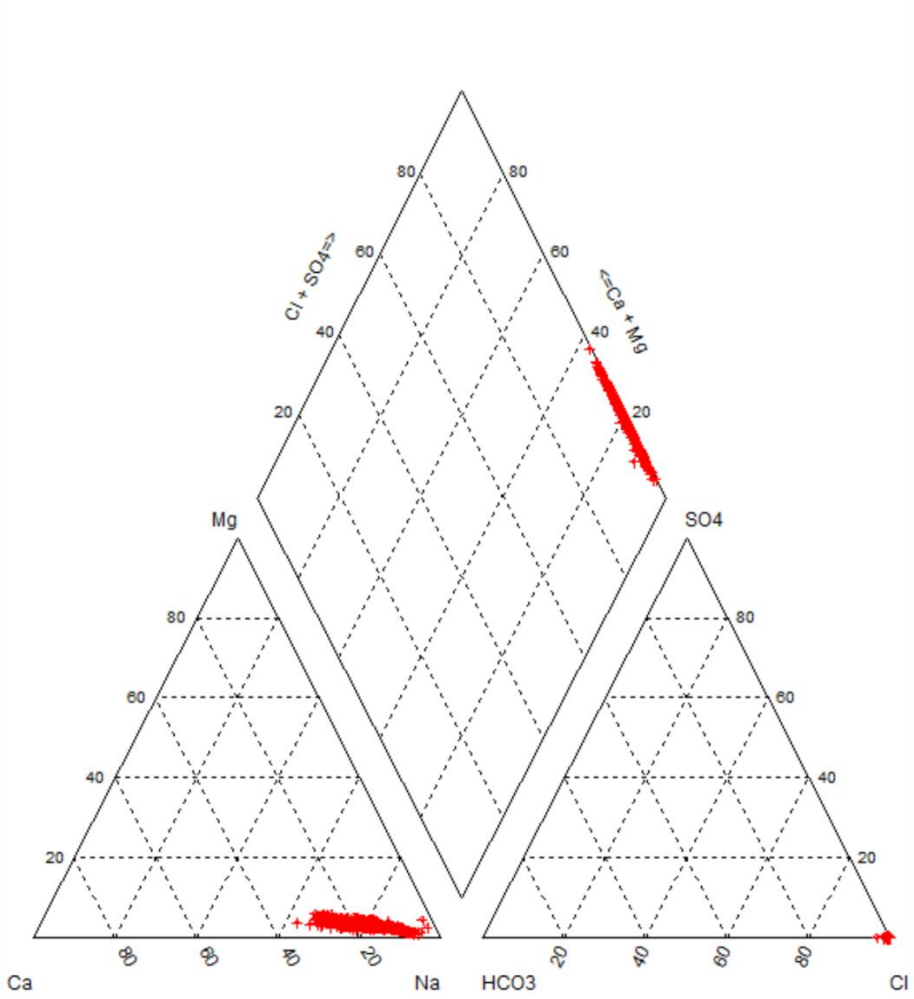

Figure 2.14. Piper plot of Montney Formation water analyses (n = 908) culled from the BCOGC online data portal (BCOGC, 2017a).

While the mean concentration of Montney formation water, and thus produced water according to the inferences presented above, is around 150 g/L, there is potential for this waste to become more concentrated as it is recycled and used to hydraulically fracture new wells (Ron Stefik, personal communication). An analysis of wastewater for disposal by the Encana Corporation (see Appendix C) reveals TDS values of 260 g/L. This wastewater is typically stored on the surface prior to disposal, causing it to equilibrate to ambient air temperature. It will occasionally be heated prior to disposal, but, for the purposes of this study, wastewater temperature is assumed to be 15°C (James Armstrong, personal communication, March 6, 2017). Water temperature and salinity alter the fluid's density and viscosity, potentially affecting its migration in the subsurface during and after injection (see Chapter 3).

Paddy-Cadotte Formation Water Chemistry

The Paddy-Cadotte formation water chemistry has been characterized by Petrel-Robertson and Canadian Discovery (2011) based on 55 vetted formation water samples covering roughly the same area as that shown in Figure 2.9. Figure 2.15 shows a piper plot compiled by Petrel Robertson of the available data and indicates formation waters in the Paddy-Cadotte to be dominantly Na-Cl type, though some samples show greater concentrations of Ca and HCO_3 (Petrel Robertson and Canadian Discovery, 2011).

Encana (2014) also compiled formation water chemistry data for the Paddy-Cadotte (source unknown), producing a salinity map of the formation (Figure 2.16). This map is contoured using 61 irregularly spaced data points resulting in large areas in which contour lines can only be inferred. Based on the interpreted TDS contours, TDS within the Paddy-Cadotte varies spatially, ranging throughout the region from ~40 g/L in the south to <5 g/L near the study area. The study area lies almost entirely within the 6 g/L contour line (though is noted that this line is poorly defined based on only 2 data points), and so is considered to host formation waters with a salinity of 5 g/L.

It is noted that Petrel Robertson and Canadian Discovery (2011) also produced a salinity map of the Paddy-Cadotte, which indicates that salinity in the study area is on the order of 30 g/L (though only one data point is used to constrain this value), and as such, differs from the Encana map. It is felt that Encana's map better represents conditions in the study area as it includes more recent measurements taken from disposal well WA 10677 prior to disposal operations beginning.

The average water temperature within the Paddy-Cadotte is roughly 45°C, based on two estimates: 42°C (personal communication, James Armstrong, Encana Corporation March 6, 2017) and 47°C (Petrel Robertson and Canadian Discovery, 2011).

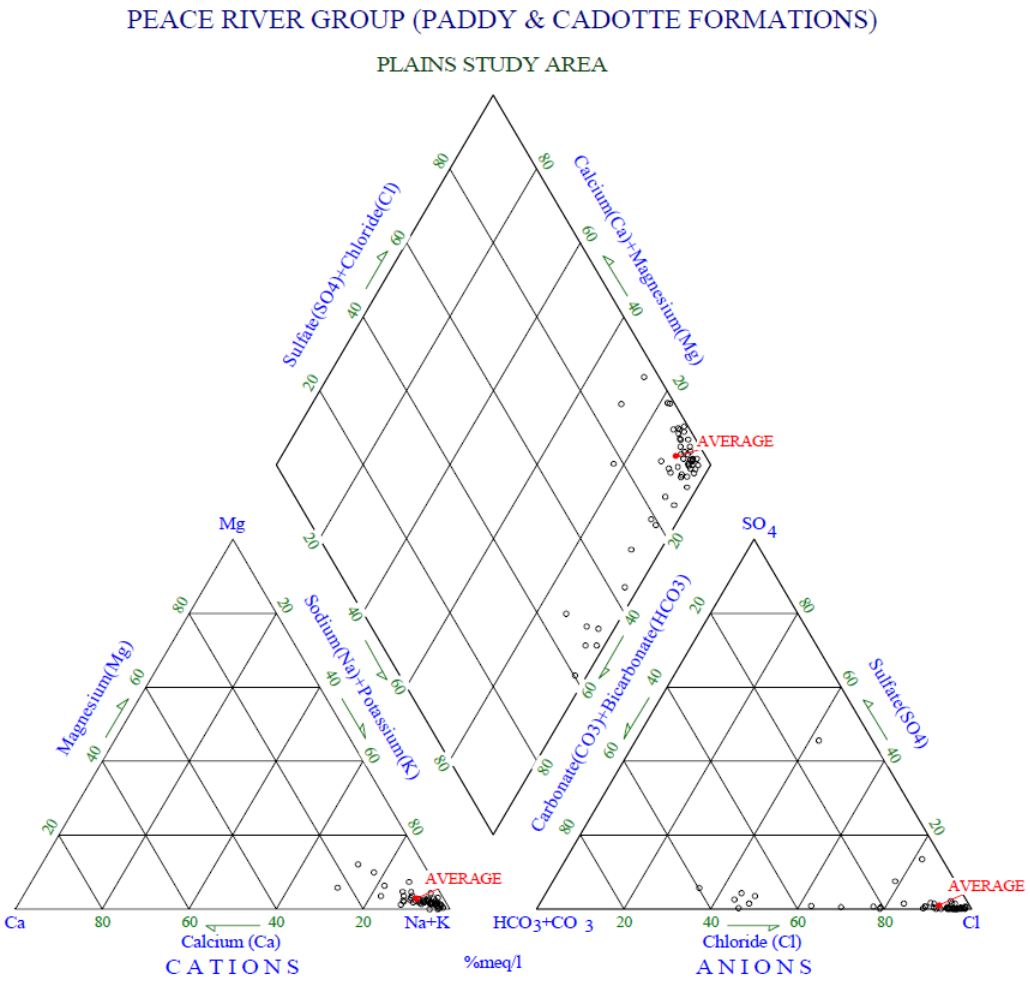

Figure 2.15. Piper plot for 55 formation water samples from throughout the Paddy-Cadotte (Petrel Robertson and Canadian Discovery Limited, 2011).

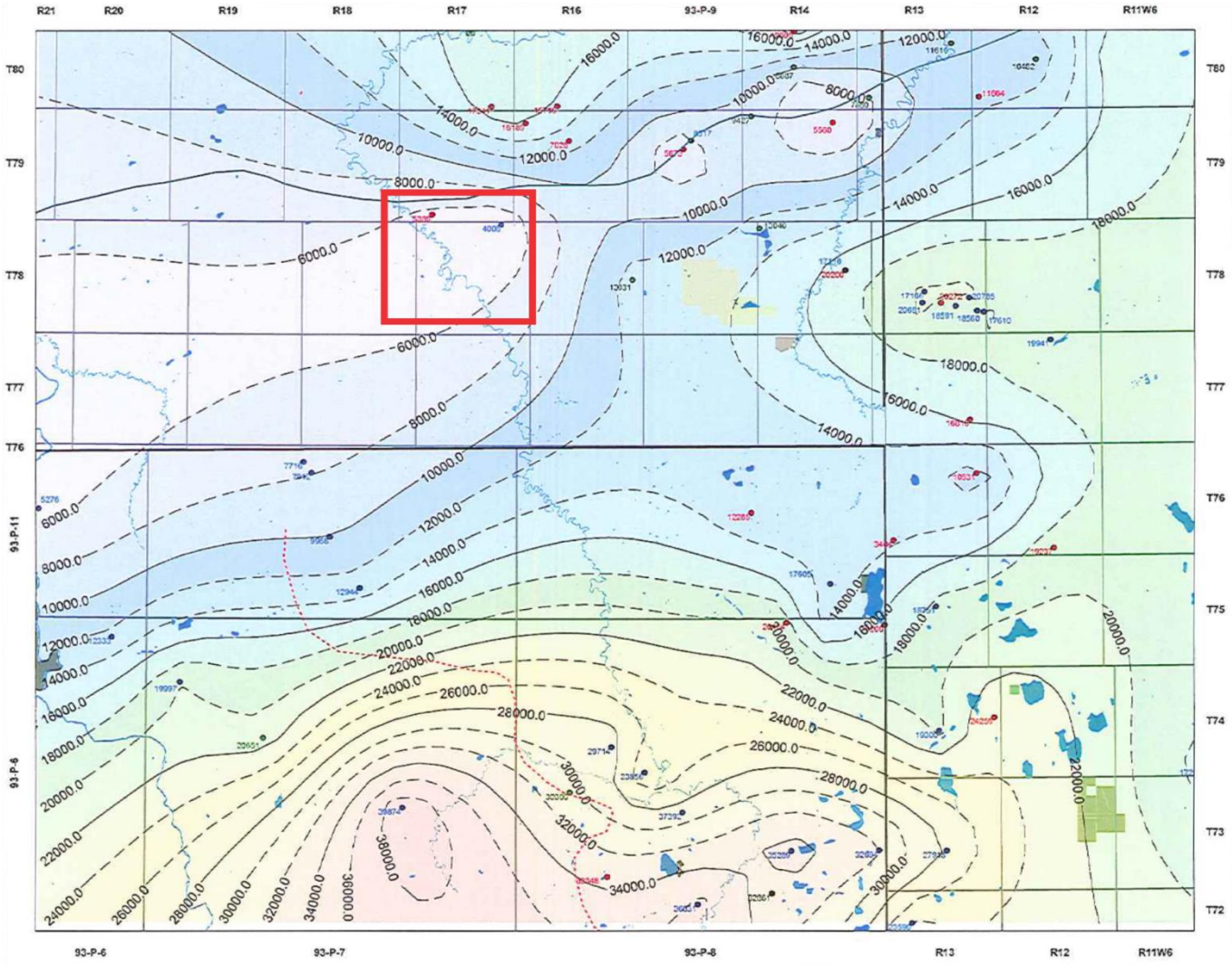

Figure 2.16. Salinity map of the Paddy-Cadotte showing measurements in the Cadotte (blue dots) and in the Paddy (red dots). The red box shows the location of the well cluster. Contour interval is 2,000 mg/L (Encana, 2014).

2.4. Summary

This chapter described the regional hydrogeological setting and the hydrogeological information for the study area in order to better parameterize the numerical models for the sensitivity analysis (Chapter 3) and the multi-well investigation (Chapter 4). Data for the Paddy-Cadotte are sparse (e.g., permeability values are derived from a single core log), or else are variably spaced (e.g., water samples or DST pressures are limited to locations at which hydrocarbon wells have been drilled). Based on the information detailed in previous sections, a summary of the representative formation and fluid parameters are presented in Table 2.4.

Table 2.4. Modeling parameter values established for the Paddy-Cadotte (P-C) disposal formation, wastewater chemistry, and P-C formation water chemistry.

Parameter	Value/Range	Parameter	Value/Range
Formation Properties		*Wastewater Properties*	
Permeability of HSU 1 and 3 (mD)	1 - 100	Temperature (°C)	15
Porosity of HSU 1 and 3 (%)	14 – 19	Salinity (g/L)	40 - 300
Permeability of HSU 2 (mD)	200 - 500	*P-C Formation Water Properties*	
Porosity of HSU 2 (%)	20 - 30	Temperature (°C)	45
		Salinity (g/L)	5 - 40

The Paddy-Cadotte is targeted for both wastewater disposal (five wells) and source water extraction (six wells), with operations having begun less than five years ago. The disposal formation can be divided into 3 hydrostratigraphic units (HSUs) which are stacked on top of one another. The HSUs were first determined based on neutron and density porosity logs for 5 wells located across the study area (WA 24223, 25267, 26671, 10677, 26327) and limited core data from one well (WA 00019 drilled in 1951) available for the study area. The upper and lower HSUs (HSU 1 and HSU 3) are of relatively low permeability and porosity (roughly 1-100 mD and 14-19%) in comparison to HSU 2 (200-500 mD and 20-30%). HSU 2 is the primary target of the disposal wells and source wells in the Paddy-Cadotte. Based on an analysis of 385 neutron and density porosity logs (discussed in greater detail in Chapter 4), HSU 1 and 3 are considered continuous throughout the Paddy-Cadotte, but HSU 2 is observed to pinch out to the north, west, and south of the study area.

Two types of water need to be considered for modeling: wastewater that is disposed and Paddy-Cadotte formation water. For the purposes of the modeling, which involves simulations of density-dependent groundwater flow (see Chapter 3), the temperature and salinity of these fluids are characterized. The wastewater injected into the disposal formation is assumed to represent formation water from the Montney produced during the extraction of hydrocarbons, which, based on available data discussed in Section 2.3.3., was determined to range in salinity from 40-300 g/L, with the dominant ions comprising this salinity being Na and Cl. The temperature of the disposed wastewater is defined as 15°C due to being kept in storage tanks on the surface prior to disposal. The formation waters of the Paddy-Cadotte range in salinity from 5-40 g/L with Na and Cl being the dominant ions in solution. The salinity of the formation water near the disposal wells is towards the low end of this range (5 g/L). The temperature of this formation water is defined as 45°C.

Chapter 3.

Single Well Simulations of Wastewater Disposal

To understand the structure and evolution of dense wastewater plumes, a series of generic box models were constructed in which wastewater disposal was simulated for differing model parameterizations. The high salinity of this wastewater imparts a greater density than for freshwater, which is further influenced by variations in temperature and pressure. Situations in which large density differences are present (e.g. when saline wastewater is injected into a formation host to less saline water) necessitate the use of a specialized modeling code that is capable of solving density-dependent flow and solute transport. The program selected for this research is the finite-element code FEFLOW v.7.0 (Diersch, 2005a).

Modeling density-dependent flow and transport is complex, requiring time-intensive computer codes to arrive at a solution. This is because the solution for groundwater flow depends on fluid density, which in turn depends on solute concentration and temperature. Solution of the solute and heat transport equations integrates the groundwater velocity, which depends on the hydraulic head distribution generated by solving the groundwater flow equation. Both parts of the problem depend on information from the other in order to arrive at a solution; the problem is “two-way coupled” (Zheng and Bennett, 2002) and must be solved iteratively.

In the first part of this chapter, I identify the equations solved in FEFLOW relevant to the single well and study area density dependent flow models introduced above. In the second part, I discuss the design, construction, simulation, and results of the single well Base Case model approximating simplified disposal conditions in the Paddy-Cadotte. A sensitivity analysis is performed on the Base Case in order to ascertain the influence of various formation and fluid characteristics on the overall structure and extent of a wastewater plume created by a disposal well.

3.1. Using FEFLOW for Density-Dependent Flow Modeling

This section presents the equations used in FEFLOW to solve the density dependent groundwater flow models developed for this thesis. The major balance equations for

groundwater flow, heat transport, and mass transport solved by FEFLOW, along with the relevant equation of state for density and the density settings, are summarized from Diersch and Kolditz (1996). Additional constitutive equations that serve to complete the equations below are excluded from this thesis, but are described in detail in Diersch and Kolditz (1996) and Diersch and Kolditz (2002).

3.1.1. Governing Equations

To solve for the density dependent groundwater flow regime, FEFLOW solves the groundwater flow equation (Equation 3.1):

$$S_s \frac{\partial h}{\partial t} + \frac{\partial q_i}{\partial x_i} = Q \tag{3.1}$$

where:

S_s = specific storage coefficient
h = hydraulic head
t = time
q = Darcy flux
Q = fluid source/sink

in which the Darcy flux, q_i is written as:

$$q_i = -K_{ij} f_\mu \left(\frac{\partial h}{\partial x_j} + \frac{\rho - \rho_0}{\rho_0} e_j\right) \tag{3.2}$$

where:

q = Darcy flux
K_{ij} = tensor of hydraulic conductivity
f_μ = constitutive viscosity relation function
ρ, ρ_0 = fluid density, reference fluid density
e_j = components of the gravitational unit vector
h = hydraulic head

t = time

These equations can also be written in terms of pressure-permeability instead of hydraulic-head-conductivity (Zheng and Bennett, 2002), though FEFLOW employs the latter. However, hydraulic head can be easily converted to pressure using Equation 2.2, and this thesis uses whichever of these two terms is most appropriate given the context of the discussion. For example, when discussing regional flow in the Paddy-Cadotte, hydraulic head is a more appropriate metric than pressure as it is more intuitive to interpret in regards to the direction of groundwater flow. When discussing disposal conditions, pressure is more appropriate than hydraulic head, since it is the term used in BCOGC regulations.

The models presented in this thesis involve the transport of both mass and heat, and so require additional equations that work in conjunction with the groundwater flow equation (Equation 3.1) to describe their distribution throughout the model. These two variables have the potential to impact the density of water in the models, and so are considered coupled and must be solved iteratively (see Numerical Approach, below). In addition to the groundwater flow equation, FEFLOW solves the mass transport (Equations 3.3 and 3.4) and heat transport (Equation 3.5) equations. Two different forms of the mass transport equations are presented: convective (Equation 3.3) and divergent (Equation 3.4). Both forms are equivalent within the model domain, but have different effects concerning boundary conditions (Diersch, 2005b), i.e. when mass and/or heat are entering or leaving the model. This includes when mass is being injected into the model via a simulated disposal well, and is discussed further in Section 3.2.1.

$$\frac{\partial}{\partial t}(RC) + \frac{\partial}{\partial x_i}\left(q_i C - D_{ij}\frac{\partial C}{\partial x_j}\right) + R\theta C = Q_C \qquad (3.3)$$

where:

R = retardation factor
C = concentration
q = Darcy flux
D_{ij} = tensor of hydrodynamic dispersion
θ = chemical decay rate

Q_C = mass source/sink

$$R_d \frac{\partial C}{\partial t} + q_i \frac{\partial C}{\partial x_i} - \frac{\partial}{\partial x_i}\left(D_{ij} \frac{\partial C}{\partial x_j}\right) + (R\theta + Q)C = Q_C \quad (3.4)$$

where:

R = time derivative of the retardation factor

t = time

C = concentration

q = Darcy flux

D_{ij} = tensor of hydrodynamic dispersion

θ = chemical decay rate

Q = fluid source/sink

Q_C = mass source/sink

$$\left[n\rho c^f + (1-n)\rho^s c^s\right]\frac{\partial T}{\partial t} + \rho c^f q_i \frac{\partial T}{\partial x_i} - \frac{\partial}{\partial x_i}\left(\lambda_{ij} \frac{\partial T}{\partial x_j}\right) = Q_T \quad (3.5)$$

where:

n = porosity

ρ, ρ^s = fluid and solid density, respectively

c^f, c^s = specific heat capacity of fluid and solid phases, respectively

T = temperature

t = time

q = Darcy flux

λ_{ij} = tensor of hydrodynamic thermodispersion

Q_T = heat source/sink

3.1.2. Density-Related Equations

Equation of State for Density and Viscosity

Fluid density is a function of temperature, salinity, and pressure, and in a density-dependent groundwater model, density is not constant. FEFLOW calculates fluid density throughout the model using an equation of state that relates temperature, salinity, and pressure (Diersch and Kolditz, 2002). Assuming a single species is present, it can be linearly approximated in relation to a reference fluid (see Reference Fluid below) as:

$$\rho = \rho_0[1 + \beta(p - p_0) + \alpha(C - C_0) - T_E(T - T_0)] \quad (3.6)$$

where:

ρ, ρ_0 = fluid and reference fluid density, respectively
β = fluid compressibility
p, p_0 = pressure and reference pressure, respectively
α = solutal expansion coefficient
C, C_0 = concentration and reference concentration, respectively
T_E = thermal expansion coefficient
T, T_0 = temperature and reference temperature, respectively

in which the values for fluid compressibility (β) and solutal expansion coefficient (α) are typically treated as constants.

It is noted that in situations where large temperature differences are present, the thermal expansion coefficient (T_E) can undergo significant variation (Marsily, 1981), becoming a function of temperature that is expressed as a 6th order polynomial (Perrochet and Tacher, 1997). The literature is unclear as to what is deemed a significant temperature difference (this was referenced as a personal communication between Diersch and Kolditz and Perrochet), but it is felt that the temperature differences simulated in this thesis (30°C) can likely be considered significant, and so the thermal expansion coefficient is modelled as the polynomial described by Perrochet and Tacher (1997).

The length of the equation for calculating fluid viscosity precludes its inclusion in this text (see Diersch and Kolditz (1998) for the full equation), but is a function of temperature

and salinity similar to that for density. An increase in fluid viscosity can result from an increase in salinity, a decrease in temperature, or a combination of the two.

Hydraulic Conductivity

Hydraulic conductivity is dependent on both density and viscosity which vary as a function of temperature and salinity (and, in the case of density, pressure). Hydraulic conductivity (K) is expressed as:

$$K = \left(\frac{\rho g}{\mu}\right) k_i \tag{3.7}$$

where:

ρ = fluid density
g = gravitational acceleration
μ = fluid viscosity
k_i = intrinsic permeability[7]

k_i is a property of the porous medium, while the bracketed term, the extrinsic permeability, is a property of the fluid. In density-dependent models, the hydraulic conductivity of a given porous medium will change depending on the density and viscosity of the fluid passing through it. For this reason, hydraulic conductivity in FEFLOW is assigned based on the properties of a user-defined reference fluid (see below).

Reference Fluid

In FEFLOW, the user specifies properties of a reference fluid (density, viscosity, salinity, temperature), which are then incorporated into Equations 3.2 and 3.6. The default values for the reference fluid are those of freshwater (0 g/L salinity) at 10°C with a density of 999.8 kg/m^3, but can be modified to suit the needs of the model. The initial K for a particular model element is based on the density and viscosity of the reference fluid. Throughout the simulation, K is adjusted according to the properties of the fluid passing

[7] Intrinsic permeability is commonly expressed in the oil and gas industry using the unit of a Darcy, with one Darcy being equivalent to 9.869 x10^{-13} m^2.

through the element at a given time step. The density of this fluid is calculated using Equation 3.6, while viscosity is calculated as a function of salinity and temperature (Diersch, 2002).

Equivalent Freshwater Head

Hydraulic head is related to solute concentration through the $\mathrm{p_g}$ variable in Equation 2.2, which is equivalent to fluid density multiplied by the acceleration of gravity. In a model with water of varying density, it is necessary to normalize head in order to properly understand the direction of groundwater flow (Post et al., 2007), which FEFLOW does using the density of the reference fluid. Most commonly, the reference fluid represents freshwater, and so FEFLOW translates pressure throughout the model into equivalent freshwater head (see Equation 2.2).

Density Difference Ratio

The density difference ratio ($\bar{\alpha}$) relates concentration differences throughout the model to appropriate densities and is defined as:

$$\bar{\alpha} = \frac{\rho_C - \rho_0}{\rho_o} \tag{3.8}$$

where ρ_0 is the density of the reference fluid and ρ_C is the density of the fluid at a user-defined salinity. These densities must be calculated at the reference temperature ($\mathrm{T_0}$). In assigning a value to the density difference ratio over the model domain, density dependency of the fluid due to solute concentration is activated according to the magnitude of the assigned value. If mass transport is active in the model but no value is assigned for the density difference ratio it is assumed that solute concentration has no influence on fluid density. This can be useful when solute is present at such low concentration that its contribution to fluid density can be ignored, or if the solute is being used as a tracer.

Boussinesq Approximation

The Oberbeck-Boussinesq approximation often referred to as the Boussinesq approximation, serves to simplify the mass, momentum, and energy conservation equations (not presented in this thesis) solved in FEFLOW (Diersch and Kolditz, 2002). Using this approximation, density related effects can be ignored except when they are

related to buoyancy, i.e. when gravity is considered. This approximation is not appropriate to use when significant density differences occur, such as in the presence of large temperature or salinity gradients (Bear, 1972). Evans and Raffensperger (1992) found that using the Boussinesq approximation under such conditions could lead to errors of up to 10% in terms of calculated flow field, though this was after 600 years of simulation time. As described below, the Boussinesq approximation was invoked for the simulations described in this chapter (see Section 3.2.1), but all simulations were run for much less time than the 600 years in the Evans and Raffensperger (1992) study, and so it was felt that any potential error introduced by this approximation was minor even though large concentration differences are present in many of the simulations.

3.1.3. Numerical Modeling Approach

In finite element models, the domain is divided into a number of elements with nodes located at each vertex (Anderson et al., 2015). Solutions for the primary variables (head, solute concentration, and heat) are obtained at each node and interpolation functions (also called 'basis functions') are used to obtain values for these variables within each element. In this manner, solutions are considered piecewise continuous, as opposed to piecewise discontinuous in the case of finite difference models, where solutions are obtained for the primary variables at nodes (located either in the center of a cell or on the corners, depending on the code) and then applied as a constant value to the entirety of the cell in which the node is located (Anderson et al., 2015). Finite element models are typically more mathematically complex than finite difference models, but provide a greater degree of versatility in terms of mesh discretization (Zheng and Bennett, 2002). This versatility is less important for the models presented in this chapter, all of which have rectangular domains with relatively simple features, but becomes more important for the study area model presented in Chapter 4, which includes more complicated topography and disposal and source well distribution. The models presented in this thesis are all transient, as they are designed to simulate the evolution and migration of a wastewater plume over time, though the study area model presented in Chapter 4 is initially calibrated to steady-state conditions and then converted to a transient model in which disposal and source well activities are simulated.

In density-dependent simulations, where a solution for hydraulic head is dependent on fluid density (and thus heat and mass transport), and the distribution of heat and mass

throughout the model is dependent on the hydraulic head distribution, the equations for groundwater flow (Equation 3.1), mass (Equation 3.3 or 3.4), and heat (Equation 3.5) must be solved iteratively as a coupled set (Zheng and Bennett, 2002). For a given time step, the groundwater flow equation is solved first using an assumed density distribution in order to produce an initial solution for head. The groundwater flux field obtained from this solution is then used to solve for heat and mass transport, producing a new density distribution throughout the model, which is then used as input for the groundwater flow equation again. This process is repeated until both sets of equations converge below a user-specified residual error, at which time the simulation will move to the next time step.

In more complicated groundwater flow models, such as those in which density-dependent flow is a major component, it can be difficult to design a time step schedule that allows for an accurate result to be produced. FEFLOW provides the option of using an automatic time step control, which increases or decreases the length of time steps throughout the simulation based on error estimates (Diersch, 2013; Diersch and Kolditz, 1998). The user can specify the maximum allowable length of a time step, preventing it from becoming too large, as well as specific times at which a time step should be performed.

3.2. Generic Single-Well Simulations - Base Case Model

A box model representing disposal conditions for a single well in the Paddy-Cadotte was used to investigate the evolution of a dense wastewater plume. The model presented below is the Base Case, which serves as the standard to which other cases in the subsequent sensitivity analysis are compared (Section 3.3). This section also establishes some of the metrics used to quantify wastewater disposal that are used in the sensitivity analysis.

The Base Case was parameterized to approximate disposal conditions for a single disposal well in the Paddy-Cadotte. In instances where a range of values was possible for a given parameter (e.g. formation permeability, wastewater salinity, etc.), a value within the range that was considered to be most representative of disposal or (hydro)geological conditions was chosen and the full range of values was investigated in the sensitivity analysis. The model simplifies conditions in the disposal formation and the model domain is limited in vertical extent to the main disposal horizon, HSU 2 (see

Chapter 2). The bounding, lower permeability, hydrostratigraphic units are considered impermeable in the Base Case, though are included in a separate simulation as part of the sensitivity analysis to observe the effect of including them (Section 3.2.3).

3.2.1. Model Design and Parameterization

The model domain is represented by a simple box model approximating a saturated cross section through the disposal horizon (HSU 2) in the Paddy-Cadotte. An axisymmetric projection (Figure 3.1) was chosen for this model as it has been shown to greatly reduce the computation time relative to an equivalent, full 3D model (Langevin 2008). A limitation of this projection type is that conditions are assumed to be radially symmetric around the disposal well, meaning that a hydraulic gradient, variations in permeability, sloping topography, and other nearby wells cannot be simulated. These factors are investigated in a study area model of the Paddy-Cadotte (Chapter 4).

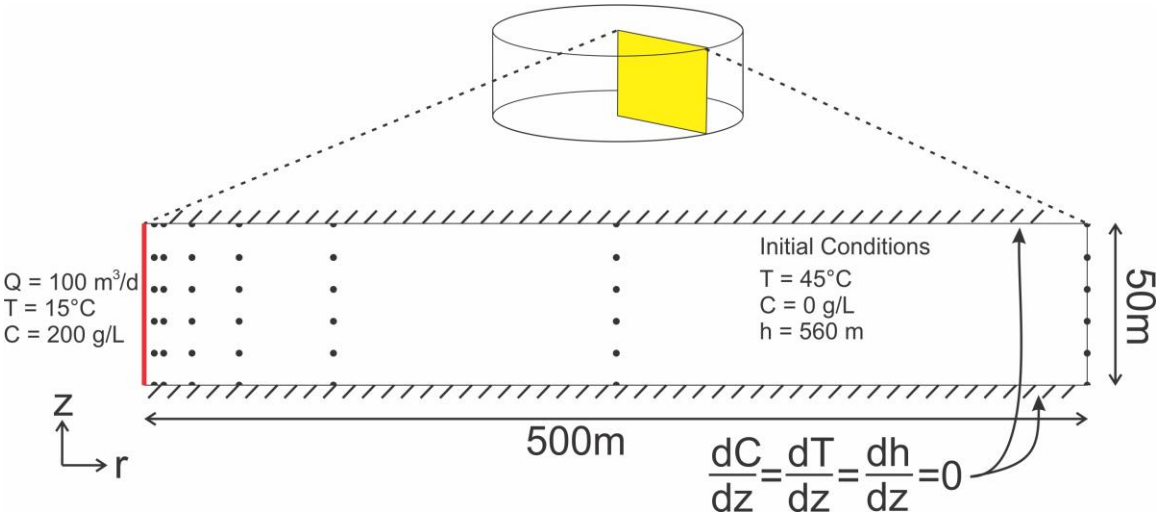

Figure 3.1. Axisymmetric projection showing a zoomed view of the model domain (yellow slice) as well as select parameters and initial and boundary conditions. The disposal well is simulated on the left boundary of the domain (red line). Dots show locations of specified observation points. Vertical exaggeration is 1.7x.

The model domain was 500 m in the radial direction and 50 m in the vertical direction, with a total of 159,809 mesh elements. In order to guide discretization of the domain, observation points were placed throughout the model (as seen in Figure 3.1) and a line segment was drawn along the leftmost boundary. FEFLOW's built-in meshing algorithm, under the 'Triangle' setting, recognizes these point and line features and discretizes the

domain according to their locations, allowing for finer resolution in areas of interest. The left side of the model represents the disposal well, and so greater detail was desired in that location. A finer mesh discretization was used around the observation points to obtain precise locations for output of pressure, temperature, and concentration. Element sizes around the observation points and disposal well are on the order of 0.1-0.2 m, and on the order of 1.0-1.5 m in the coarsest parts of the model. Mesh discretization is too fine to display in Figure 3.1.

Initial Conditions

The model domain was assigned uniform initial temperature and salinity values of 45°C and 0 g/L, respectively, approximating conditions in the disposal formation (discussed in Chapter 2). The value of 0 g/L for salinity is slightly outside the range of salinity observed in the Paddy-Cadotte (5-40 g/L), but serves as a good baseline against which to compare other cases. Ultimately, it is the density difference between fluid types that is important that is important, which is investigated in the sensitivity analysis.

Pressures measured by DSTs in the Paddy and Cadotte around the disposal and source wells ranged from 4000-8000 kPa, and so a value of 5000 kPa was selected to represent the disposal formation. In the default coordinate system of the model, this is equivalent to assigning a uniform hydraulic head value of 560 m to the model domain. The pressure within the model increases with depth according to the hydrostatic gradient of freshwater (9.8 kPa/m), resulting in greater pressures at the bottom of the model (~5500 kPa) in comparison to the top (5000 kPa).

Boundary Conditions

The top and bottom of the model domain represent the low permeability Harmon and Shaftesbury shales that restrict disposed wastewater to the disposal formation. These edges were assigned specified flux boundaries of $\frac{\partial h}{\partial z} = 0$, i.e. a no flow boundary (Figure 3.1). The entire left side of the model represents the disposal well, which was simulated using FEFLOW's well boundary condition. An injection rate of 100 m^3/day was desired for the Base Case, which necessitated dividing this value by the number of nodes along the left edge of the model (259 nodes), and then further dividing it by 2π (to account for the axisymmetric projection types). With the well boundary condition, FEFLOW recognizes negative values as a source of water, and so the final value

applied to each node along the left side of the model was -0.0615 m^3/day. The right side of the model was assigned a head-dependent (aka fluid-transfer or Cauchy) boundary condition with a reference head value of 560 m (the same as the initial head value throughout the rest of the domain). This boundary condition can be used to simulate the presence of a constant head boundary (the reference head value) at some distance from the model edge without requiring a large model domain, potentially leading to shorter run times. The elements along this boundary were assigned out-transfer rates of 9.87×10^{-10} s^{-1}, which is calculated by dividing the mean hydraulic conductivity of the formation in the interval between the edge of the model domain and the distance of the reference head by the distance of the reference head from the model boundary. In this case, the hydraulic conductivity was assumed to be 1.48×10^{-6} m/s (discussed below) and the reference head was assumed to be 1.5 km from the edge of the model. The flux of water through this boundary is controlled by the head in the elements adjacent to it. If head in these elements is higher than the reference head (560 m), then water will flow out of the model at a rate that is proportional to the difference in heads and the out-transfer rate in the elements along the boundary. The effect of this boundary is investigated in the sensitivity analysis.

Specified concentration and temperature boundary conditions of 200 g/L and 15°C were applied to all nodes along the left edge of the model, simulating the injection of cool, saline wastewater. Specified heat and mass boundary conditions were applied only to the edge representing the disposal well. The top and bottom of the model were considered impermeable to heat and mass transport, despite the potential presence of thermal and solute gradients across these boundaries. The right edge of the model did not require specified boundaries, as mass and heat are carried out of the model domain according to the head-dependent flow boundary previously discussed.

Fluid Properties

The injected wastewater simulated in the Base Case model has a temperature of 15°C and a salinity of 200 g/L. The chemical composition of this wastewater is assumed to be entirely Na and Cl. This allows for a molecular diffusion coefficient of 1.99×10^{-9} m^2/s to be used (Haynes, 2014). The density of this fluid at the reference temperature and pressure was calculated using a tool from Driesner and Heinrich (2007), and found to be 1126.1 kg/m^3. Using Equation 3.8, a density difference ratio of 0.126 was calculated and

applied to the model domain. Both the volumetric heat capacity (c) and thermal conductivity (λ) of the modeled fluids were kept as the FEFLOW default values for freshwater of 4.2×10^6 J/m^3/K and 0.65 J/m/s/K. Chloride is a conservative ion, and so solute sorption and retardation are assumed to be negligible. Any potential sorption and retardation of sodium is ignored.

Formation Properties

As mentioned in Section 3.1.2, FEFLOW compares solute concentration and temperature throughout the model to that of a user-defined reference fluid in order to determine fluid density using the equation of state (Equation 3.6). The reference fluid chosen for the model is the FEFLOW default, representing freshwater (0 g/L) at 10°C and atmospheric pressure. Using the properties of the reference fluid, hydraulic conductivity of the formation can be calculated using Equation 3.7. An intrinsic permeability of 200 mD was applied to the model domain, roughly in the middle of permeability values observed in the Paddy-Cadotte, resulting in a hydraulic conductivity of 1.48×10^{-6} m/s. This value was assigned uniformly as K_x in the model domain. Hydraulic conductivity in the vertical direction (K_z) was assumed to be one tenth that in the horizontal direction, falling roughly in the middle of the range of anisotropy ratios reported by Meyer (2002) for a similar sandstone (the Viking formation of west central Alberta).

A porosity of 0.25 was applied to the model, as this value was in the middle of the porosity range observed in HSU 2 of the Paddy-Cadotte and is reasonable for a sandstone (Manger, 1963). Specific storage was calculated using:

$$S_s = \rho g(\alpha + n\beta) \tag{3.9}$$

where the porosity (n) was used to calculate aquifer compressibility (α) using Hall's correlation for sandstones (Hall, 1953), and determined to be 4.82×10^{-10} Pa^{-1}. The compressibility of water (β) varies slightly with temperature, pressure, and solute concentration, but is assumed to remain constant at 5.0×10^{-10} Pa^{-1}. Specific storage (S_s) is a function of fluid density, which varies throughout the simulation. However, FEFLOW only accepts a single, invariant value. Therefore, a range of possible S_s values was calculated using Equation 3.9 and the density of the end member fluid types (freshwater at 0 g/L with a density of 997.4 kg/m^3, and the most saline brine at 300 g/L with a density

of 1177.4 kg/m^3) and found to be roughly 5.9 to 7.0x10^{-6} m^{-1}, though this range was expanded for the sensitivity analysis (see Section 3.3.9).

The volumetric heat capacity (c) and thermal conductivity (λ) assigned to the disposal formation are 2.46 MJ/m^3/K and 1.79 J/m/s/K, respectively, based on estimates by Eppelbaum et al. (2014) for sandstones, and were applied uniformly to the model domain.

Gelhar et al. (1992) showed that longitudinal dispersivity is scale-dependent. Values typically range over 2-3 orders of magnitude for any porous medium, with the largest values being equivalent to the scale of the problem considered. The scale of the Base Case model is considered to be 50-100 m, and so a conservative value of 5 m is selected for the longitudinal dispersivity. Transverse dispersivity is modeled as one tenth of longitudinal dispersivity. The same values are used for thermal dispersivity.

Time Settings

The Base Case was run for one year of active injection, during which time all the boundary conditions along the left side were turned on. After one year of injection, the disposal well was turned off and the model was run for 20 years (post injection period). Time steps were determined using FEFLOW's automatic time-step control (Diersch and Kolditz, 1998), with an initial time step length of 0.001 days and a final simulation time of 7665 days (21 years). Fixed output times were 10, 100, 365 (1 year), 730, 4015, and 7665 days to allow for comparison between simulations. An error tolerance of 10^{-3} was selected, as well as a maximum of 12 iterations per time step. Limiting the number of iterations per step prevented the model from spending too much time on any particular step; if convergence was not reached by the 12^{th} iteration in a particular time step, the simulation would move on to the next one (though this never occurred in any of the simulations described here).

Other Settings

The model was initially run without using the Boussinesq approximation, but this was found to produce significant imbalances in the fluid rate budget (heat and mass balance were unaffected). Invoking the Boussinesq approximation fixed this imbalance, potentially at the expense of simulation accuracy. The results of both model runs were compared (Appendix D), and it was found that there were only minor differences

between the two, most notably the extent of the 10 g/L concentration contour extending 0.5 m further along the base of the formation under the Boussinesq approximation, a difference of roughly 0.005%. It was felt that the increased accuracy in terms of fluid balance outweighed the error introduced, and so the Boussinesq approximation was incorporated into the final Base Case model.

The model was run using the convective form of the mass transport equation (Equation 3.3), as using the divergent form (Equation 4.4) produced anomalously high (>200 g/L) concentrations in later time steps. The dependency of fluid density on temperature was set to non-linear, to allow for the thermal expansion coefficient in Equation 3.6 to be a function of temperature. Solute dispersion was modeled as non-linear (Hassanizadeh and Leijnse, 1995), and fluid viscosity was set as dependent on solute concentration and temperature.

3.2.2. Results

The results of the Base Case simulation at various time-steps throughout the disposal and post injection periods are shown in Figure 3.2. The wastewater plume is demarcated by select isohalines (lines of constant salinity) at irregular contour intervals, which were selected so as to most clearly display concentration differences within the plume. The estimated radius of the plume based on the volumetric calculation (Equation 1.1) is shown at each time-step by a white dashed line, displayed overtop the model results to allow for a direct comparison between the two methods for estimating the lateral extent of plume migration (numerical model versus the volumetric calculation approach discussed in Chapter 1). The position of the line defined by Equation 1.1 moves along the radial direction throughout the disposal period as the volume of wastewater injected increases. In the post injection period, when wastewater injection stops, the position of this line no longer changes because the volumetric calculation assumes that the injected mass would remain fixed in space.

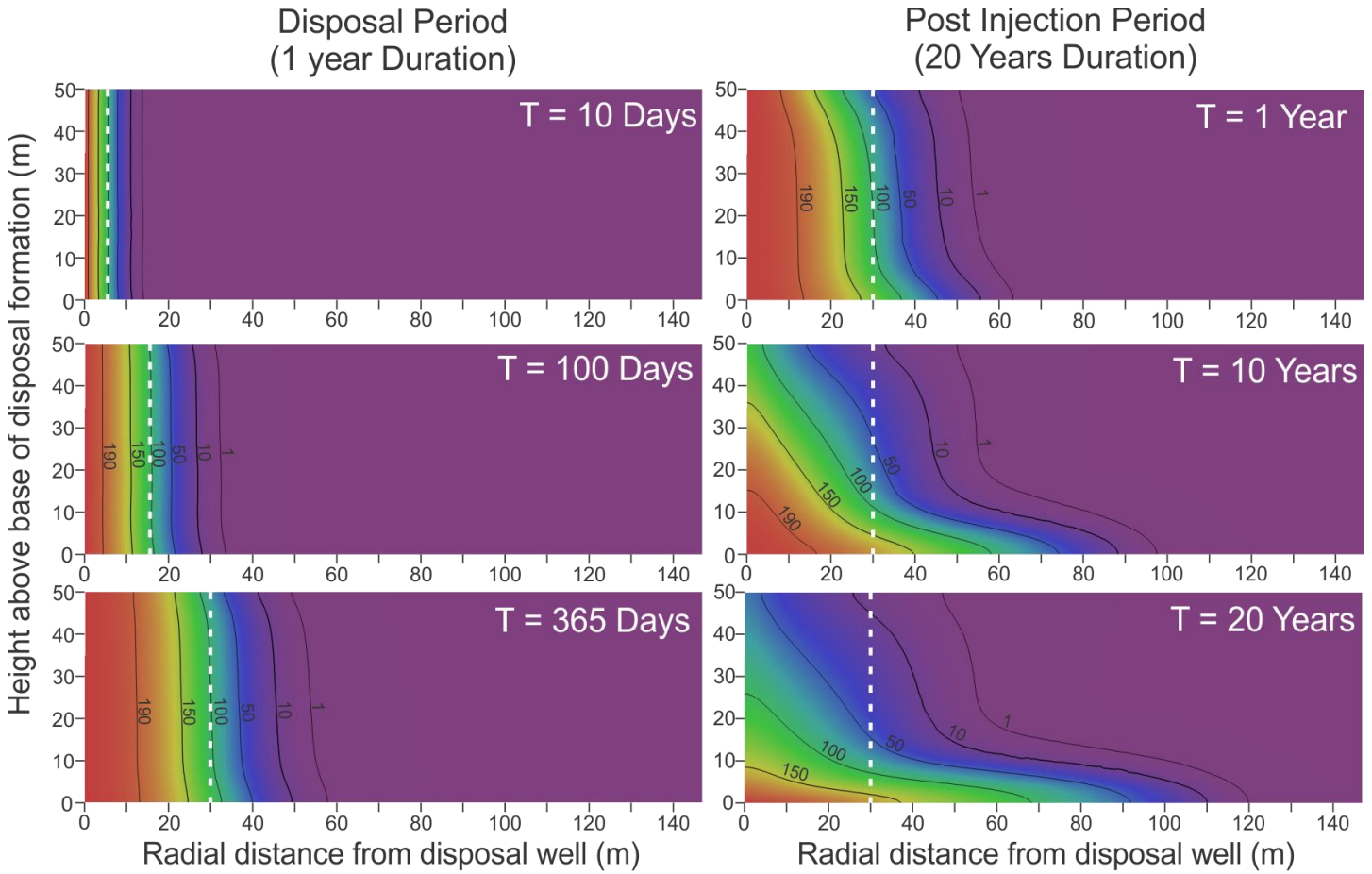

Figure 3.2. **Results of the Base Case simulation showing the extent and structure of the wastewater plume at different time steps during the disposal period (one year duration) and post injection period (20 year duration), which begins immediately after the disposal period. The plume is delineated by select concentration contours (in g/L), which are at irregular intervals. From right to left at all time steps, the order of the contours is 1, 10, 50, 100, 150, and 190 g/L. Labels are excluded from T = 10 days for clarity. The white dashed line in each box shows the estimated extent of the wastewater plume using the volumetric calculation (Equation 1.1).**

In early time steps of the disposal period (T = 10 days), the volumetric calculation shows good agreement with the model results, and all isohalines are parallel to the disposal well. As injection continues, however, the extent of the plume based on the volumetric calculation deviates somewhat from the simulated plume. Isohalines begin to deviate from parallel as the negative buoyancy of the wastewater causes the plume to spread further along the bottom of the model than at the top. Dispersion and diffusion have a notable effect on the extent of the plume; after 365 days of disposal, the volumetric calculation estimates a plume radius of roughly 30 m, whereas the model results show that the 1 g/L isohaline extends a distance of almost 60 m from the disposal well. Throughout the disposal period, the volumetric calculation aligns closely with the 100 g/L isohaline, which is half the concentration of the injected wastewater and equivalent to the advective front. The bulk of the plume's mass is located within the radius predicted by the volumetric calculation.

In the post injection period, the wastewater density begins to significantly affect the plume's structure. Close to the disposal well, where salinity is highest, the most notable changes occur. The plume begins to sink as the wastewater spreads along the bottom of the aquifer. The maximum concentration of the plume decreases, as evidenced by the disappearance of the 190 g/L isohaline after 20 years of post-injection. At late time-steps, the plume deviates significantly from the volumetric calculation, extending four times further than calculated volumetrically. The pronounced sinking of the wastewater plume suggests that any slope or irregularities to the base of the disposal formation could strongly influence the evolution and migration of a disposed wastewater plume.

Formation pressures during the simulation are reported; Figure 3.3 shows the change in pressure at various locations throughout the model during both the disposal and the post injection periods measured at the same height in the formation. Pressures are initially uniform throughout the model (5250 kPa), but increase at relatively high rates in the first few days of injection (as expected based on basic well testing theory) and continue to rise at a lower rate after 100-150 days to a maximum pressure of approximately 5600 kPa at the well itself. Once the injection period ends (at 365 days), pressures drop rapidly at all distances from the well and gradually return to initial values after roughly 100 days (as in a recovery test). The greatest maximum pressures are observed directly at the disposal well, with maximum pressures decreasing with increasing distance from the well (again consistent with well testing theory).

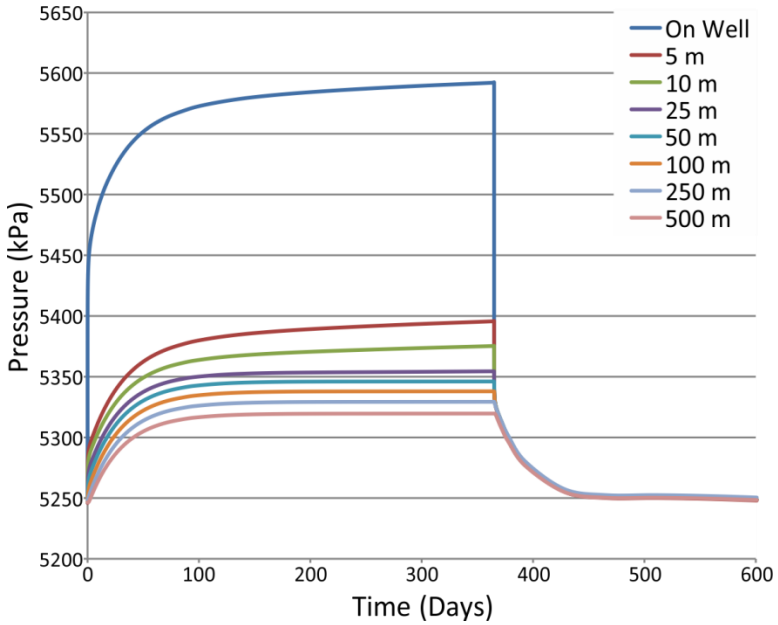

Figure 3.3. Simulated pressure changes in the Base Case at increasing distance from the disposal well. All pressures are recorded at 25 m (mid-way depth in the disposal formation). Pressures were output for the entirety of the simulation (7665 days), but no significant changes in pressure were observed in later time steps, and so results are only shown for the first 600 days.

The pressures calculated along the well are shown as a function of height above the base of the disposal formation in Figure 3.4 for initial conditions (T = 0 days) and for the maximum pressure attained (T = 365 days). Initial pressures along the well increase linearly with depth according to the hydrostatic gradient. After a year of injection, the pressure gradient remains similar, but is shifted to the right (higher pressure) because fluid is injected uniformly along the well. However, the profile is more jagged, likely due to minor heterogeneities in the mesh (i.e. unequal spacing of nodes along the left boundary) as a result of FEFLOW's meshing algorithm. As well, large pressure spikes are observed at the very top and bottom of the model (Figure 3.4, inset). This is assumed to be a boundary effect due to the nodes being located along the upper and lower no-flow boundaries.

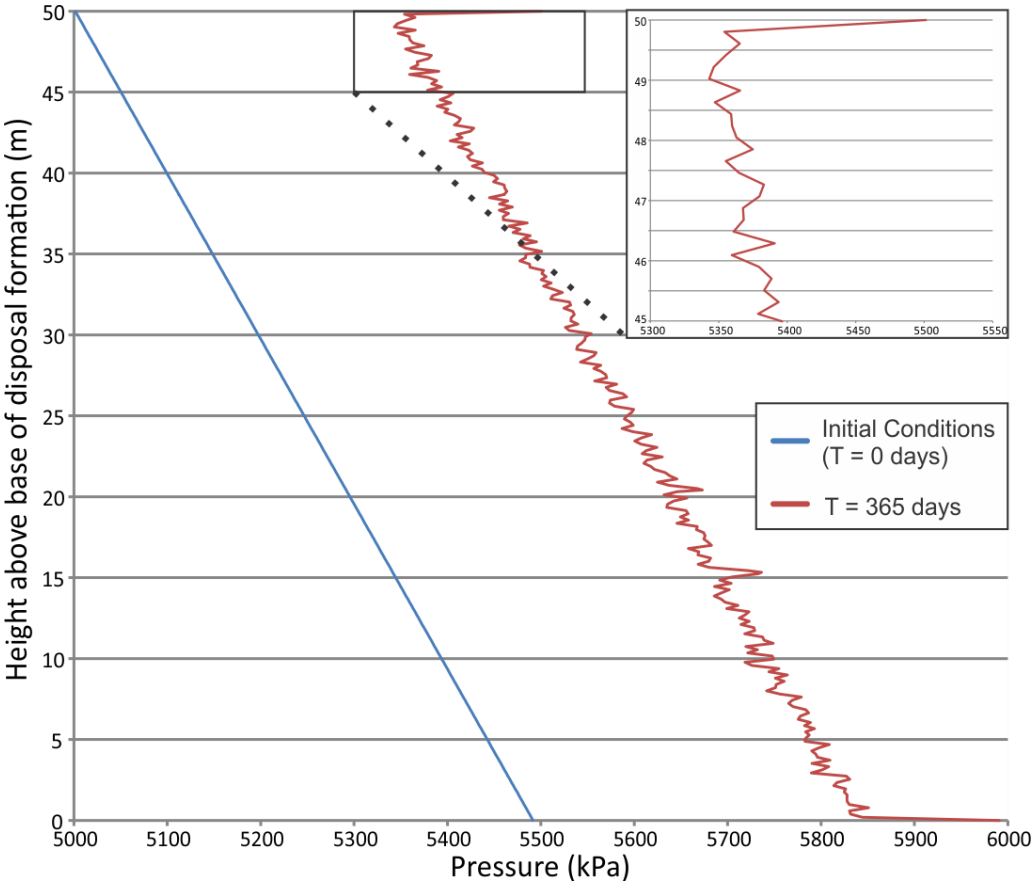

Figure 3.4. Simulated pressures along the well prior to injection (T = 0 days) and after one year of injection (T = 365 days). Inset graph shows the pressure spike at the upper boundary of the model in greater detail. A similar spike is seen at the bottom of the model.

For each time step in the simulation, the mean pressure along the disposal well was calculated and plotted in Figure 3.5. Disposal formation pressures at the well increase at the greatest rate during the first few days after injection is initiated, and gradually slow to a near constant rate of increase. Peak pressure of just under 5600 kPa is reached after a year of injection, equivalent to a 6.5% increase over the IVRP. When injection stops at 365 days of simulation time, pressures rapidly drop and return to near initial reservoir pressure after approximately 50 days.

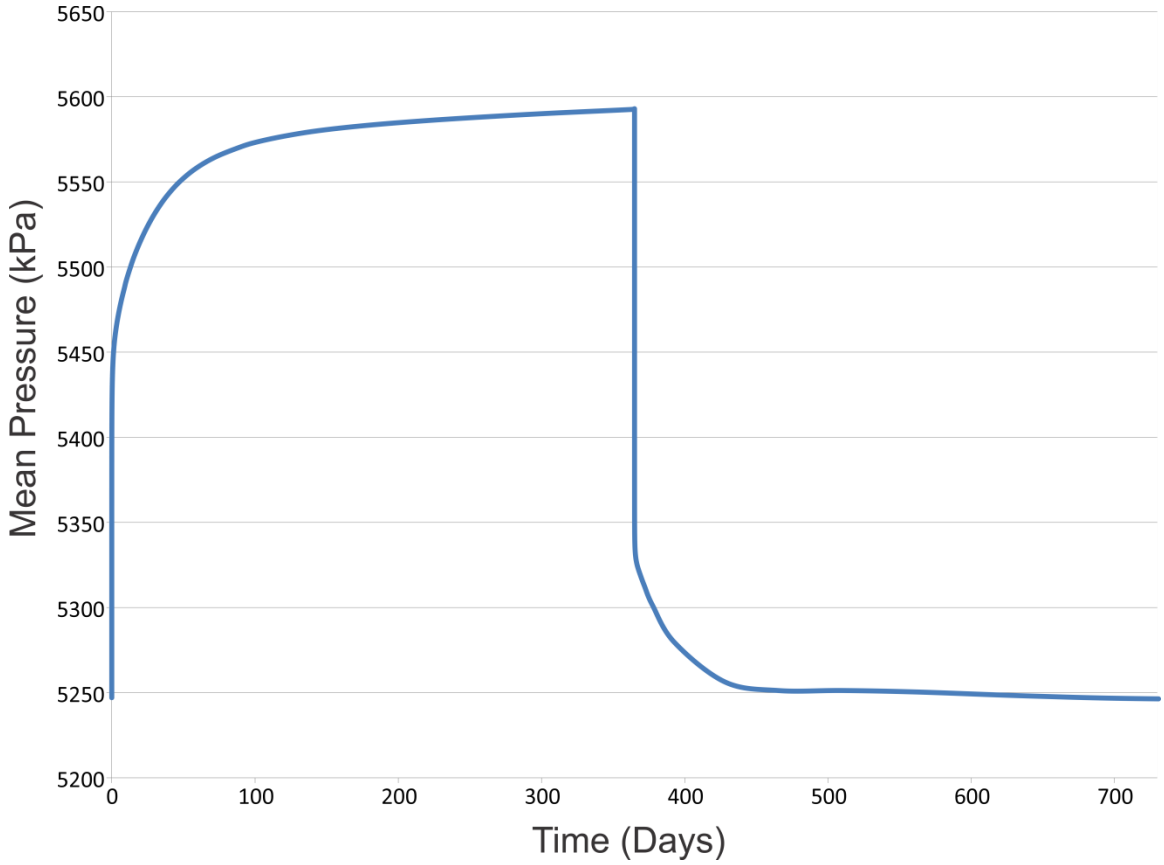

Figure 3.5. Mean pressure increase in the formation along the disposal well in the Base Case model. Formation pressures remain constant after 700 days and so were not plotted past this time.

3.2.3. Discussion

The results of the Base Case model simulations show that mass transport processes and density-related effects exert a strong control on wastewater migration, which leads to notable differences in the isohaline extent and configuration in the post disposal period when compared to the lateral extent determined using the volumetric calculation (Equation 1.1). These differences are less evident during disposal (Figure 3.2). In early time steps, the wastewater plume is largely driven by advection due to the high pressure gradient leading away from the well, and so the isohalines remain vertical and parallel to the disposal well. The isohalines have the same vertical orientation as the white dashed line representing the extent of wastewater according to the volumetric calculation, though dispersion and diffusion cause the simulated results to extend twice as far. Comparison of the contour results of the simulation and the contour estimated using the volumetric approach indicates that the bulk of the mass is contained within the extent

calculated by the volumetric calculation, showing that this calculation provides a generally suitable estimate for plume extent during disposal. When disposal stops, however, the advective driving force of injection diminishes, allowing density-driven flow to play a greater role in plume migration. Thus, the plume sinks towards the bottom of the formation, spreads out, and has lower maximum concentrations. This leads to differences between the model results and the volumetric calculation, which predicts that the wastewater plume will remain cylindrical (vertical in cross section). Clearly Equation 1.1 cannot be used to fully predict the behavior of disposed wastewater after disposal has stopped, but the significance of this depends on whether or not accuracy is actually required in a given disposal scenario. For instance, if disposed wastewater had the potential to migrate off of the lease owned by the disposal well operator into a lease owned by another party, then a greater degree of accuracy might be required. Ultimately, the need for accuracy may have to be considered on a case by case basis. Further, since the saline wastewater was observed to sink, any slope to the base of the formation has the potential to cause the plume to migrate down-dip. The effect of a sloping base is examined in the regional model (see Chapter 4).

Formation pressures as a result of wastewater disposal are shown in Figure 3.5 to increase sharply in the time period immediately after injection is initiated, but gradually level off to a near constant rate of increase after 100 to 200 days. Once injection is stopped, simulated pressures drop rapidly and reach near initial conditions after 50 days of post injection. These results suggest that in the ideal case considered here – namely, a homogeneous disposal formation of uniform thickness and 100% well efficiency - the most significant pressure increases should occur soon after injection begins. However, most geological formations are not homogeneous. The permeability may decrease away from the well, the formation may thin, or structural traps can laterally bound a formation. These heterogeneities could lead to disposal pressures following a different curve than that shown in Figure 3.5. Likewise, well inefficiencies may exist or develop over time, such as the buildup of scale in the well/formation or the mobilization of fine particulates injected into the formation which could reduce permeability. None of these factors are incorporated into the models investigated in this thesis, and, as a result, none of these simulations are appropriate replacements for in-situ formation pressure tests in assessing the performance of any particular well. Instead, the pressure results obtained

from these simulations illustrate the potential for pressure increases in a disposal formation due to variations in disposal and formation conditions.

3.3. Sensitivity Analysis

In order to assess the control of various formation and fluid parameters on the migration of disposed wastewater and the resulting increases in formation pressure, a sensitivity analysis was performed on the Base Case. The ranges of values investigated are those that could potentially be encountered during wastewater disposal in the Paddy-Cadotte that were discussed in Chapter 2 and are presented in Table 3.1. In most cases discussed in this section, results are presented as both model cross-sections showing concentration contours over time (similar to Figure 3.2) and as pressure plots (similar to Figure 3.5). In place of modeling a 20 year recovery (post-injection) period, the disposal period for each case is 10 years.

For some cases, the parameter being investigated necessitated modifications to either the model itself or the means of presenting the results of the simulation. For example, in the case of varying formation water density, new initial hydraulic head conditions had to be applied to the model domain to account for the greater pressure gradient created due to denser formation waters. These details are discussed as necessary in the introduction to each case.

Table 3.1. Parameters investigated in the sensitivity analysis and their associated ranges.

Parameter	Range	Base Case Value
Formation Extent (km)	0.25-0.5 (no flow), 1.5-200 (reference head)	1.5 (reference head)
Permeability (mD)	20-500	200
Salinity Contrast (g/L)	50-300	200
Injection Rate (m^3/d)	100-1000	100
Dispersivity (m)	0.5-50	5
Diffusion Coefficient (10^{-9} m^2/s)	0-4	1.99
Permeability Anisotropy (K_z/K_x)	0.01-1	0.1
Formation Thickness (m)	25-50	50
Specific Storage (1/m)	1.0×10^{-5} – 1.0×10^{-7}	1.0×10^{-5}

3.3.1. Downgradient Model Boundary Condition

In this case, the boundary condition along the right edge of the model was modified in order to assess its control on formation pressures and wastewater distribution. In the

Base Case, this edge was simulated as a head dependent boundary of 560 m, with the elements adjacent to it assigned an out-transfer rate of 9.87×10^{-10} s^{-1}, which is equivalent to a constant head boundary of 560 m at a distance of 1.5 km from the right side of the model domain. This out-transfer rate value was modified to simulate a constant head boundary of 560 m at 3, 100, and 200 km from the edge. Additionally, two different instances of no-flow boundaries were simulated: one in which the extent of the model was unchanged and one in which the model domain was halved to 250 m by deactivating the elements in the right half of the model.

The 10 g/L isohalines were plotted for the cases in which reference head is located at 1.5 and 100 km from the model edge, as well as for the case in which all model elements are active and a no-flow boundary is implemented. All of these isohalines were found to overlap, indicating that the extent of the wastewater plume is largely unaffected by varying the out-transfer rate at the downgradient boundary (Appendix D).

Formation pressures at the disposal well boundary resulting from the different downgradient boundary cases are shown in Figure 3.6. In all other pressure plots in the sensitivity analysis, a common y-axis is used to enable comparisons between cases. Because much greater pressures are reached when modifying the downgradient boundary condition than when modifying any other parameter, a different y-axis scale is used. Additionally, simulation time is plotted on a log scale.

It is evident from Figure 3.6 that the downgradient boundary condition exerts a strong control over simulated pressures. When the boundary reference head is closer to the model edge, as in the 1.5 km (Base Case) and 3 km cases, pressures remain low. This boundary is acting as a strong sink and prevents pressures from building up within the domain. In the extreme case, where the out-flow boundary is replaced with a no-flow boundary, pressures rise indefinitely, never reaching a plateau as seen in Figure 3.5. The closer this no-flow boundary is to the well, the faster the rate at which pressure builds. For example, in the case of the no-flow boundary simulated 250 m from the disposal well, pressures increase very rapidly and reach a final value of 42 MPa, over eight times greater than the IVRP and roughly four times greater than when the no-flow boundary was simulated at 500 m from the disposal well after the same simulation time of 3650 days (Figure 3.6). Such a no-flow boundary condition could represent lateral confinement of the formations due to, for example, a geological pinch out or an

impermeable structural feature. For the cases in which the reference head is positioned 100 and 200 km from the model edge, pressures approach those simulated in the no-flow boundary case.

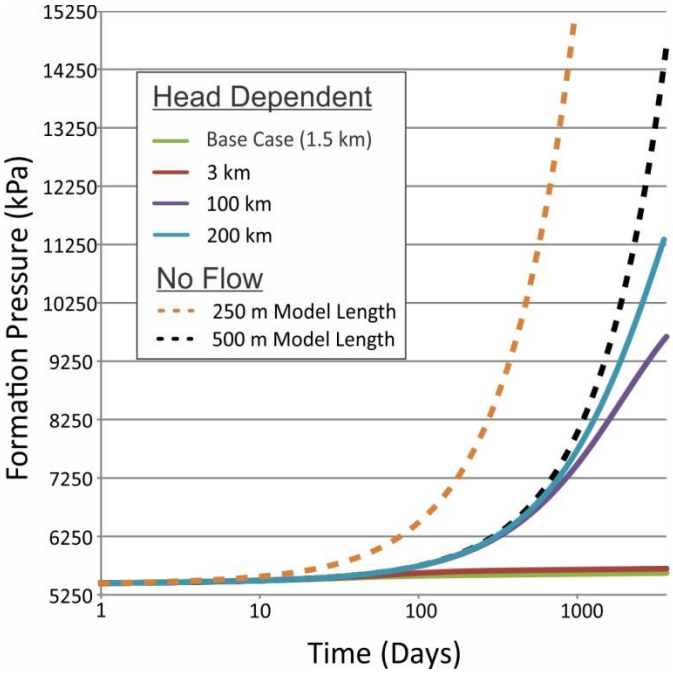

Figure 3.6. Mean formation pressure along the disposal well for various outflowing boundary conditions applied to the right side of the model domain. For head dependent boundaries, labels indicate the distance at which the reference head is simulated. For No Flow, distances indicate the length of the model domain. X-axis is on a log scale.

This analysis shows that choice of downgradient boundary condition has the potential to greatly affect simulated disposal formation pressures. The Base Case boundary was selected as it was initially felt that it would have minimal influence on formation pressures, but this is clearly not the case. Pushing the reference head to greater distances closely approximates a no-flow boundary, which is also likely not realistic, as the extent of the disposal formation in the Paddy-Cadotte is known to stretch for tens of kilometers.

The variations observed due to this boundary condition could potentially arise from the specific storage of the area between the model edge and reference head not being accounted for. Ultimately, the role of this boundary condition was not entirely understood, and which reference head distance best represents actual disposal conditions is unclear. Because of this, the absolute pressure results from these

simulations are not to be interpreted literally. Instead, the relative changes in pressure between parameter values should be used to interpret the proportional pressure response in the disposal formation as a result of increasing or decreasing parameter values.

3.3.2. Permeability

This case considers a range of homogeneous formation permeability from 20-500 mD, which is equivalent to a hydraulic conductivity range of 1.48×10^{-7}-3.70×10^{-6} m/s (see Equation 3.8). Figure 3.7 shows the extent of the 0.05C isohaline, where C is equal to the concentration of the injected wastewater (200 g/L) for 20, 250 and 500 mD.

In early time steps (one year of disposal), the extent of the wastewater plume does not vary much between permeability cases, but differences become evident in later time steps (Figure 3.7). For the 20 mD simulation, the plume retains its upright structure as the isohalines remain parallel to the disposal well, showing only slight differences between the extent of its top and bottom even nearing the final time step. Conversely, in the 500 mD simulation, the plume elongates on the bottom of the disposal formation, and extends 60 m further than the 20 mD case. This indicates that permeability exerts a strong control on the overall extent of the wastewater plume. The green line in Figure 3.7 shows the extent of the wastewater plume after 10 years determined using the volumetric calculation (i.e. no dispersion or diffusion). This line is most similar to that of the 20 mD case, suggesting that the volumetric calculation more closely approximates advective and dispersive transport in lower permeability formations. When permeability is greater, the density of the wastewater exerts a greater control, leading to larger disagreements between the two methods of estimating plume extent (i.e. numerically modelled versus volumetrically calculated).

Mean formation pressures for the three different values of permeability are shown in Figure 3.8. In all cases, pressures rapidly rise in the days following onset of injection and slowly level off. After 10 years of injection, the 200 and 500 mD cases reach pressures of 5650 and 5440 kPa, equivalent to 107/103% of the IVRP, and continue to rise at a slow rate. In the 20 mD case, however, the pressure rises rapidly and reaches 8340 kPa (159% of IVRP) by the end of the simulation. These results highlight the importance of permeability in influencing formation pressure response due to disposal of wastewater.

In practice, the disposal wells in the Paddy-Cadotte typically do not target sections of the formation with permeability this low (HSUs 1 and 3), instead opting for the higher permeability HSU 2.

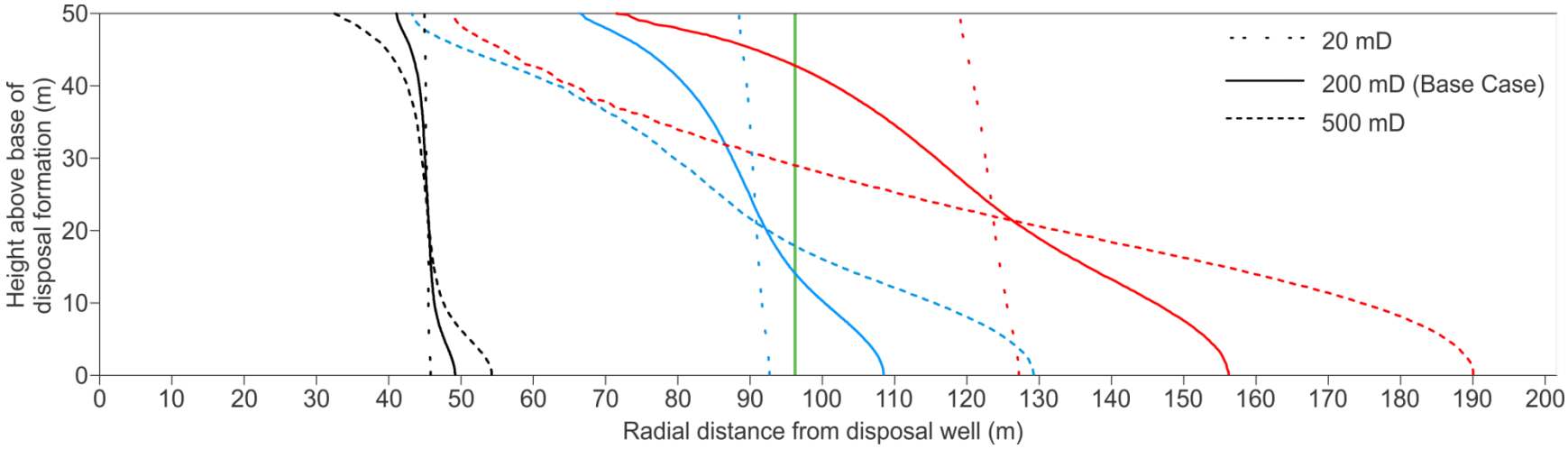

Figure 3.7. **Plot showing extent of 0.05C (10 g/L) isohalines, where C = 200 g/L, at multiple time-steps for different values of formation permeability. Model runs are differentiated by line style, while line color denotes length of disposal. Black lines represent one year of injection, blues lines represent five years, and red lines represent ten years. Green line at 96 m shows extent of wastewater plume after 10 years determined using the volumetric calculation.**

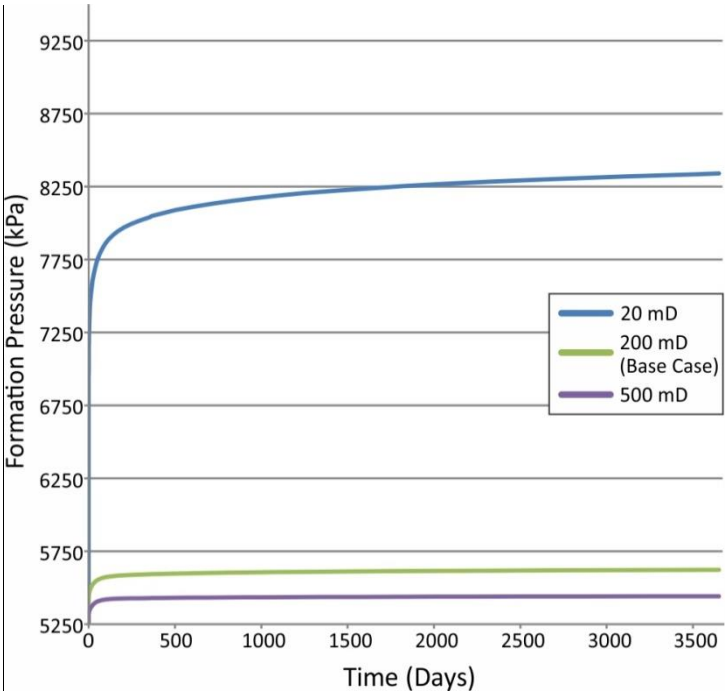

Figure 3.8. Mean formation pressure along the well for three different cases of formation permeability.

3.3.3. Salinity Contrast

This case investigates the effect of salinity differences, and thus density differences, between the disposed wastewater and formation water. This was done in two ways: 1) by increasing the salinity of the wastewater and holding formation water salinity constant at 0 g/L, and 2) by injecting 100 g/L wastewater into a formation with 50 g/L formation water and comparing it to the case from the previous set of simulations that had the same fluid concentration differences. This is done to demonstrate that it is the relative density difference between fluid types that is the main control on plume migration and formation pressures.

In the first set of simulations, a range of wastewater salinity from 50-300 g/L was modeled. The concentration contours shown in Figure 3.9 are for the 0.05C isohaline, meaning that the TDS represented by the contour changes depending on the salinity of the disposed wastewater (i.e. a fraction of the original salinity). This method of presentation was selected because absolute values of salinity do not allow for meaningful comparison between cases of varying salinity. For example, if a 10 g/L

contour was selected to represent the extent of the plume, it would be equivalent to 20% of the initial concentration in the 50 g/L case, but only 3.33% in the 300 g/L case. This results in the graph showing the plume to have spread much further in the 300 g/L case. By representing the extent of the plume using a consistent fraction of the original wastewater salinity between cases, a more meaningful comparison can be made.

The concentration contours for the various cases of wastewater salinity are shown in Figure 3.9. As the concentration (and thus density) of the wastewater increases, the plume travels further along the bottom of the disposal formation. The difference in extent between the 100 and 200 g/L cases is roughly 12 m, while the difference between the 200 and 300 g/L case is roughly 8 m. Increasing the salinity of the wastewater leads to a larger disagreement with the volumetric estimate (green line in Figure 3.9) as buoyancy effects begin to play a larger role.

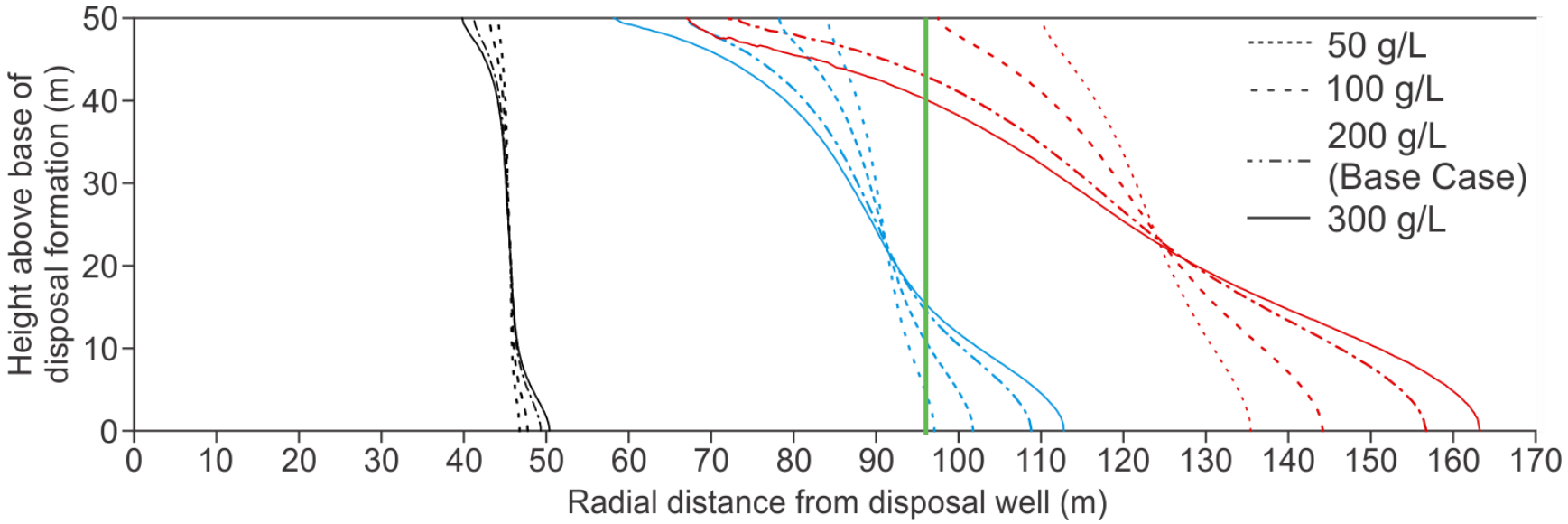

Figure 3.9. **Plot showing extent of 0.05C isohalines, where C is the concentration of injected wastewater, at multiple time-steps. For all simulations, the formation fluid has a concentration of 0 g/L. Concentrations are differentiated by line style (shown at top right of figure), while line color denotes the time-step. Black lines represent one year of injection, blues lines represent five years, and red lines represent ten years. Green line at 96 m shows extent of wastewater plume after 10 years determined using the volumetric calculation.**

Mean pressure increase along the well for each case of wastewater salinity is presented in Figure 3.10. Pressures increase sharply in the first few days after injection begins, and eventually level off to a steadily increasing value after roughly 2 years of disposal. Pressure increases ranged from 5535 to 5770 kPa between the low salinity (50 g/L) and high salinity (300 g/L) cases. The trend observed is that higher wastewater salinity results in higher pressures along the well, which is inferred to be due to the increased weight of the fluid in the formation resisting the injection of additional wastewater. This can be understood using Equation 3.7; with increasing salinity, fluid viscosity increases at a greater rate than fluid density, resulting in a lower hydraulic conductivity and making the problem similar to that investigated in the permeability case. This pressure increase becomes more pronounced as the salinity of wastewater increases; the difference in pressure at the end of the simulation between the 100 and 200 g/L cases is 65 kPa, whereas between the 200 and 300 g/L case it is 150 kPa. This, combined with the conclusions drawn from Figure 3.9, indicates that as salinity increases, the rate at which the plume spreads begins to slow, but the rate at which well pressure rises increases, though the absolute change in formation pressure as a result of increasing salinity is small in comparison to other parameters investigated in this sensitivity analysis (e.g. formation permeability).

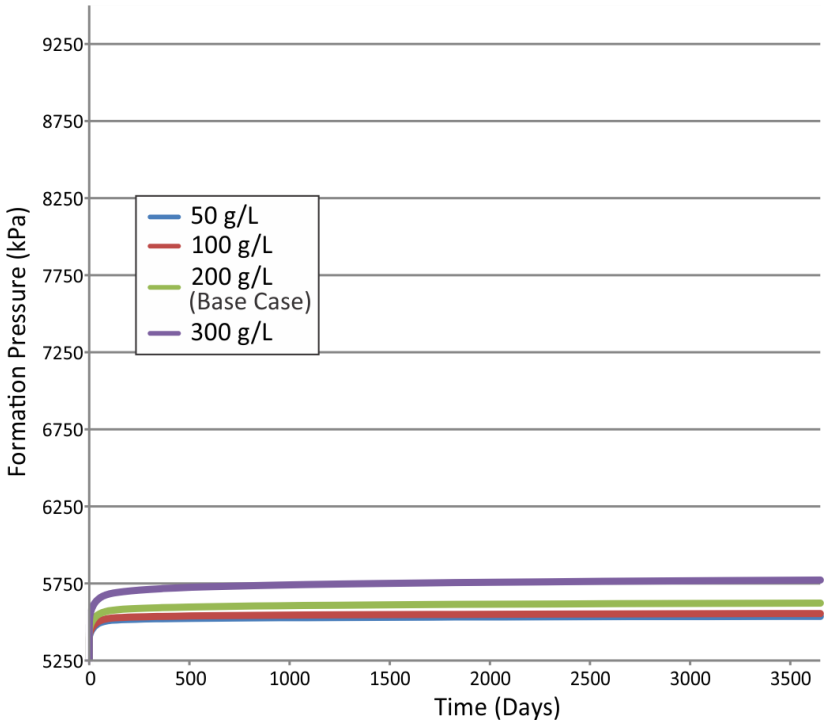

Figure 3.10. Mean formation pressure along the well for four different cases of injected wastewater salinity.

To demonstrate that plume extent and formation pressure are controlled by the salinity contrast between the fluids (disposal fluid and formation fluid), wastewater with a salinity of 100 g/L was injected into a formation with 50 g/L formation water, and then compared to the case above in which 50 g/L wastewater was injected into a formation with fresh water. This simulation necessitated modifications to the initial head distribution in the model. Because FEFLOW performs all of its calculations in terms of equivalent freshwater head, increasing the salinity of the formation water precludes the use of a homogenous head distribution in the formation. The normal hydrostatic gradient no longer applies, and must be increased to compensate for the increased density of the formation water. Failing to do so would produce lower saltwater head[8] at the base of the formation compared to the top and result in vertical flow within the model. A new hydraulic head distribution was thus assigned to the model domain using the equation:

$$h = h_0 + 0.037(50 - z) \tag{3.10}$$

[8] In situations where hydraulic head is calculated and the fluid in the formation has a density greater than freshwater, the term 'saltwater head' is commonly used.

where z is the height of the disposal formation at a given location, h_0 is the original head value (560 m), and 0.037 is the density difference ratio (Equation 3.8) calculated between freshwater and 50 g/L formation water. This produced an increasing equivalent freshwater head value with depth, which, after taking the increased fluid density due to formation water salinity into consideration, was translated by FEFLOW into a homogeneous saltwater head distribution within the model.

The concentration contours are presented in Figure 3.11. As is expected, the contours have nearly identical positions. Slight differences are visible after ten years of injection, and this is attributed to a very slight difference in density between the two simulations. The relationship between density and salinity is not linear (Figure 3.12); instead it approximates a second degree polynomial. This causes the density difference between 50 and 0 g/L fluids to be slightly more than between the 100 and 50 g/L fluids. This manifests as the slight difference in contour locations in Figure 3.11; slightly less plume elongation along the bottom of the formation occurs for the dashed contour. Fluid viscosity increases at a more constant rate than fluid density (Francke and Thorade, 2010), and so the variation in contour locations are likely not influenced by viscosity.

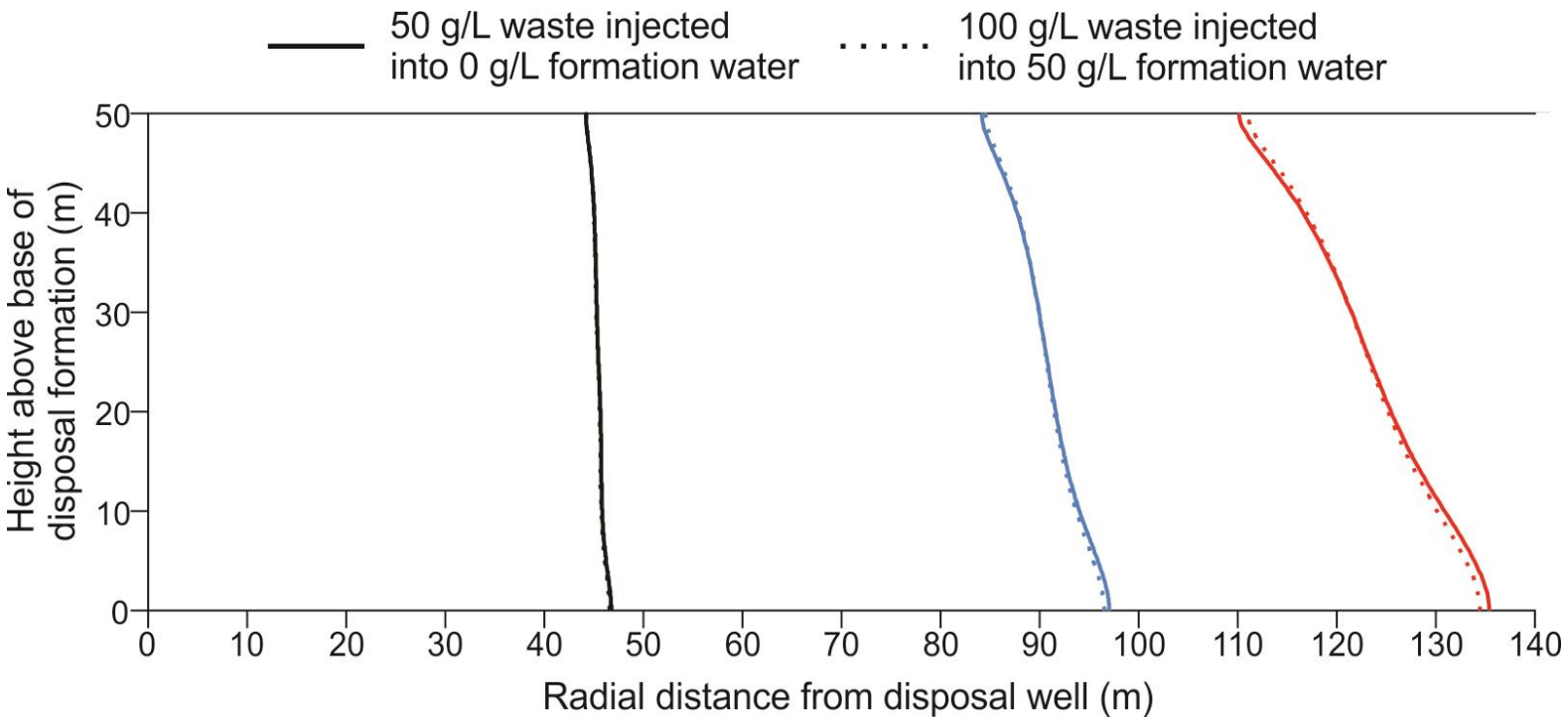

Figure 3.11. Plot showing extent of $0.05C_D$ isohalines at different time steps, where C_D is the concentration difference between the formation water and injected wastewater plus the concentration of the formation water. The dashed line represents the 52.5 g/L isohaline for that particular model run, while the solid line represents the 2.5 g/L isohaline for another run. Simulations are differentiated by line style (shown above figure), while line color denotes the time-step. Black lines represent one year of injection, blues lines represent five years, and red lines represent ten years.

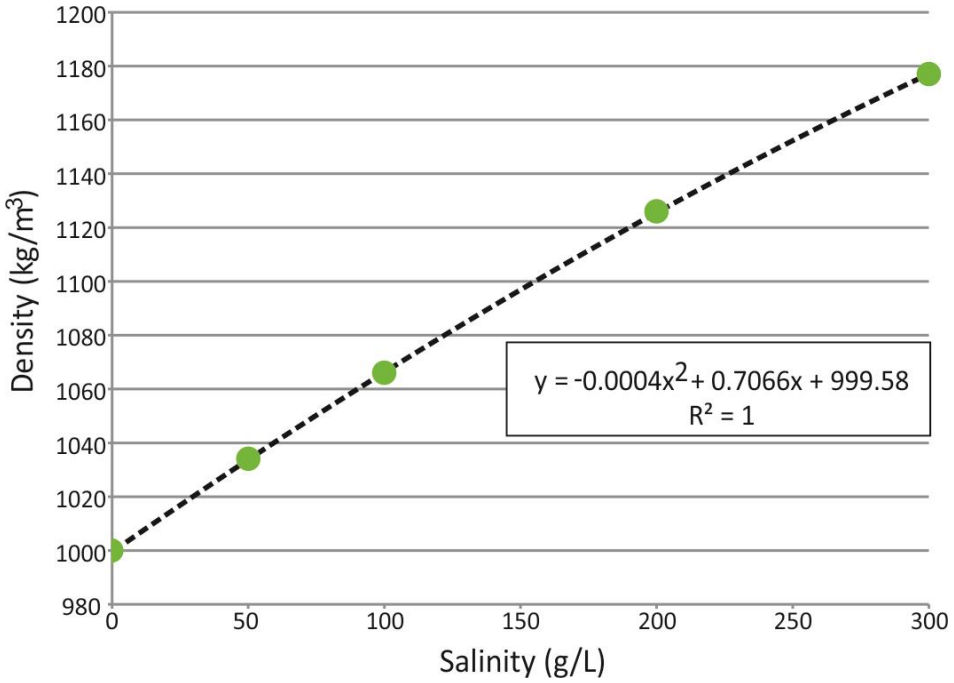

Figure 3.12. Relationship between fluid density and salinity. Calculated at 10ºC using calculator by Driesner and Heinrich (2007).

Disposal pressures for salinity contrast are shown in Figure 3.13. With the scale used in the figure, differences are hard to distinguish, but the case in which the 50 g/L wastewater is injected into freshwater is approximately 10 kPa lower than the case in which 100 g/L wastewater is injected into 50 g/L formation water. This demonstrates that disposing wastewater in formations with more saline waters can produce greater pressures, but this value is negligible in comparison to the pressures created by increasing the salinity of the injected wastewater (Figure 3.10) or by other factors varied for this sensitivity analysis.

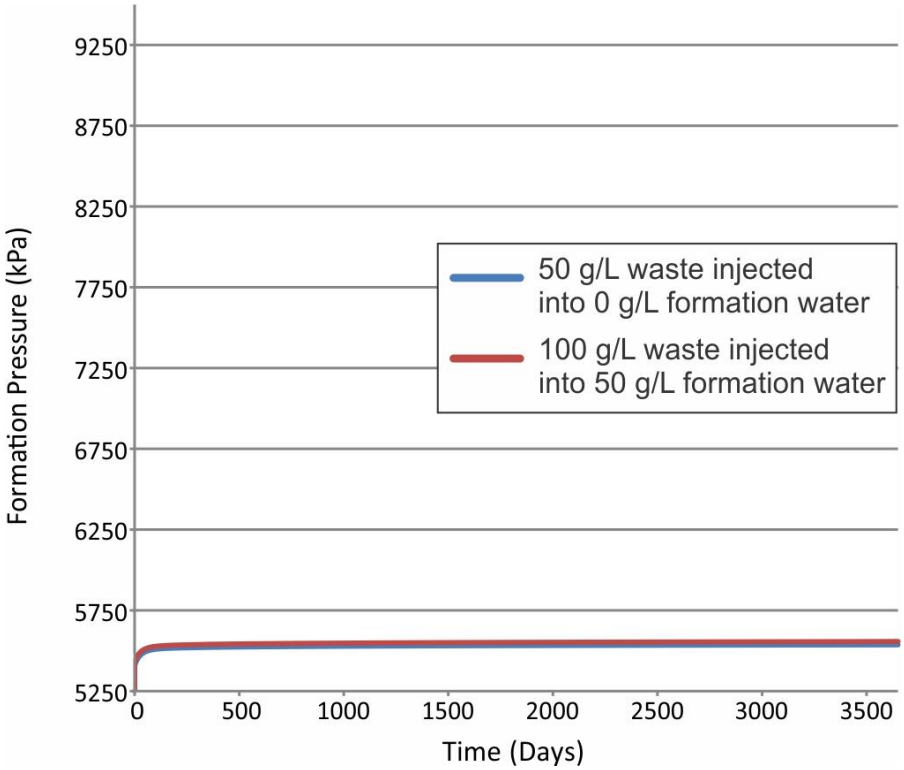

Figure 3.13. Mean formation pressure along the well for two different cases of salinity contrast.

3.3.4. Injection Rate

In this part of the sensitivity analysis, various injection rates were modeled. The operational range of three of the disposal wells discussed in Section 2.1.1 is 100-200 m^3/d, and so these values were selected for simulation. One disposal well, WA 10677, operates at a significantly greater rate of 1000 m^3/d, and so this value was investigated as well. Since neither the TDS of wastewater nor formation water changes in this case, a constant isohaline (10 g/L) was plotted in order to compare plume extent between simulations.

The extents of the wastewater plumes for various injection rates are shown in Figure 3.14. The change in lateral extent with increasing injection rate is unsurprising; as a greater volume of wastewater is injected, the plume spreads further and occupies a greater volume of the disposal formation. Showing the extent of wastewater after 10 years of injection on Figure 3.14 as determined using the volumetric calculation is difficult as the three different injection rates simulated all produce different plume extents, which would make the figure difficult to read. Therefore, the results are

presented in Table 3.2. According to the volumetric calculation, after 10 years of injection at a rate of 100 m^3/day the plume would reach a distance of 96 m; at 200 m^3/day it would reach a distance of 136 m; and at 1000 m^3/day it would reach a distance of 304 m. In order to quantify how well the volumetric calculation approximates the modelled results, the extent estimated by the volumetric calculation is divided by the furthest modelled extent (along the bottom of the disposal formation) for any given injection rate. Table 3.2 shows that, as injection rate increases, the extent of the plume estimated using the volumetric calculation more closely approximates the modelled plume extent.

Table 3.2 Values used to compare volumetric plume extent to modelled plume extent, both measured after 10 years of disposal. Modelled extent is measured along the bottom of the disposal formation.

Injection Rate (m^3/day)	100	200	1000
Volumetric Plume Extent (m)	96	136	304
Modelled Plume Extent (m)	156	202	381
Ratio of Volumetric to Modelled Extent	0.62	0.67	0.8

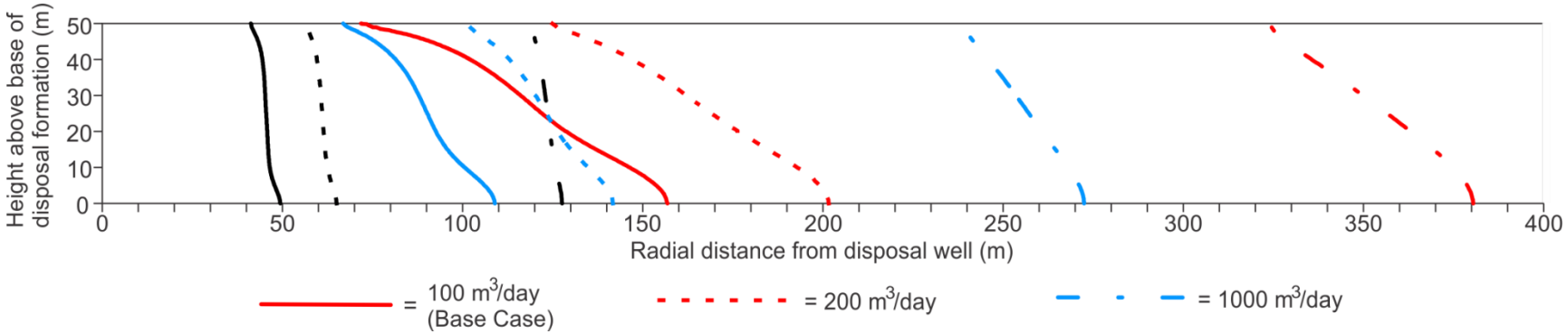

Figure 3.14. Plot showing extent of 10 g/L isohaline for different injection rates at multiple time-steps. Injection rates are differentiated by line style (shown along bottom of figure), while line color denotes the time-step. Black lines represent one year of injection, blues lines represent five years, and red lines represent ten years.

Pressure increase along the well as a result of increasing the injection rate is shown in Figure 3.15. As with the concentration contour results shown in Figure 3.14, the simulated pressures are predictable for changes in injection rate; higher injection rates lead to higher formation pressures. The 100 and 200 m^3/d cases both see modest increases in formation pressure, while the 1000 m^3/d case quickly reaches the highest pressures simulated in any part of the sensitivity analysis (9285 kPa). As discussed in Section 3.3.2, pressures of this magnitude, combined with any well inefficiencies not accounted for in the model, could potentially approach the 90% formation fracture pressures discussed in Chapter 2.

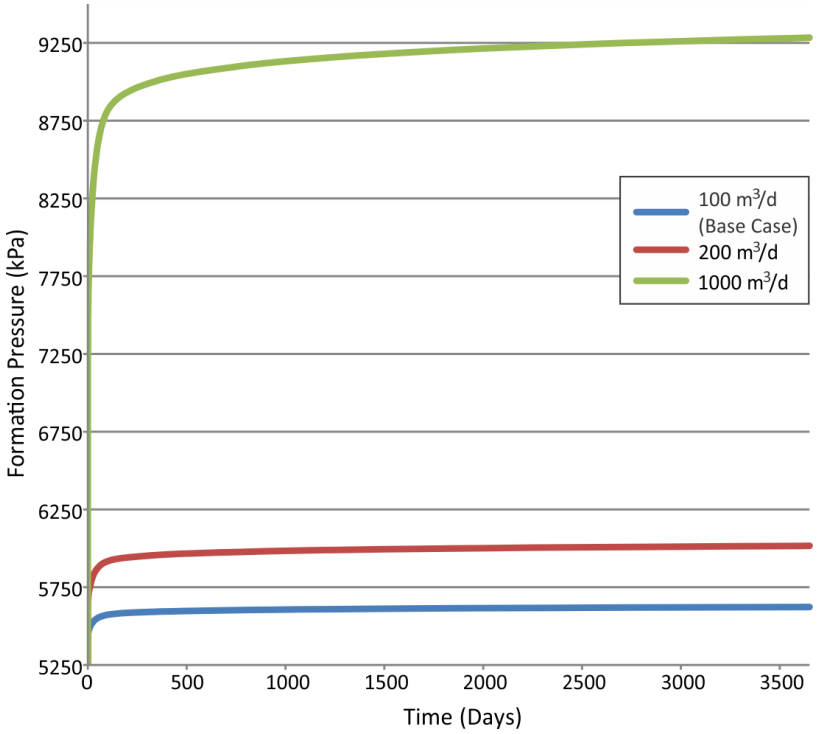

Figure 3.15. Mean formation pressure changes along the well for three different cases of injection rate.

3.3.5. Dispersivity

This part of the sensitivity analysis investigated the effect of varying mass and heat transport dispersivity (same value for both) on solute distribution and formation pressure. There were two components to this sensitivity analysis: 1) varying longitudinal dispersivity, and 2) varying transverse dispersivity. Note that in FEFLOW, transverse dispersivity is uniform in the vertical and lateral directions. For these simulations, longitudinal dispersivity is maintained at ten times greater than transverse dispersivity. A

longitudinal dispersivity of 5 m was chosen for the Base Case, and values an order of magnitude greater and smaller than this were simulated in this sensitivity analysis. A vertical transverse dispersivity of 0.5 m was chosen for the Base Case, and similarly, values an order of magnitude higher and lower were simulated. Due to time constraints, no cases were investigated in which longitudinal dispersivity was increased while transverse dispersivity was held constant. This relationship could be investigated in the future.

The effect of longitudinal dispersivity on the extent of the wastewater plume is shown in Figure 3.16, and it is evident that it exerts a strong control. Between the extreme cases (α_L = 0.5 m and α_L = 50 m), there is a difference of over 50 m in plume extent along the bottom of the aquifer after ten years of disposal. The concentration gradient (not shown here) for the 0.5 m case is quite steep, with wastewater concentration rising from 10 g/L to 190 g/L over as little as 20 m. The opposite is true in the 50 m case, with the same concentration change occurring over 180 m. As longitudinal dispersivity increases, the plume spreads further, but the salinity is distributed throughout a greater volume resulting in lower concentration gradients. Lower dispersivity values more closely approximate the volumetrically calculated plume extent (shown by the green line in Figure 3.16), which makes sense since the volumetric calculation assumes no dispersion. An attempt was made to model disposal with no dispersivity (α_L = 0 m), but this led to large numerical instabilities and the model never converged. As well, as dispersivity decreases, a finer mesh discretization is required. Theoretically, with no dispersion the mesh would have to be infinitely discretized. This scenario could not realistically be simulated, and so the α_L = 0.5 m is used as a rough analogue for the α_L = 0 m case. Plume extent, defined by the 10 g/L isohaline, is heavily influenced by the longitudinal dispersivity value.

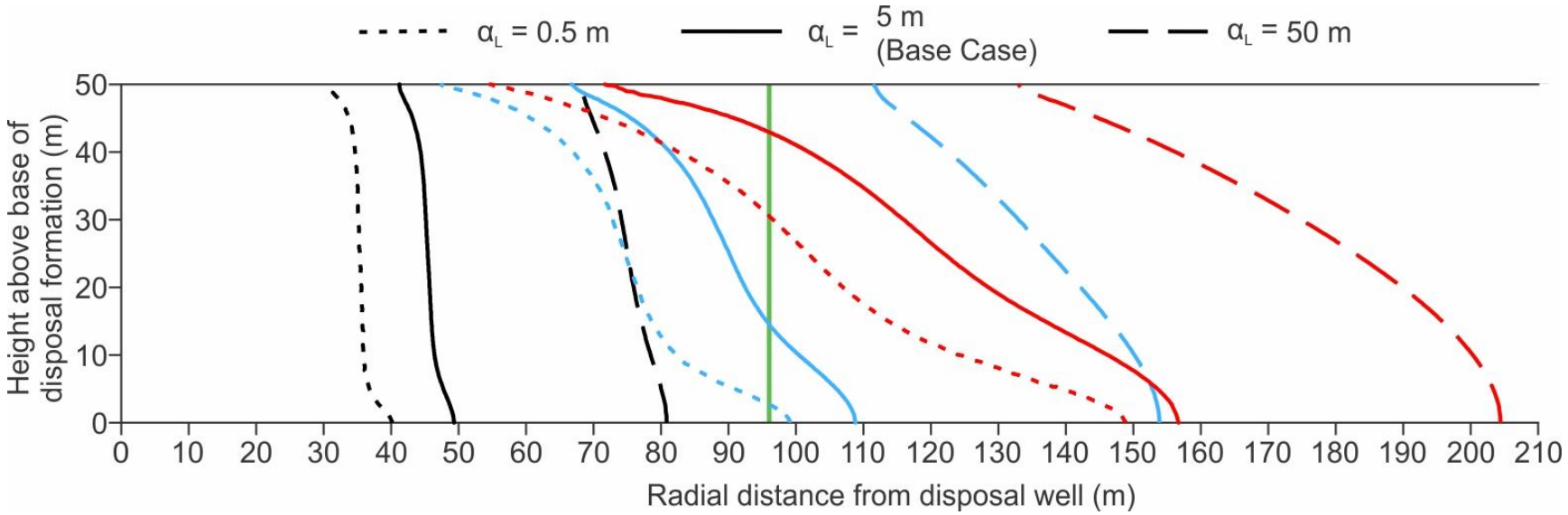

Figure 3.16. Plot showing extent of 10 g/L isohaline for different values of dispersivity at multiple time-steps. Longitudinal dispersivity values are differentiated by line style (shown along top of figure), while line color denotes the time-step: black lines represent one year of injection, blues lines represent five years, and red lines represent ten years. Green line at 96 m shows extent of wastewater plume after 10 years determined using the volumetric calculation.

Mean formation pressure along the disposal well is plotted in Figure 3.17. Differences between cases are negligible and indistinguishable given the scale used in the figure. Between the two extreme cases of 0.5 m and 50 m there is a difference in pressure of 10 kPa, indicating that dispersivity has little effect on disposal pressures.

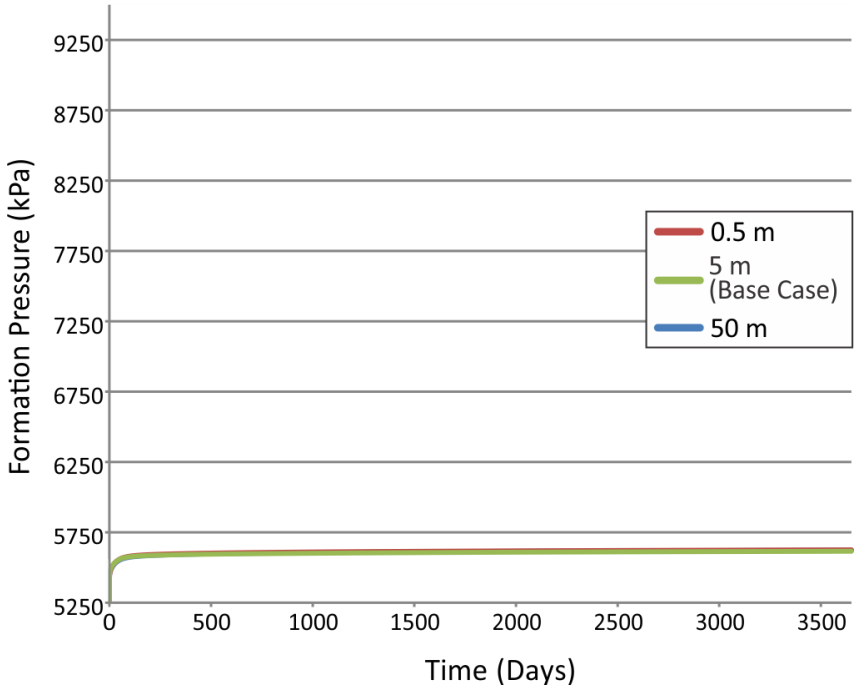

Figure 3.17. Mean formation pressure along the well for three different cases of dispersivity. Curves for all cases overlap and cannot be distinguished.

Transverse dispersivity was also investigated in greater detail by increasing and decreasing the Base Case value of 0.5 m by an order of magnitude while keeping longitudinal dispersivity constant. In doing so, disposal pressures varied by an insignificant amount (<5 kPa), and so are not plotted here. The effect of varying transverse dispersivity on solute distribution is shown in Figure 3.18. Higher values cause the plume to travel further along the top and through the middle of the formation, but not as far along the base. Solute is redistributed vertically throughout the formation, resulting in the plume travelling a smaller distance but occupying a greater volume. The variation in plume extent seen in Figure 3.18 is smaller than that observed for changing values of longitudinal dispersivity (Figure 3.16), indicating that the distribution of wastewater in the Paddy-Cadotte under the conditions modeled here is more sensitive to longitudinal dispersivity than transverse dispersivity. Higher transverse dispersivity (assuming longitudinal dispersivity remains constant) counteracts, to a minor degree, the

buoyancy effects caused by the high wastewater density, leading to a slightly better alignment with the volumetric calculation after 10 years of disposal (demarcated by the green line in Figure 3.18).

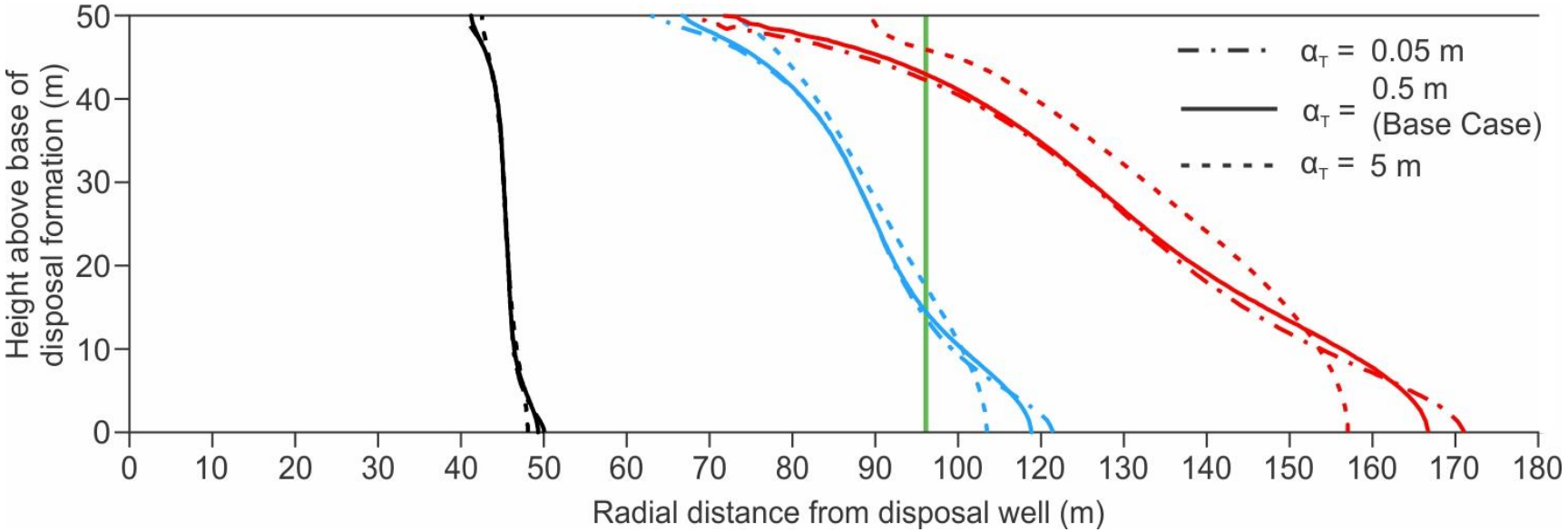

Figure 3.18. Plot showing extent of 10 g/L isohaline for different values of transverse dispersivity at multiple time-steps. Dispersivity variations between model runs are differentiated by line style, while line color denotes the time-step: black lines represent one year of injection, blues lines represent five years, and red lines represent ten years. Green line at 96 m shows extent of wastewater plume after 10 years determined using the volumetric calculation.

3.3.6. Diffusion Coefficient

The diffusion coefficient for NaCl in the Base Case was taken from the literature (1.99×10^{-9} m^2/s; Haynes, 2014). For this sensitivity analysis, simulations were run for coefficients of both 0 and 4.00×10^{-9} m^2/s. This was done to demonstrate that, even in extreme cases, diffusion does not play a large role in either plume extent or disposal pressures. No difference in formation pressure was observed between cases and so these results are not plotted or discussed here.

Simulating disposal of wastewater using the three diffusion coefficients produced no significant difference in the location of the 10 g/L isohaline after 10 years of injection. Diffusion occurs slowly, and so additional runtime was added to the models in order to assess the impact of diffusion over a greater time scale. Injection was halted after 10 years and the model run for a 30 year post-injection period. The 10 g/L isohalines for each model case at the end of this period are shown in Figure 3.19. Only minor differences are observed between cases; the two cases with the lowest diffusion coefficient overlap and cannot be differentiated, while the case with the highest value extends slightly further than the others along the top of the model domain. These results demonstrate that diffusion is a negligible factor when considering wastewater disposal in these models over the time period simulated.

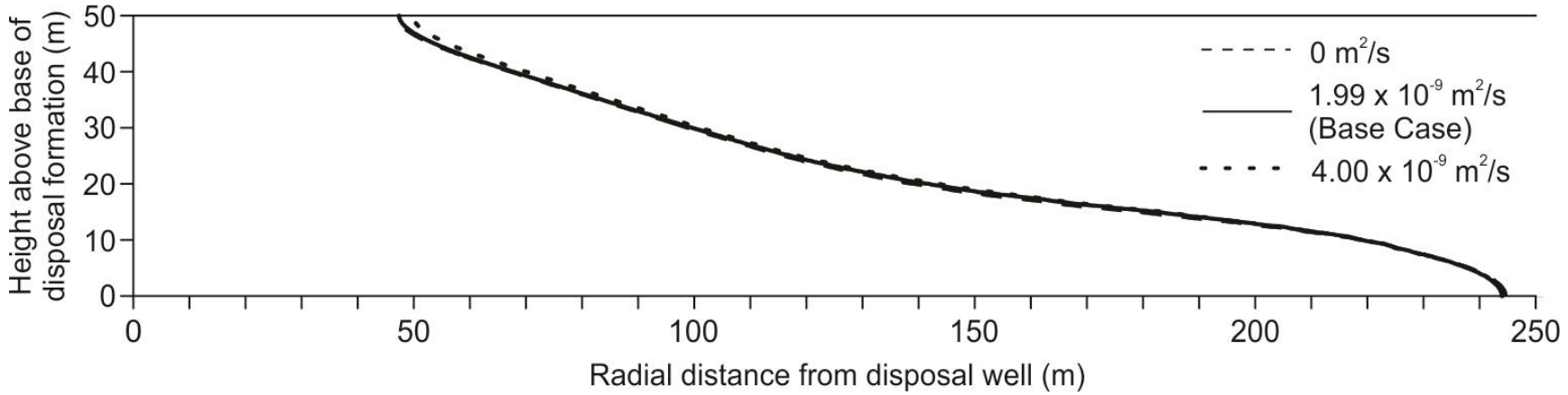

Figure 3.19. Extent of 10 g/L isohaline for different diffusion coefficients after 10 years of active disposal and a 30 year post-injection period. Cases are differentiated based on line style.

3.3.7. Permeability Anisotropy

This case investigates changes to formation permeability anisotropy. In these box models, only the maximum permeability (K_x) in the horizontal direction is assigned. The vertical permeability (K_z) is then determined by assigning the model a value for Anisotropy of Conductivity, which is equivalent to K_z/K_x. Anisotropies of 0.01-1.0 are simulated, as this is the range of values determined by Meyer (2002) for the Viking sandstone of Alberta, which is similar to the Paddy-Cadotte. In all cases, K_x is 200 mD. Disposal pressures varied by only 5 kPa between the extremes, demonstrating that permeability anisotropy has little control on formation pressures.

The extent of the wastewater plume under varying formation permeability anisotropy is shown in Figure 3.20. This parameter strongly influences the overall extent and structure of the plume; a high degree of anisotropy causes the plume to remain more upright and more closely match the plume extent estimated by the volumetric calculation, while decreasing anisotropy causes it to spread further along the bottom of the formation. In this model, gravity acts in the –z direction; thus, when the permeability value aligned with this direction increases, it causes the dense wastewater to sink towards the bottom of the formation with greater ease.

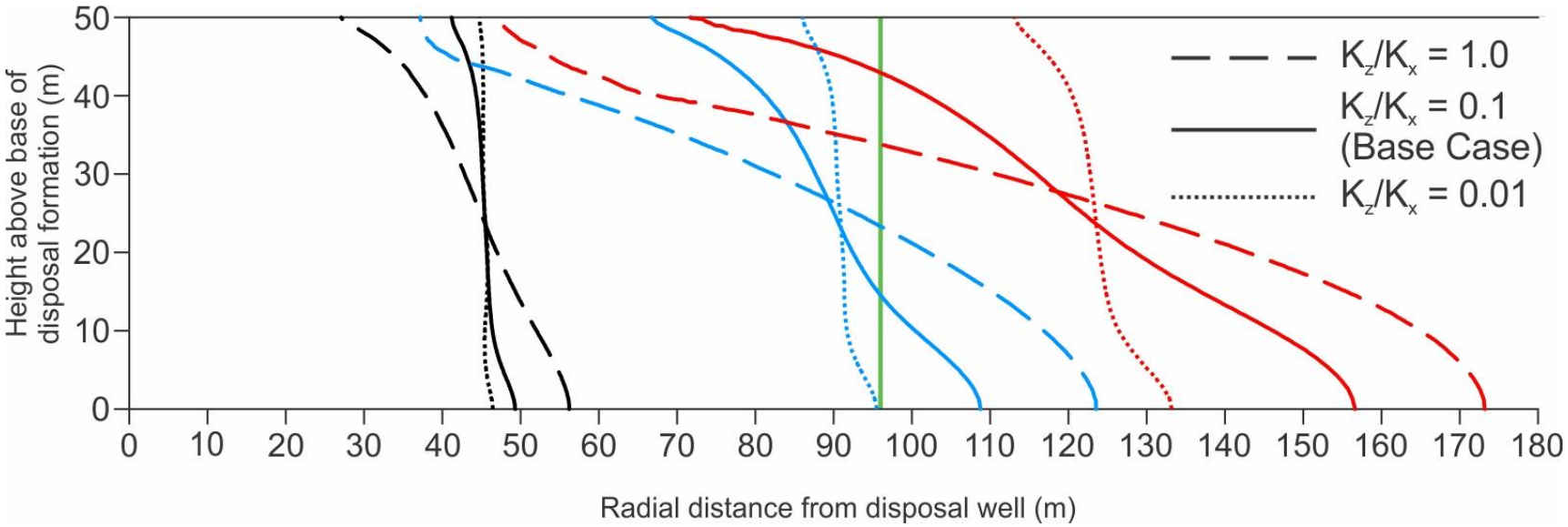

Figure 3.20. Plot showing extent of 10 g/L isohaline for different values of formation permeability anisotropy at multiple time-steps. Anisotropy is differentiated by line style (shown along top of figure), while line color denotes the time-step: black lines represent one year of injection, blues lines represent five years, and red lines represent ten years. K_x is 200 mD in all cases. Green line at 96 m shows extent of wastewater plume after 10 years determined using the volumetric calculation.

3.3.8. Formation Thickness

This case investigates the effect of formation thickness on disposal pressures and plume extent. The Base Case was designed with a thickness of 50 m, which is greater than the actual thickness of the disposal horizon, but was selected so as to better display the structure of the wastewater plumes. In this part of the sensitivity analysis, the same disposal conditions are simulated in a box model that is half the thickness of the Base Case (25 m), which is roughly equivalent to the thickness of the disposal horizon in the Paddy-Cadotte. This necessitated doubling the disposal rate assigned to the left boundary, as the number of nodes on this edge was reduced by a factor of two when the formation was thinned.

Figure 3.21 shows the effect of formation thickness on the extent of the wastewater plume. As expected, the plume extends further when the same amount of wastewater is injected into a thinner formation. As the formation thickness is halved, plume radius is increased by a factor of roughly $\sqrt{2}$, though dispersion causes this factor to vary slightly. Minor variation is observed in the structure of the plume between cases; the isohalines in the thinner formation at any given time step are less sinuous than their counterparts in the thicker formation, most likely because there is less space for buoyancy effects to manifest. Following the same method used in Section 3.3.1, the volumetric calculation estimates 61% of the modelled plume extent in the 50 m case, and 71% in the 25 m case, demonstrating that the volumetric calculation becomes more accurate when the disposal formation is thinner.

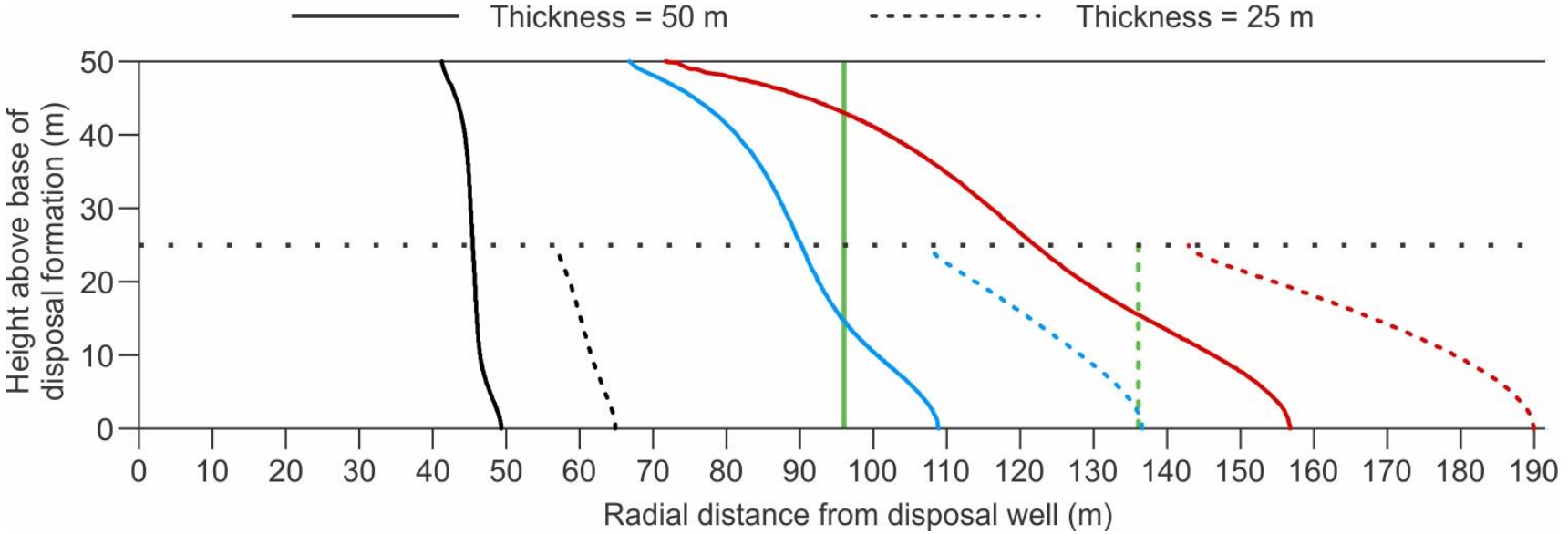

Figure 3.21. Plot showing extent of 10 g/L isohaline for different formation thicknesses at multiple time-steps. The two cases of formation thickness are differentiated by line style and the height to which the isohalines rise; the 50 m case has isohalines covering the full height of the figure, while the 25 m case isohalines reach the middle of the figure, marked by the horizontal dotted line. Line color denotes the time-step: black lines represent one year of injection, blues lines represent five years, and red lines represent ten years. Green lines show extent of the wastewater plume after 10 years of disposal determined using the volumetric calculation for the 50 m (solid line) and 25 m (dashed line) cases.

The effect of formation thickness on disposal pressure is shown in Figure 3.22, Pressures double when thickness is halved. This effect is obvious, but these results illustrate the importance of this parameter, which has the potential to strongly affect formation pressures, particularly if the formation were to abruptly thin a short distance from the disposal well.

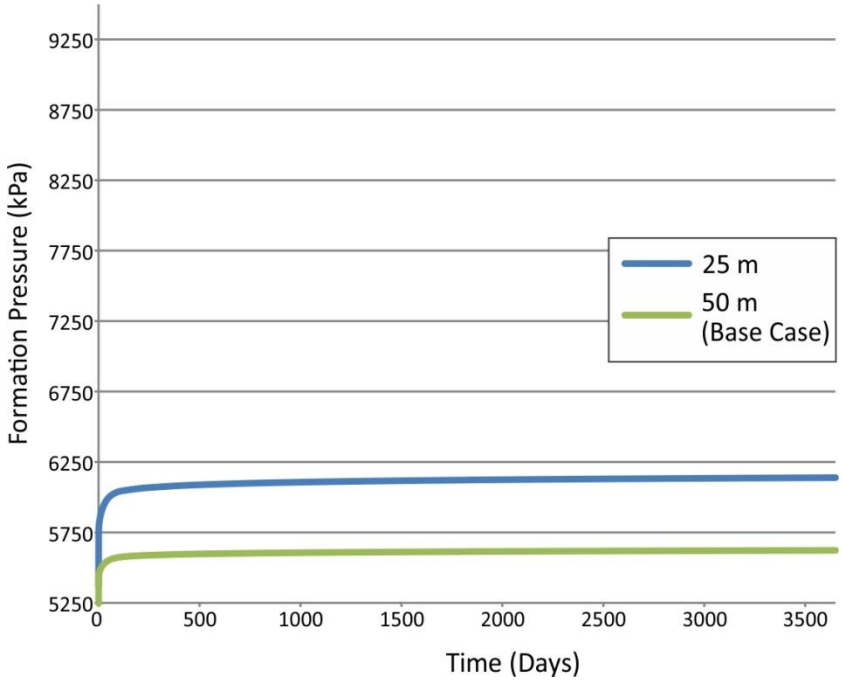

Figure 3.22. Mean formation pressure along the well for two cases of formation thickness.

3.3.9. Specific Storage

The range of specific storage investigated in this case is $1x10^{-5}$-$1x10^{-7}$ m^{-1}, an expansion of the range determined in Section 3.2.1. The concentration contours do not differ between cases and so are not plotted here.

Figure 3.23 shows the mean increase in formation pressure along the disposal well. The curves can only be differentiated in the first 140 days, and so are not plotted beyond that time. Specific storage controls the rate at which pressures increase, but not the final pressure achieved, which is the same between all cases. Lowering the specific storage results in a steeper curve, creating higher pressures at earlier time steps.

As the outflow boundary has been demonstrated to influence disposal pressures (Section 3.3.1), it is likely that the results from this case are heavily influenced by the distance from the right boundary selected for the reference head and would rise to greater values if the reference head were to be simulated further from the model edge.

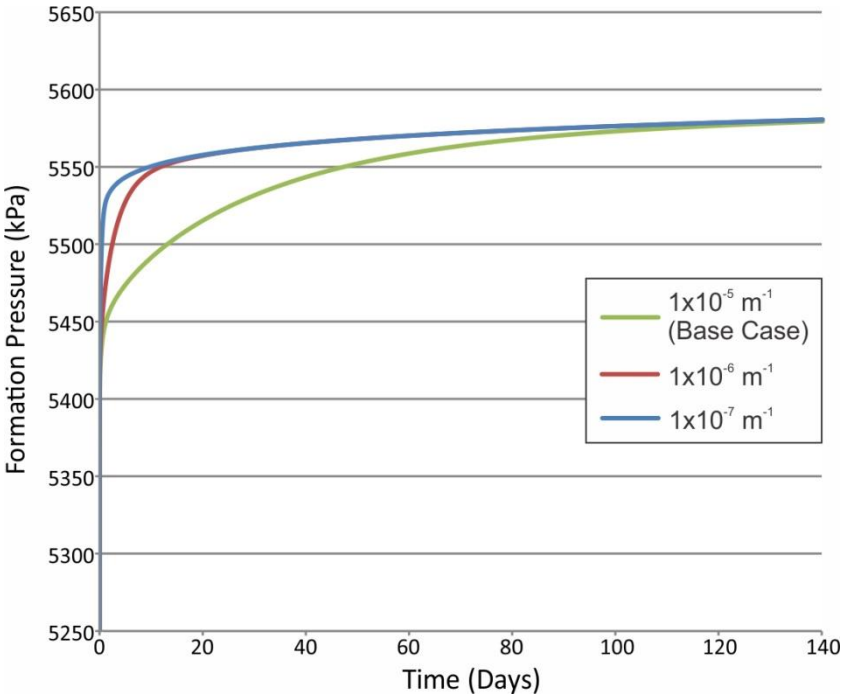

Figure 3.23. Mean disposal pressure along the well for three cases of specific storage. Curves for all cases overlap beyond 140 days and cannot be distinguished, so only the results for early time steps are shown.

3.4. Incorporation of Bounding Hydrostratigraphic Units

The model setup used throughout the sensitivity analysis is a simplification of disposal conditions within the Paddy-Cadotte. It is useful for generally conceptualizing how formation and fluid parameters affect the structure and extent of a wastewater plume, but it does not account for all of the nuances involved with wastewater disposal in the Paddy-Cadotte. In this section, the hydrostratigraphic units identified in Chapter 2, along with their associated parameter values, were incorporated into the box model for the purpose of determining how their properties influenced wastewater plumes beyond the conditions investigated in the previous box models. Unless stated otherwise, parameterization is the same as in the Base Case.

For this simulation, the model domain was rebuilt based roughly on the HSUs identified in the geophysical logs for WA 10677 (Figure 2.10). HSU 1 was assigned a thickness of 35 m, HSU 2 a thickness of 25 m, and HSU 3 a thickness of 15 m, for a total model height of 75 m. The domain was discretized using FEFLOW's triangle meshing algorithm, with smaller element size used along the disposal well and along borders between HSUs. HSU 1 and 3 were assigned the same parameters: a porosity of 0.15, a hydraulic conductivity of 1.48×10^{-7} m/s, and a specific storage of 7.4×10^{-6} m^{-1} (which was determined using Equation 3.10 using a value for sandstone compressibility correlating with a porosity of 0.15 (Hall, 1953)). HSU 2 was assigned parameter values equivalent to those used in the Base Case. Disposal was simulated only in HSU 2, assigning a well boundary condition to the nodes located along the left side of the model. An outflow boundary condition (the same as the Base Case) was applied to the entire right side of the model domain. The simulation was run for ten years of active disposal.

The results of this multi-HSU simulation are shown in Figure 3.24. The majority of the disposed wastewater remains in HSU 2, spreading preferentially along this horizon in comparison to the bounding lower permeability units. However, some wastewater does spread into the upper and lower HSUs, most notably HSU 3, as the wastewater's high density causes it to sink downwards. The overall extent of the plume is compared to the most similar case from the sensitivity analysis, that in which the formation thickness was reduced to 25 m. In this multi-HSU model, the plume extends 175 m from the disposal well after ten years of injection, whereas in the case from the sensitivity analysis the plume spread 15 m further to 190 m. This reduced plume extent is attributed to wastewater spreading into HSUs 1 and 3 as opposed to extending further along HSU 2.

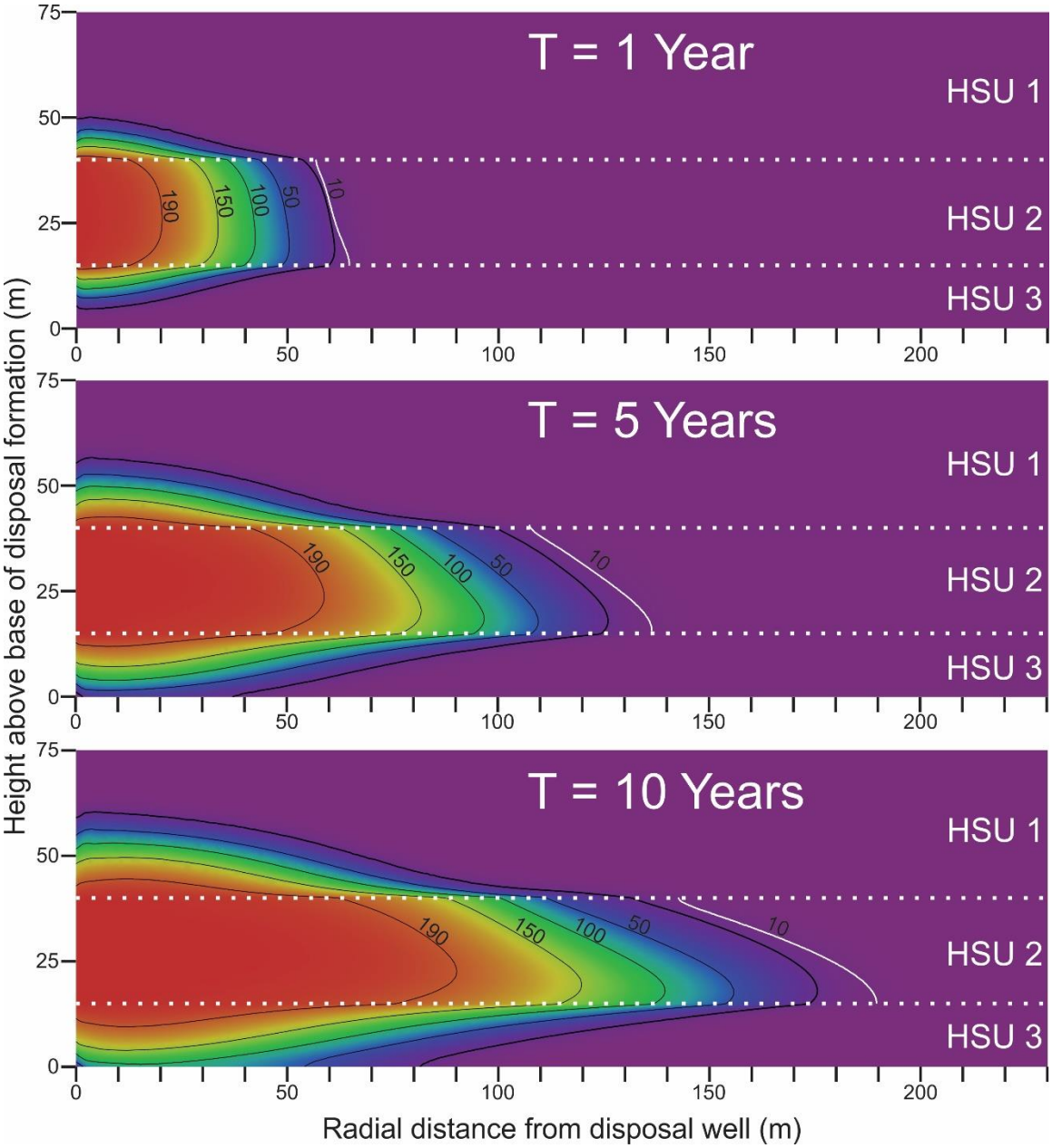

Figure 3.24. Extent of wastewater plume in multi-HSU model incorporating HSU 1, HSU 2 and HSU 3 of the Paddy-Cadotte. The plume is demarcated by select isohalines (in g/L). The two rightmost contours are the 10 g/L isohalines, with the black contour demonstrating the results for this simulation, and the white line showing the results from Section 3.3.8 in which the formation is thinned to 25 m.

The evolution of formation pressures in this model approximate those of the 25 m case in Figure 3.22, but reach a final value that is 105 kPa lower. This is attributed to the fact that, though disposal occurs over the same thickness of formation, the multi-HSU model has a greater total thickness and allows for pressures to be distributed throughout a

greater volume. It is noted that the pressure spikes at the top and bottom of the disposal well observed in the Base Case (Figure 3.4) are no longer present in the multi-HSU model. By extending the model domain above and below the injection interval, pressures are able to dissipate throughout HSUs 1 and 3, eliminating the pressure spikes as previously simulated.

3.5. Model Upscaling

An overly coarse mesh can contribute to inaccuracy in salinity distribution. Therefore, the mesh discretization chosen for the Base Case was made especially fine to display the extent of a wastewater plume in the greatest detail and with a high degree of precision. While this discretization is reasonable for a small-scale box model, requiring run times of 5-10 minutes, it is not feasible for regional-scale modeling as presented in Chapter 4. In order to determine the coarsest possible mesh for use in the regional model (i.e. one that offers a suitable compromise between simulation time and an accurate portrayal of wastewater plume extent), the mesh in the Base Case was gradually coarsened.

Four mesh variations were produced as shown in Figure 3.25. Mesh A, which was used in the Base Case, is the finest mesh, with elements adjacent to the disposal well and observation points being on the order of 0.1-0.2 m, and elements further from these features being on the order of 1.0-1.5 m. At the other extreme, Mesh D was of the coarsest resolution, with all elements being roughly 7-10 m in size. Each mesh was used to run the Base Case, with 200 g/L wastewater being injected into the disposal formation for a period of ten years.

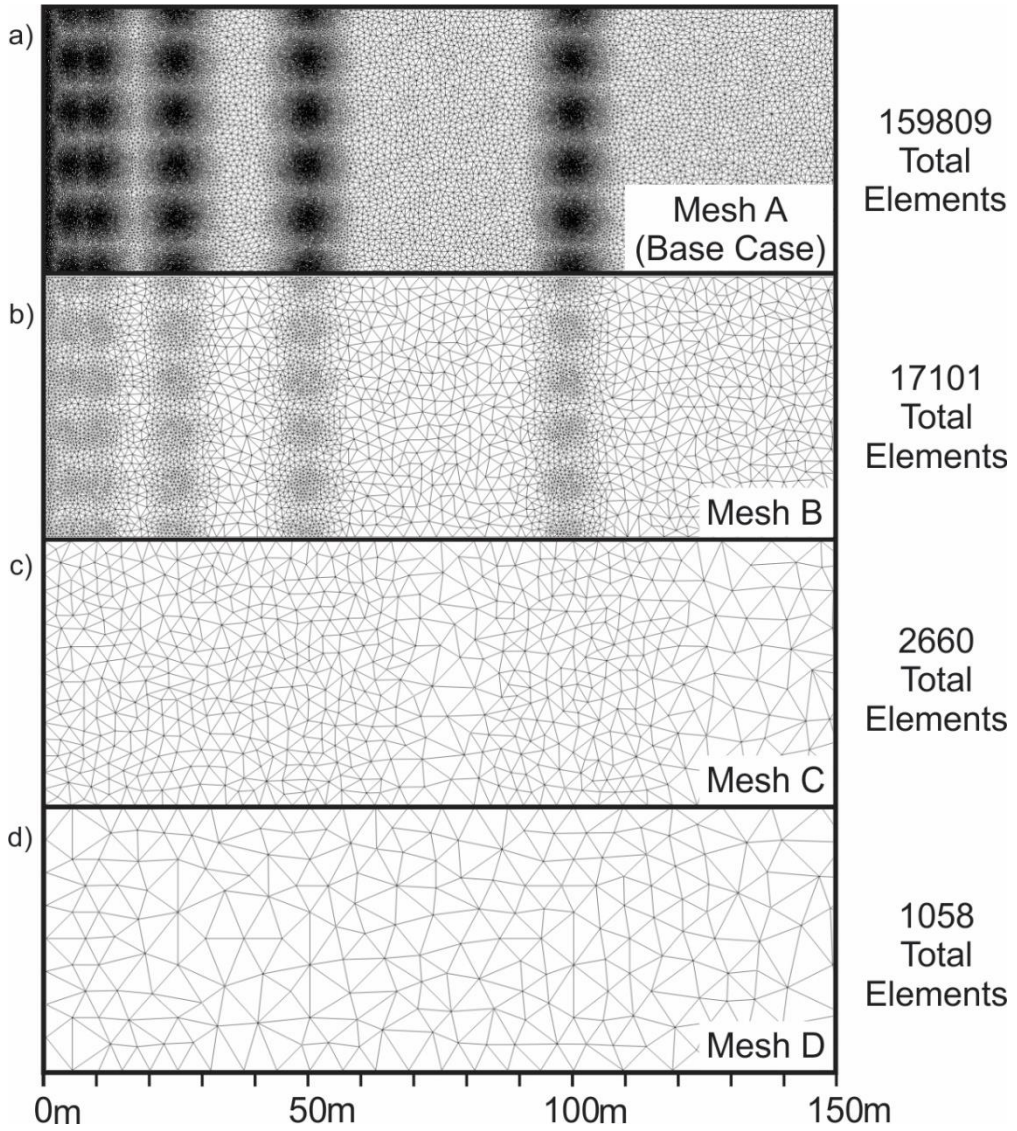

Figure 3.25. Variations in mesh discretization used to determine optimal element size for a regional model of the Paddy-Cadotte. In order to better illustrate element size, only the first 150 m out of the total 500 m model domain is shown.

The results of the above simulations were compared by plotting the extent of the 10 g/L isohaline produced in each model run (Figure 3.26). Overall, only minor variations are observed between different mesh cases. Mesh A produces the smoothest contour and the most precise transport results. Coarsening the mesh has the effect of underestimating the extent of the wastewater plume relative to Mesh A, though these variations are small. The most extreme case, Mesh D, calculated the 10 g/L isohaline to reach 163 m from the disposal well, just 3 m short of that calculated using Mesh A. These results show that, relative to the overall extent of a wastewater plume, increasing

the element size does not significantly affect the simulation results. In the case of a regional model, an element size of 10 m should be acceptable in the areas around disposal and source wells, reducing the computation time required to complete a simulation.

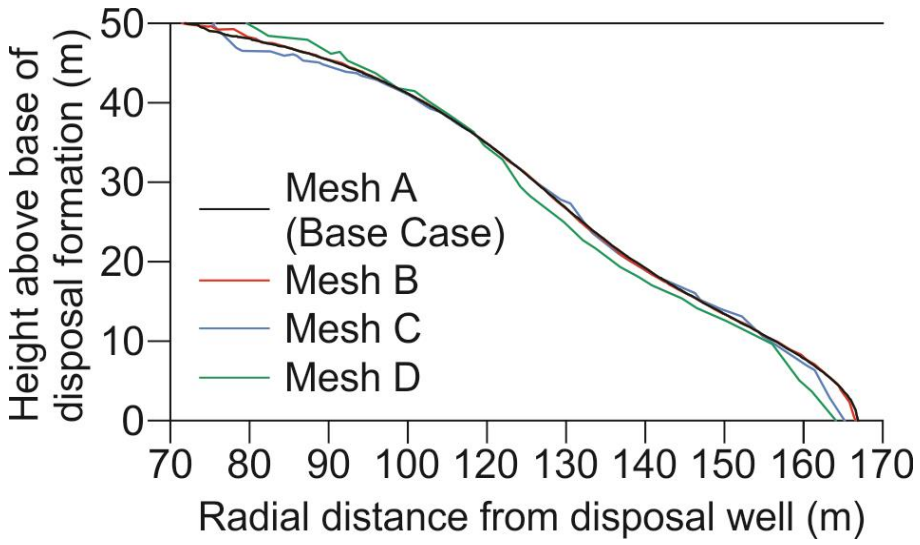

Figure 3.26. Extent of 10 g/L isohalines after 10 years of injection for differing mesh discretization.

3.6. Discussion

The sensitivity analysis outlined above serves to quantify changes in plume extent/structure and formation pressures as a result of modifications to fluid, formation, and disposal rate characteristics. The Base Case and subsequent models investigated in the sensitivity analysis were not calibrated to any particular disposal well scenario and so are not representative of site specific conditions. Additionally, the model scenarios were not designed to reflect formation pressure testing methodologies employed by industry as required by regulator and do not account for well specific factors or inefficiencies. The purpose of the sensitivity analysis was not to predict the absolute change in pressure or plume extent for a given well, but rather to provide insights regarding the relative influences of the variables investigated on wastewater plume configuration and extent as well as potential effects on reservoir pressure for the scenarios modeled. These insights are discussed below.

The box models presented in this chapter are highly simplified, but this was intentional so as to best characterize the effect of formation and fluid characteristics on the plume

extent and formation pressures. Simplifications include constant disposal rates (whereas in reality these rates vary considerably from month to month), a flat disposal formation (necessitated due to the nature of the projection type chosen), and a homogeneous permeability and porosity distribution throughout the model domain. In reference to the latter, an attempt was made to use a FEFLOW plug-in to stochastically generate a porosity and permeability field for the model based on geostatistics gathered from core permeability measurements from the Paddy-Cadotte. Unfortunately, the Paddy-Cadotte is data-sparse and meaningful statistics could not be determined, and so the stochastic modeling effort was abandoned.

3.6.1. Plume Extent

During active disposal, the volumetric calculation can be used to obtain a general estimate of plume extent, predicting the location of the advective front within which the highest salinities are observed. However, when disposal ends buoyancy effects begin to dominate and the plume sinks to the bottom of the disposal formation. The majority of the injected saline wastewater is still observed to remain within the extent predicted using the volumetric calculation (Figure 3.2).

The results of the Base Case and subsequent sensitivity analysis demonstrate that the volumetric calculation does not accurately predict the extent of the disposed wastewater, primarily because it does not account for dispersivity and buoyancy related effects. The significance of this is debatable though, as the need for accuracy will vary depending on the situation, and often there will not be enough data available to perfectly model a deep reservoir used for disposal. If a conservative approach for estimating plume extent is sufficient, the results from the permeability and dispersivity sections of the sensitivity analysis (the two cases that show the greatest difference between the modeled extent and volumetrically calculated extent) show that the estimate of plume extent obtained from the volumetric calculation can be increased by a factor of 1.5 to 2.0. However, this adjustment would only be valid during active disposal as the wastewater plume is observed to travel four times further than the volumetric estimate after the disposal well had been shut down for 20 years. Therefore, if a long term estimate of plume extent is required, the volumetric approach is inadequate. It is noted, however, that these simulations did not account for other influences, such as sloping formation topography, regional hydraulic gradient, or the influence of nearby wells, all of which could cause the

plume structure and extent to deviate from those observed in the models presented in this chapter.

Estimating plume extent using the volumetric calculation more closely matches the results in the multi-HSU model (Section 3.4) than in the models used in the Base Case and sensitivity analysis, all of which had a single HSU. This is because, when using Equation 1.1 to estimate plume extent, only the thickness of the disposal horizon is used (20-25 m), as opposed to the entire thickness of the formation (>50 m). The equation assumes that wastewater will remain in the higher permeability unit, but Figure 3.24 shows that this is not the case. Some wastewater will be pushed up into HSU 1 or sink into HSU 3, resulting in a plume that does not travel as far through the disposal horizon, thereby reducing the error of the volumetric calculation.

3.6.2. Formation Pressures

The pressure results presented above are not meant to be used to inform disposal practices for any particular well as there are multiple factors, such as well inefficiencies and variable formation thickness, that were not investigated in the sensitivity analysis and that have the potential to influence disposal pressures. As such, modeling results are not meant to replace wellhead monitoring or annual pressure testing performed on a disposal well.

Of the parameters investigated, injection rate and formation permeability were found to have the strongest effect on formation pressures at the disposal well. The 20 mD permeability and 1000 m^3/day injection rate cases produced the highest disposal pressures observed in the sensitivity analysis, over 8000 and 9000 kPa, respectively. These have the potential to be greater if well inefficiencies are incorporated, and so were discussed in terms of the 90% formation fracture pressure limitation imposed by the BCOGC (see Section 1.1.3). The results from these two parameter cases, along with other parameters found to influence disposal pressures to a lesser degree, can be used to conceptualize a scenario in which the exceedance of the 90% formation fracture pressure limit is most likely, namely the injection of high salinity wastewater at a high rate into a thin, low permeability formation.

Another of the pressure regulations concerning disposal well operations in BC is the 120% IVRP limitation. Under this regulation, background formation pressures are not to exceed 120% of the pressures that existed in the formation prior to any water extraction or wastewater injection. This pressure is measured annually during a falloff test in which the disposal well is temporarily shut down, and formation pressures measured in the well are extrapolated to a 60-day value. The sensitivity analysis presented in this chapter did not incorporate this fall-off test, and so cannot be used to comment on the potential for disposal operations to exceed the 120% IVRP limit. The pressure results from the Base Case scenario are the most applicable to this regulation, as the simulated disposal in this case is stopped after a year of operation and the resulting pressure fall-off curve is shown in Figure 3.5. The 120% IVRP limit is never reached in this case, even at the end of disposal, but pressures are observed to return to IVRP after roughly 100 days. Parameters that could potentially affect the rate at which pressures fall off include specific storage and permeability. As shown in Figure 3.23, a lower specific storage would result in a faster drop in pressure. Increasing permeability would allow pressures to propagate through the formation more quickly, resulting in a steeper drop in formation pressure after disposal is stopped.

3.6.3. Applicability to Study Area Model

The modeling results presented in this chapter demonstrate potentially important influences of permeability and dispersivity on plume extent; dispersivity strongly influences plume extent while permeability affects both disposal pressures and plume extent. Unfortunately, the Paddy-Cadotte has only became economically interesting within the past few years, when it was identified as a good candidate for wastewater disposal, and so there are relatively few data available and parameterization of these two important variables is difficult.

The models presented in this chapter all used a homogeneous permeability value, simply because there are too few permeability measurements available in the Paddy-Cadotte to confidently simulate any form of heterogeneity. Permeability values can be broadly assigned to the different HSUs identified in the formation, but this is a large simplification and will likely lead to uncertainty in the study area model. Any change in permeability at some distance from a disposal well would lead to deviation from the

idealized plumes and pressure curves obtained from the homogeneous permeability models from the sensitivity analysis.

Dispersivity is even more difficult to parametrize than permeability, as it can only really be determined by taking field measurements of plume transport, and this is prohibitively expensive to do in a formation as deep as the Paddy-Cadotte. Instead, literature values for dispersivity will be used when parameterizing the study area model (see Chapter 4), which is recognized as a potentially large source of error in terms of plume extent.

Any abrupt thinning or thickening of the disposal formation that is not accounted for in the study area model could lead potentially significant inaccuracies for predictions of plume extent and formation pressures using the numerical modelling approach, as shown in Section 3.3.8. Fortunately, the topography of the Paddy-Cadotte is well constrained due to the number of oil and gas wells that pass through it to access the Montney, so any changes to formation thickness can easily be incorporated into the study area model. Structural traps, such as folds or impermeable faults, that have the potential to act as impermeable boundaries and increase formation pressures (as in Section 3.3.1) are not present in the area, and modeling the disposal in this formation is made easier than other more structurally complicated areas such as the Appalachians. However, there still remains the potential for stratigraphic traps, such as layer pinchouts, that may be present within the Paddy-Cadotte. Such traps would likely affect plume extent and disposal pressures. The most evident stratigraphic trap is the pinching out of HSU 2, the main disposal horizon, and this pinchout will be incorporated into the study area model.

Chapter 4.

Study Area Model

This chapter details the construction, calibration, and results of a numerical model of historical and future wastewater disposal and water source wells operating in the Paddy-Cadotte in the study area. The goal of this model is to understand how factors, such as a regional hydraulic gradient, formation dip, and interference between wells, potentially influence the migration of disposed wastewater and pressures generated during injection, neither of which could be simulated using an axisymmetric projection. Unless stated otherwise, model parameterization and settings are the same as those used in the Base Case in Chapter 3.

4.1. Model Development

4.1.1. Model Design and Construction

Model Domain

The model domain was initially intended be relatively small, roughly 20 km x 20 km and centered on the well field shown in Figure 2.2, but results from the axisymmetric box models in Chapter 3 indicated that this could potentially lead to boundary conditions influencing pressure results. The selection of boundary conditions to constrain the model domain was complicated because topographic or hydraulic features, such as topographic divides or rivers, which are usually used when designing near-surface models, are not useful for defining boundary conditions in deep disposal formations. Therefore, the 600 m hydraulic head contour line produced by Petrel Robertson and Canadian Discovery (2011) for the Cadotte (Figure 2.9, top) was chosen to define the northern, western, and southern parts of the domain, as it was the most distal feature available and so would have the least impact on results. The eastern side of the model was defined using the BC-Alberta border, as the data used in this study are only available for BC. The outline of the model domain is shown in Figure 4.1.

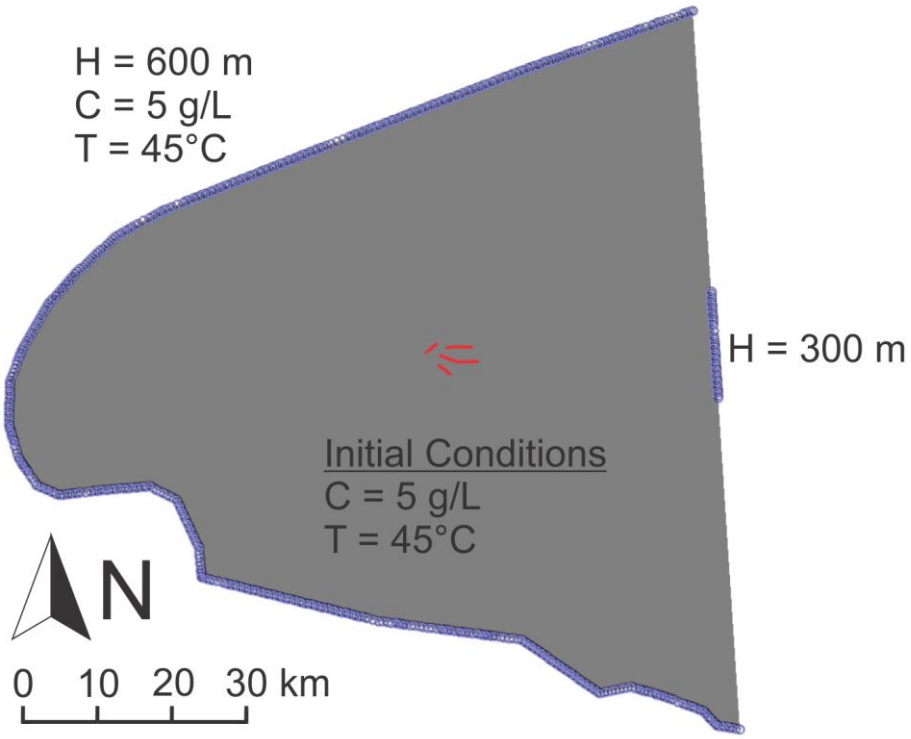

Figure 4.1. Model domain of study area showing boundary and initial condition values. The blue lines along the north, west, south and center east of the domain show the location of constant head (H), concentration (C), and temperature (T) boundary conditions defined later in this section. Red lines in the center of the domain show the location of the source wells from Figure 2.2.

The top and bottom of the model represent the low permeability Harmon and Shaftesbury shales, which are considered to be completely impermeable for the purposes of this study. These surfaces were defined by extracting formation elevation data from Accumap (IHS Energy, 2016) for the top of the Harmon (n = 2204) and Paddy (n = 2049) for all wells within the model domain. These XYZ data were imported into FEFLOW and surfaces were created by interpolating between the points using the kriging method. Some anomalous points were present, producing sharp increases or decreases in elevation over a short distance, and were assumed to be a result of either data entry error or misidentification of the formation tops. These points were manually removed in order to produce smoother surfaces and increase the stability of the model.

Mesh Discretization

Mesh discretization was guided by the locations of the disposal and source wells, which were imported as point and line data, respectively, because mesh discretization was

performed in a 2D map view in which the vertical disposal wells appeared as points and the horizontal source wells as lines. The Triangle mesh builder setting was used, which produced finer discretization in the areas surrounding the disposal and source wells. Results from Chapter 3 indicated that an element size of up to 10 m would be sufficient to produce accurate solutions to the mass and heat transport equations, and so elements around the wells were initially created at this scale. However, early model runs produced large numerical oscillations with elements of this size, and so the mesh was refined in the area around the wells to a final size of roughly 3 m. Further from the well field, where more accurate solutions were not required, element size was approximately 300 m. After the element size was finalized, FEFLOW's mesh smoothing feature was used to correct for any irregularly shaped elements produced during mesh generation. The final mesh discretization (Figure 4.2) had 3.6 million elements.

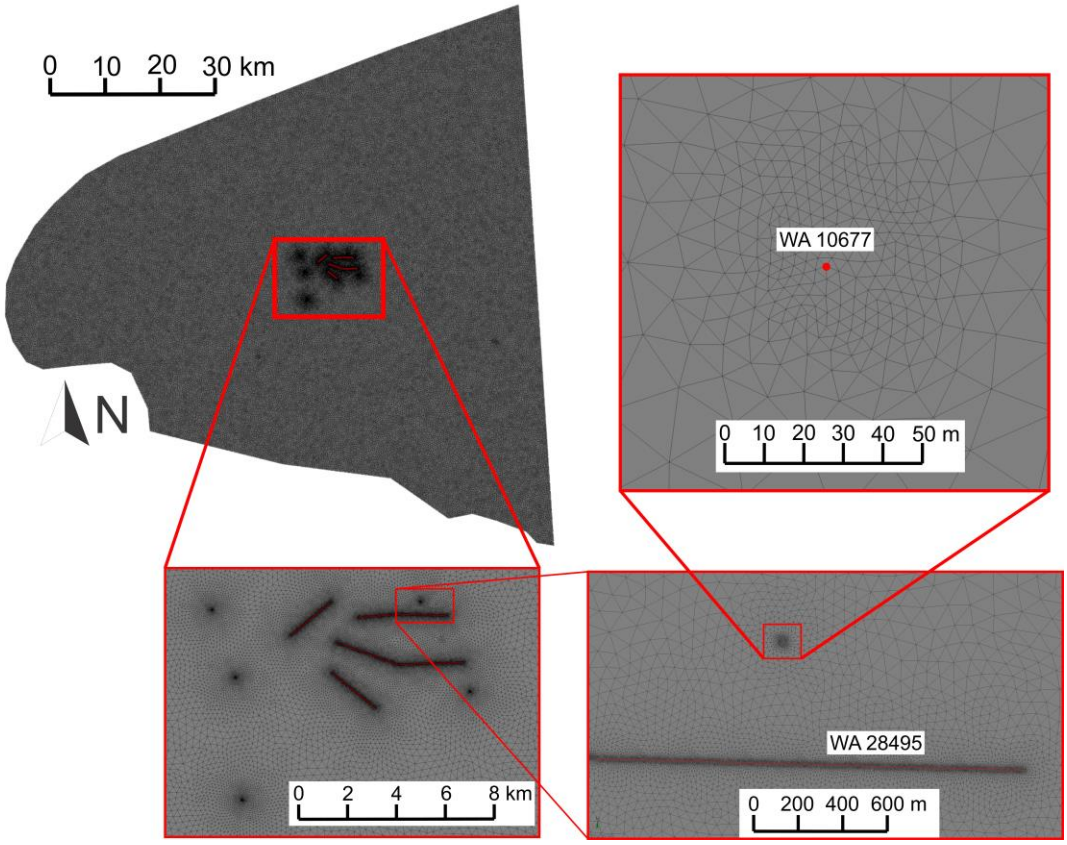

Figure 4.2. Mesh discretization in the study area model.

Layer Geometry and Vertical Mesh Discretization

To define the boundaries between the hydrostratigraphic units identified within the Paddy-Cadotte, 385 neutron and density porosity logs within the study area were

manually checked for a zone of higher porosity indicating the presence of HSU 2, the main horizon targeted by most disposal wells and all source wells. When this HSU was identified in a log, the top and bottom elevations of the high porosity zone were noted, along with the coordinates of the well (Appendix E). When the high porosity zone was not present in a log, it was marked as absent and assigned a thickness of 0 m at that location. In this way, the extent and thickness of HSU 2 could be estimated. The XYZ point data for the top and bottom of HSU 2 were imported into FEFLOW, and the kriging method was used to interpolate between the points to create continuous surfaces. In areas where HSU 2 had a thickness of 0 m, the unit was assigned a thickness of 0.1 m and given the properties of the overlying unit (HSU 1). In this way, FEFLOW was used to simulate the unit pinching out. The overall extent of HSU 2 is shown in Figure 4.3.

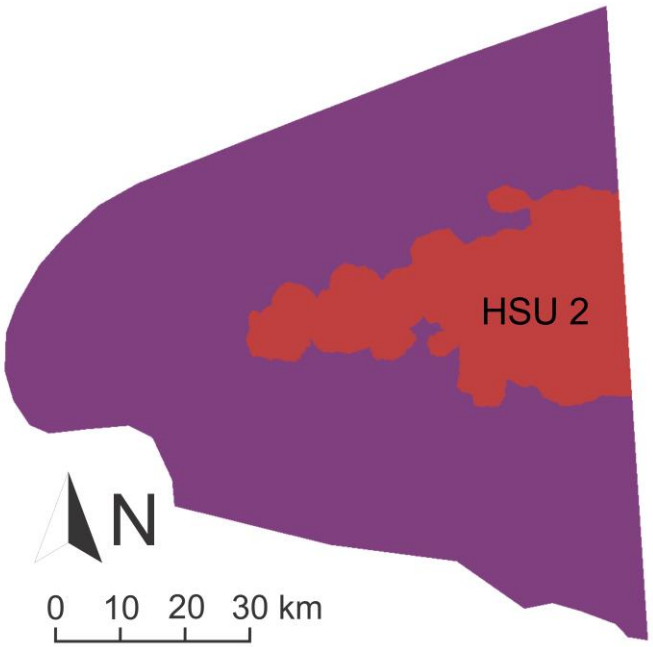

Figure 4.3. Extent of HSU 2 (red) determined using neutron and density porosity logs.

Incorporating HSU 2 into the model resulted in a total of three layers, one for each HSU. Finer vertical discretization was desired within each HSU in order to increase the accuracy of heat and mass transport solutions, and so additional slices were created within each layer (distributed evenly), increasing the total number of layers in HSU 1 to six, in HSU 2 to four, and in HSU 3 to four. Resulting vertical discretization ranged from 0.1 m (where HSU 2 pinched out) to 10 m (in HSU 1).

The source wells in the model were intended to be simulated as a continuous series of discrete nodes, each of which would have a well boundary placed on it (see below), meaning that the nodes making up each well had to exist on the same slice. Since the slice elevations within each HSU were generated automatically and evenly distributed within the layer, they did not automatically coincide with elevations of the water source wells. Therefore, elevations of the nodes along sections of the slices representing the water source wells were manually adjusted to be consistent with the actual water source well elevations (Figure 4.4). This initially resulted in a jagged, irregular slice geometry in the areas near the source wells, and so these slices were smoothed in 3D using FEFLOW's automatic mesh smoothing feature.

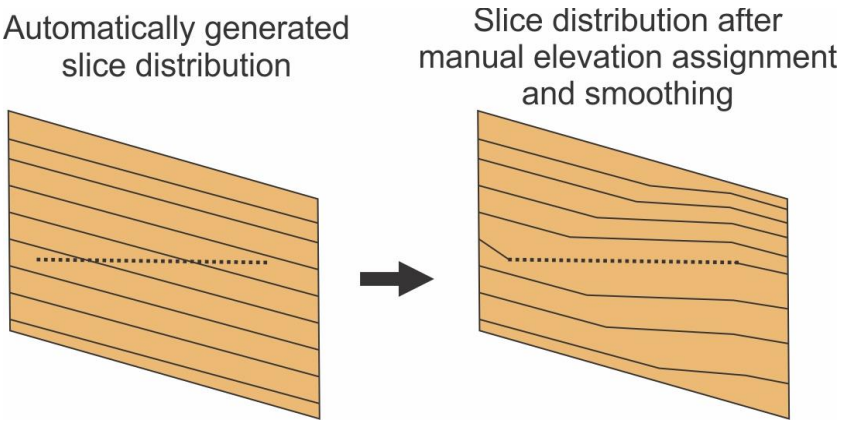

Figure 4.4. Example of the slice correction method used to more accurately model source well elevation. Solid lines indicate slices. Dotted line shows the actual elevation of the source well. This figure is for illustrative purposes only; HSU 2 in the model contains only three slices (four layers).

Boundary Conditions and Initial Conditions

The boundary conditions assigned to the model were shown in Figure 4.1. The north, west, and south boundaries were assigned a constant head boundary condition of 600 m (Figure 4.1), based on the hydraulic head contours from Petrel Robertson and Canadian Discovery (2011, Figure 2.9). It is recognized that using equivalent freshwater heads to define regional flow can produce inaccuracies, particularly when variations in temperature and salinity are not incorporated (Bachu, 1995). Additionally, equivalent freshwater heads cannot be used to determine vertical flow in a formation, only horizontal flow (Bachu, 1995). However, due to the low data availability in the Paddy-Cadotte, the equivalent freshwater head contours from Petrel Robertson and Canadian Discovery (2011) are the best data available with which to define boundary conditions,

and so are used in spite of the potential errors that they may introduce. The mid-portion of the eastern side of the model, representing the BC-Alberta border, was assigned a constant head value of 300 m, again consistent with the hydraulic head contours from Petrel Robertson and Canadian Discovery (2011, Figure 2.9). The remainder of the eastern edge of the model domain was assigned a no-flow boundary, because the hydraulic head maps indicate that groundwater flows parallel to this portion of the border (Petrel Robertson and Canadian Discovery, 2011; Figure 2.9). Regional hydraulic head contours are commonly used to define the domain boundary conditions (Anderson et al., 2015). In this study area, these were the only available hydraulic features in the formation that could be used to define boundary conditions along the model edges. In addition, it is recognized that hydraulic heads towards the south of the Cadotte are greater than 600 m, but this area is also hydrogeologically complex, data sparse, and far from the study area, and so the boundary condition in this area was simplified. As a result, calibration to drill stem test data in this area was not attempted (see Section 4.1.2). No initial head condition was assigned within the model domain. Instead, the head distribution was determined based on steady state calibration runs discussed in Section 4.1.2.

Salinity of the formation water in the Paddy-Cadotte is variable, ranging from 40 g/L in the south of the model area to 5 g/L in the study area (Figure 2.16). To simplify the model, and since results from the model are only taken from within the study area, a homogenous salinity of 5 g/L was assigned to the entire model domain as an initial condition (Figure 4.1). A constant mass-concentration boundary condition of 5 g/L was assigned along the entire north, west, and south model edges (Figure 4.1). No mass boundary was assigned to the eastern edge.

The temperature of the formation waters within the Paddy-Cadotte is roughly 45°C (James Armstrong, Encana Corporation, personal communication), and so this value was assigned homogenously within the model domain as an initial condition. A constant temperature boundary condition of 45°C was assigned along the entire north, west, and south model edges (Figure 4.1). No heat boundary was assigned to the eastern edge.

Model Parameterization

Parameter values unique to a particular HSU are summarized in Table 4.1. Values for permeability (and thus hydraulic conductivity, related through Equation 3.7) and porosity

for each HSU were determined based on core data from WA 00019 (Figure 2.11), though this core only had measurements for HSU 1 and 2. HSU 3 was initially planned to be assigned the same parameter values as HSU 1 as it was felt that they were similar; however, discussion with the Encana Corporation (Katherine Murphy, Encana Corporation, personal communication) revealed that HSU 3 is roughly an order of magnitude less permeable than HSU 1, and also of lower porosity, due to the presence of interbedded muds and sands. Permeability in the Z-direction for all units was assumed to be an order of magnitude lower than in the X- and Y-direction. Specific storage for each unit was calculated using Equation 3.9, which incorporated the value of porosity for that unit and an aquifer compressibility value related to said porosity through Hall's correlation for sandstones (Hall, 1953).

Table 4.1. Parameter values assigned to each HSU in the study area model.

HSU	Permeability (mD)	Hydraulic Conductivity (m/s)	Porosity	Specific Storage ($x10^{-6}$ m^{-1})
1	20	1.48E-07	0.15	6.6
2	200	1.48E-06	0.25	5.95
3	2	1.48E-08	0.05	9.9

The salinity of the wastewater simulated as injection at the disposal wells was 260 g/L (discussed below), which was calculated to have a density of 1157.5 kg/m^3 (Dreisner and Heinrich, 2007). Using Equation 3.8 and a density of the reference fluid of 999.8 kg/m^3, a density ratio of 0.157 was calculated and applied to the entire model domain.

Mass and heat longitudinal dispersivity values were set to 400 m, a value that was suggested by the FEFLOW support staff; the value is greater than any values investigated in Chapter 3 and was suggested so as to increase the stability of the model. Dispersivity has been shown to be scale dependent (Gelhar et al., 1992), and since the study area model is larger than the axisymmetric models a greater dispersivity value is justified. However, there are no contaminant transport data available for the Paddy-Cadotte that can be used to better constrain this parameter, and it is recognized that this is potentially a source of error (see Section 4.3.2). Transverse dispersivity was assigned a value one order of magnitude lower than longitudinal dispersivity.

In initial transient model simulations, oscillations in heat and mass were observed around the disposal wells. This could have been resolved by increasing the

discretization around the wells, but model run times were already on the order of 18 hours. Therefore, in order to keep simulation times reasonable, increasing the mesh resolution was not attempted. Instead, full upwinding was activated in the model. Upwinding is a process that dampens numerical oscillations, but does so at the expense of accuracy as it adds artificial numerical dispersion to the model (Diersch, 2013; Figure 4.5). The implications of invoking upwinding in this model are that the concentrations near the well may undergo a more smoothed increase and that the plume extends further than it would otherwise for the same parameterization.

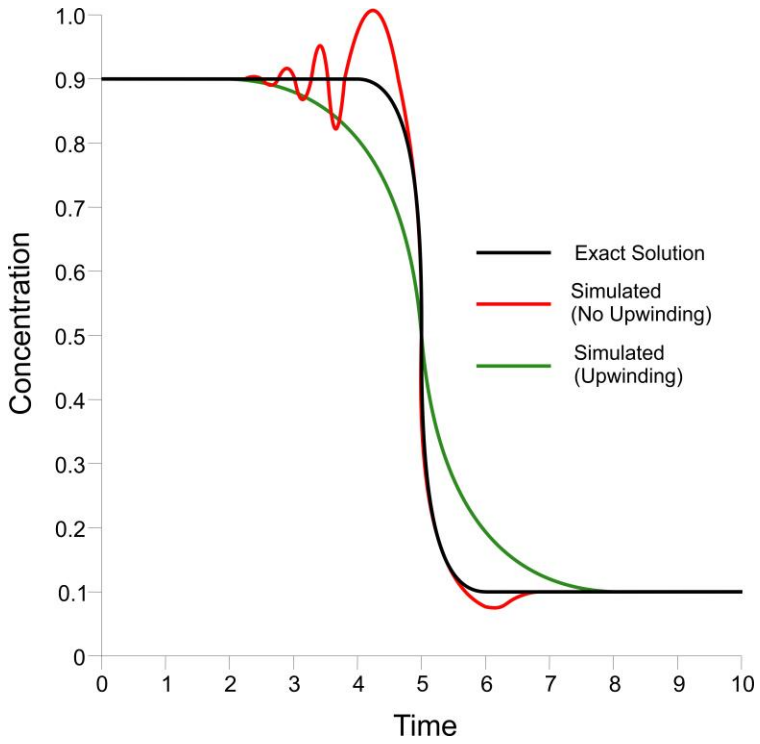

Figure 4.5. Example of using upwinding to dampen numerical oscillations in a synthetic mass transport scenario.

4.1.2. Steady State Calibration

In order to produce an initial head distribution for the transient model in which disposal could be simulated, the model was calibrated to pressure measurements from the Paddy-Cadotte under steady state conditions. No concentration data with which to help calibrate the model were available from the wells at which the pressure measurements were taken, and so the calibration lacks vigor. The pressure measurements used for calibration were taken using DSTs in the Paddy-Cadotte, and were compiled and converted to hydraulic head by Petrel Robertson and Canadian Discovery (2011). A total

of 57 data points were available within the model domain; however, 13 were located towards the south of the Paddy-Cadotte (Figure 2.9), an area that is hydrogeologically complex and difficult to calibrate accurately given the sparsity of data in this location. For this reason, calibration in the south was not attempted and these 13 points were excluded. This left a total of 44 calibration points: 18 in the Cadotte and 26 in the Paddy. Additionally, IVRP pressures at the middle of the perforated interval of each disposal well were determined using each well's approval letter (Appendix B) and converted to calibration points. When calibrating the model, more emphasis was placed on these five points than on the other 44 as they are found within the study area. In total, 49 XYZ calibration points with associated hydraulic head values were imported to the model as observation points.

In initial model calibration runs, the permeability of HSU 2 was increased to 300 mD and the constant head boundary condition along the north, west, and south of the model domain was reduced to 550 m. This provided a good calibration result, but Encana geologists felt that the permeability value assigned to HSU 2 was unrealistic (Katherine Murphy, personal communication), and so it was lowered back to 200 mD and permeabilities in all HSUs were kept constant throughout calibration. Instead, only the north, west, and south head boundaries mentioned above were modified. Lowering this head boundary to 440 m produced the best model calibration results (Figure 4.6).

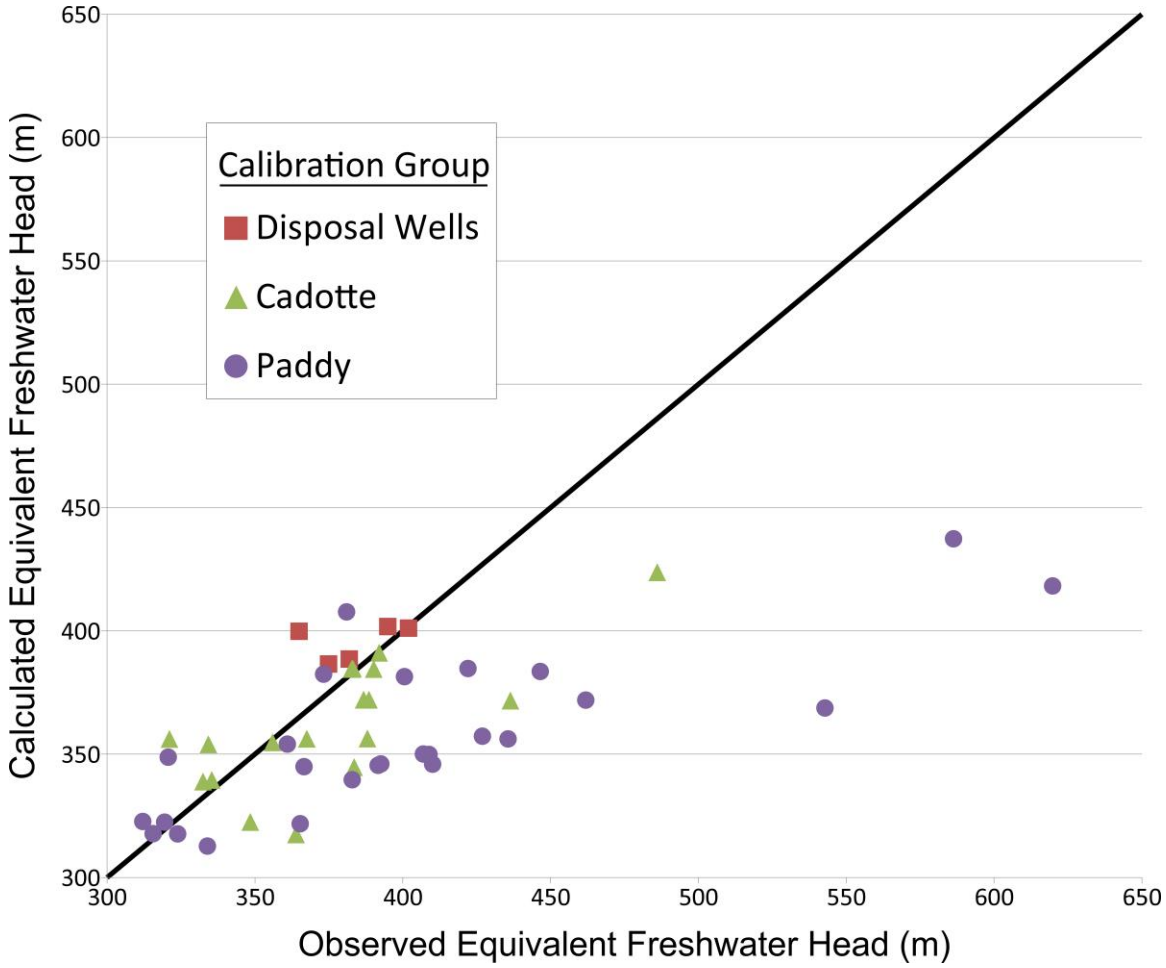

Figure 4.6 **Steady state calibration results for hydraulic head in the study area model. Calibration points in the southern Paddy-Cadotte are not included in this figure.**

The metric used to gauge model calibration is the normalized root mean square (NRMS) error. This is a measure of the deviation of computed values at the observation points from the observed values divided by the difference between the maximum and minimum values within the data set considered. Typically, a NRMS error of <10% is considered to be representative of a well calibrated model (Anderson et al., 2015). The NRMS errors for the study area model, categorized by data type (Paddy, Cadotte, Disposal Well), are presented in Table 4.2. The NRMS error for the study area model could not be reduced below 10%, for reasons discussed below. Overall error for the model was 18.4%, while the error for the disposal wells was 45.6%. This value is high, but it is noted that the RMS for the disposal wells is only 17 m, much better than the Paddy or Cadotte data points. The NRMS error for the disposal wells is so high because this data set is

comprised of only five points, and so the difference between the maximum and minimum values is low.

Table 4.2. Data used to calculate NRMS error for the various hydraulic head calibration data groups.

	Cadotte	Paddy	Disposal Wells	All Points
Max. Value (m)	486.1	619.9	402.0	619.9
Min. Value (m)	321.1	312.2	365.0	312.2
Range (m)	165.0	307.7	37.0	307.7
RMS (m)	29.6	73.4	16.9	56.7
NRMS Error (%)	18.0	23.9	45.6	18.4

Model calibration could be improved if spatial variations in permeability were better understood. However, data sparsity in the Paddy-Cadotte precluded any justifiable modifications to the permeability that would result in a better fit of the calculated head values to the observed values. The permeability values recommended by Encana are considered the most reliable, and so permeabilities were not changed from the recommended values. Additionally, the salinity value applied to the entire model (5 g/L) well reflected conditions in the study area, but was not appropriate for the rest of the model (which were as high as 40 g/L). This potentially caused the calculated heads in these areas to be lower than the observed values. If the more accurate, higher salinities had been incorporated into the model, the greater fluid density would have caused hydraulic heads to be slightly higher and thus more consistent with the observed results. Ultimately it was felt that the potentially poorer calibration results outweighed the difficulty that would arise from attempting to accurately model formation salinity in areas further from the well field. The final steady state calibration results are recognized as not being optimal, but are the best that could be achieved given the data available.

4.1.3. Historical Transient Simulation and Forecasting

The calibrated steady state model was converted to a transient model with the calibrated head values set as initial conditions and the disposal and source wells activated. For source wells, this meant assigning a well boundary condition to each node making up a given well, ranging from 300 to 800 nodes depending on the well's horizontal length. The total pumping rate for that well was then divided by the number of nodes in order to

distribute the rate evenly amongst the nodes. The number of nodes per source well is greater than the number of actual perforations in the well, but was felt to be reasonable in distributing source water extraction along the length of the well.

Disposal wells were modelled using FEFLOW's multilayer well boundary condition. This boundary condition consists of a Discrete Feature Element (DFE) assigned to the edges between elements representing the well, passing through multiple layers, with a well boundary condition applied to the lowest node as is convention with this specialized boundary type. A DFE can be assigned properties that differ from the surrounding elements, and, in the case of the multilayer well boundary condition, is assigned an arbitrarily high hydraulic conductivity. This allows for water injected at the bottom-most node to be distributed evenly along the DFE before passing into the elements immediately surrounding it. In this way, pressures are distributed more evenly across the model layers than they otherwise would be if only standard well boundary conditions were applied to the nodes making up the disposal well. If just the well boundary conditions were used, pressures would likely be high directly on the nodes but lower between the nodes, potentially affecting the model pressure results.

Injection and pumping rates for the disposal and source wells were assigned as time series using historical data taken from Accumap (IHS Energy, 2016) and the BCOGC data repository (Appendix A). Operations began in April 2013, and so data are available from this time onwards. The historical data for the study area model at the time the model was constructed were available up until in October 2017 (day 1704 of the simulation). Beyond this time, a simple forecasting scenario was implemented; the mean injection/pumping rate for each well over the historical period was calculated and assigned to the well for an additional ten years past October 2017 (for a total run time of roughly 14.75 years). It is recognized that this is an unlikely scenario as injection/pumping rates are highly variable, and wells may be shut down if the 120% IVRP limitation is surpassed during an annual pressure test. In addition, new wells are also planned for the Paddy-Cadotte, specifically up to 14 new source wells (Encana Corporation, 2014), which will likely modify the groundwater flow regime. Nevertheless, it was of interest to extend the time period to examine potential long term effects of injection, and so a simple forecasting scenario was used.

The node at the bottom of each disposal well was also assigned constant mass and heat boundary conditions that operated on the same schedule as the well boundary condition, so that heat and mass would only be added to the model when the well is active. These boundary conditions were only applied to the bottom node, as opposed to all nodes along the length of the DFE, so as to coincide with the node injecting water into the model. A constant temperature of 15°C and constant salinity of 260 g/L were used for all disposal wells, in accordance with recommendations from Encana and available wastewater chemical analysis data (Appendix C).The DFEs composing the multilayer wells were assigned an arbitrarily high mass and heat dispersivity so that solute and temperature would be distributed evenly along the well before entering the formation. If this had not been done, the majority of the mass and heat injected into the model would have remained at the bottom of each disposal well instead of being distributed along their entire length.

For this simulation, FEFLOW's automatic time step control was used (see Section 3.1.3) with a maximum allowable time step of ten days. In order to determine the influence that the source wells have on disposal conditions, the model was run twice: once with all disposal wells and source wells operating, and again with only the disposal wells operating.

4.2. Results

Despite the run stabilization techniques employed during model construction and parameterization (mesh refinement and upwinding implementation) some numerical oscillations were still observed. These oscillations were manifest as negative concentrations that occurred immediately around the well in the layers penetrated by the disposal wells. The oscillations mostly occurred in those time steps shortly after a new stress (i.e. injection) started, and disappeared within a few days of simulation time. Negative values were also observed in some of the layers above the top of the disposal wells as mass began to advance into this new area. These negative values are interpreted to be a result of too coarse a mesh, and likely could have been eliminated by refining the mesh both horizontally and vertically. However, time constraints precluded refining the mesh further. Despite these negative values, the results of the simulation are consistent with results from Chapter 3 and are discussed below. The mass balance error ranged from 1 to 4%, depending on the time step.

4.2.1. Pressure

The initial hydraulic head distribution in the model is compared to the head distribution at the end of the simulation in Figure 4.7. Changes to the head distribution are greatest in the study area and diminish with distance, with the greatest changes occurring around WA 10677. No changes are observed at a distance greater than roughly 20 km from the well field.

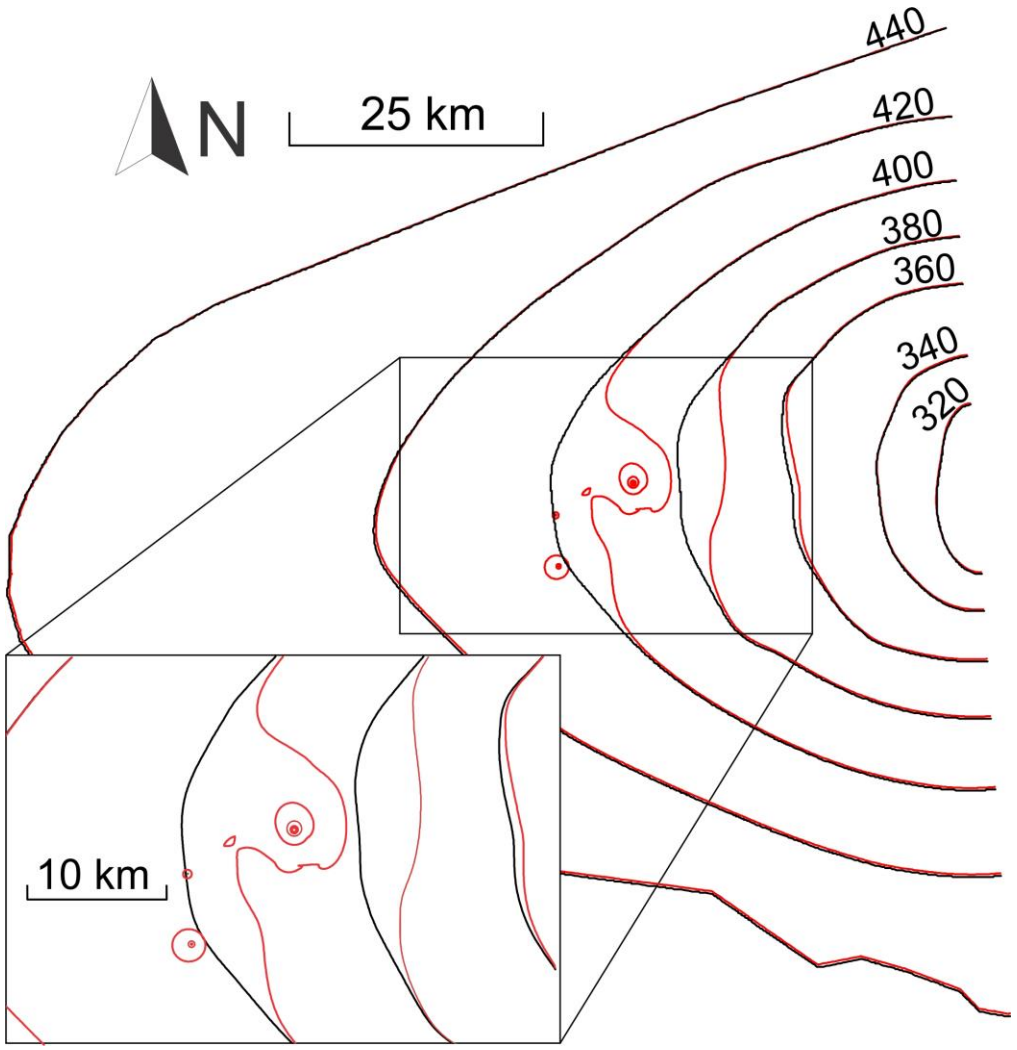

Figure 4.7. Initial (black) and final (red) hydraulic head distribution after 14.75 years in the study area model. Contour interval is 20 m.

Pressures modelled at the midpoint of the perforated interval of each disposal well throughout the simulation are shown in Figure 4.8. In the first 500 days (Figure 4.8a), no changes are observed in any of the wells as disposal has not yet begun. But shortly after this period, source well WA 28495 begins pumping water from the Paddy-Cadotte and

results in a decrease in pressure measured at WA 10677, roughly 500 m away. A maximum pressure drop of 160 kPa is observed before WA 10677 is turned on and pressures rise, which indicates that communication between disposal well WA 10677 and the water source well WA 28495 is possible. This communication is investigated further in Section 4.2.3.

All disposal wells are active by around day 800 of the simulation and follow highly variable injection schedules, resulting in equally variable pressure curves for each well (Figure 4.8b). The greatest pressures, just over 10,700 kPA, occur in WA 10677, which is injecting at a rate of 1,800 m^3/day. WA 19319 reaches similar pressures, although this well only reaches a max injection rate of 250 m^3/day, less than one sixth the rate of WA 10677. This occurs because, while WA 10677 is injecting into the permeable and porous HSU 2, WA 19319 is only injecting into HSU 1, which is an order of magnitude less permeable and 10% less porous. Similarly, WA 26366 is also injecting into HSU 1 at a maximum rate of 245 m^3/day and reaches pressures of 9,910 kPa. WA 24139 targets HSU 2 and pumps at relatively low rate of at most 370 m^3/day, and so does not reach any significant pressure. WA 27024 operates at such low rates that pressure changes at this well are minimal in HSU 2, just over 100 kPa.

As a point of reference, the modelled pressures are compared to the 90% formation fracture pressures calculated for each well (see Chapter 2). The lowest and most likely to be reached is 18,950 kPa for WA 19319. None of the modelled pressures exceed this value nor come close to this value. The highest modelled pressure is in WA 10677, which is more than 8,000 kPa from the fracture limit.

Disposal pressures past the historical period (ending in October 2017, day 1704 of the simulation) become much less variable, which is to be expected given that a constant injection rate was applied to each well in this simple forecasting scenario. In wells injecting at relatively low rates (WA 27024 and 24139), the pressures remain somewhat constant, with only slight increases (Figure 4.8a). In wells injecting at higher rates or targeting less permeable parts of the Paddy-Cadotte (WA 10677, 19319, and 26366, respectively), pressures gradually increase, but do not reach the peak pressures observed during the historical period.

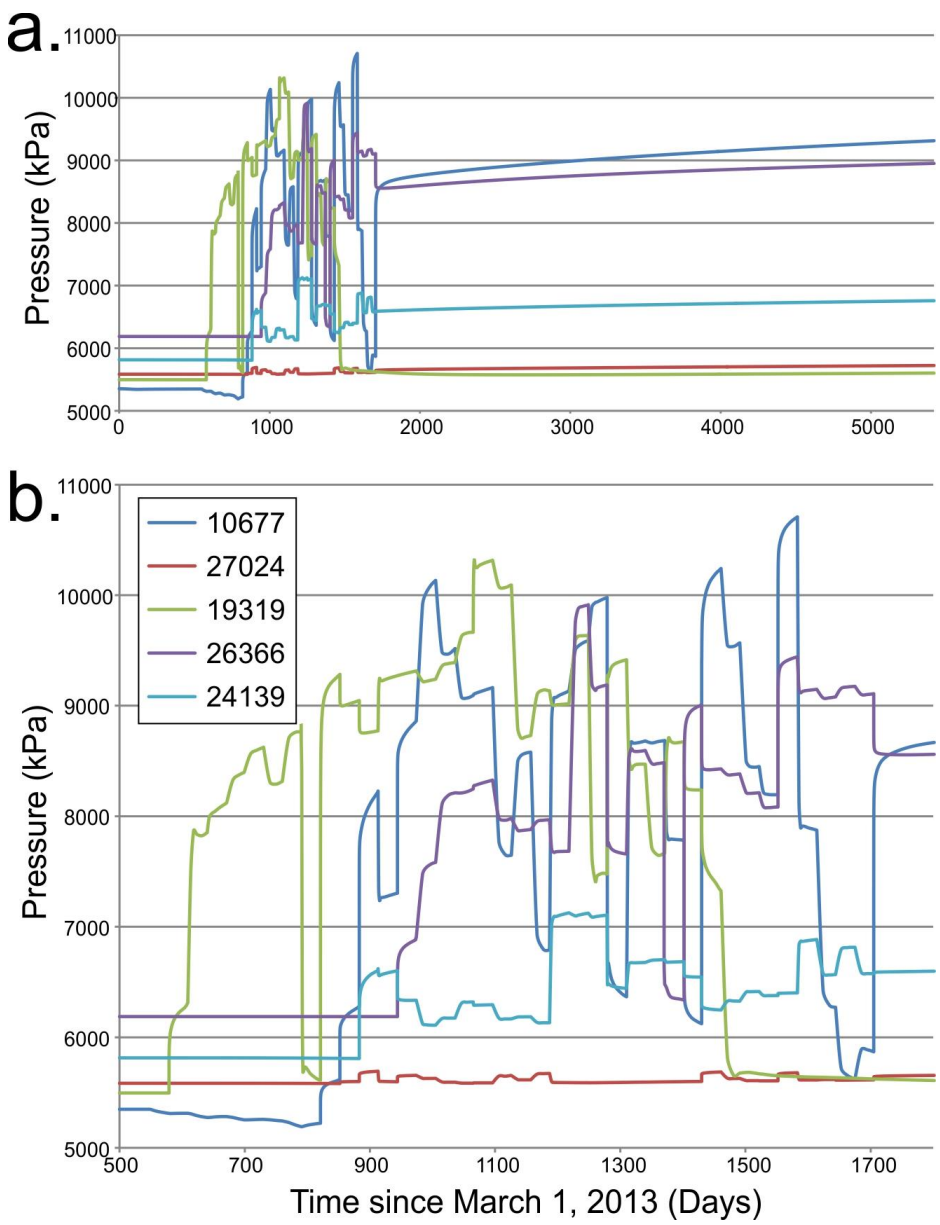

Figure 4.8. Modelled pressures measured in the middle of each disposal well for a) the full simulation and b) a portion of the historical period in which the disposal wells were most variable.

Another pressure limit imposed on wastewater disposal by the BCOGC is that background formation pressures must remain below 120% IVRP (see Chapter 1), which is tested during an annual pressure fall-off test. This type of testing was not simulated in the model, as it would complicate the injection time series and necessitate multiple additional model runs. However, in an annual pressure test occurring in February 2017, WA 19319 was found to have exceeded 120% IVRP with an extrapolated formation

pressure of 7900 kPa (Petro Management Group Ltd., 2017) and was shut down (BCOGC, 2017b). This is represented in the time series for WA 19319 in the model as an assigned injection rate of 0 m^3/day from March 2017 (day 1461 in the simulation) to the end of the simulation. The modeled pressure at WA 19319 over the time period immediately after it was shut down is presented in Figure 4.9 and compared to the 120% IVRP limit of 6600 kPa for this well (determined based on the IVRP at the midpoint of WA 19391 in the model of 5500 kPa). As a check for model accuracy, pressures in the formation 60 days after well shut-down should be greater than 120% IVRP, though Figure 4.9 shows that this is not the case. Pressures quickly drop back to near IVRP shortly after the well is turned off. The results suggest that the model does not accurately simulate actual pressure measurements obtained from an in-situ fall off test. Based on the box model results, permeability heterogeneity was one of the dominant controls on formation pressures, and so more data related to this parameter would be useful in better calibrating the model.

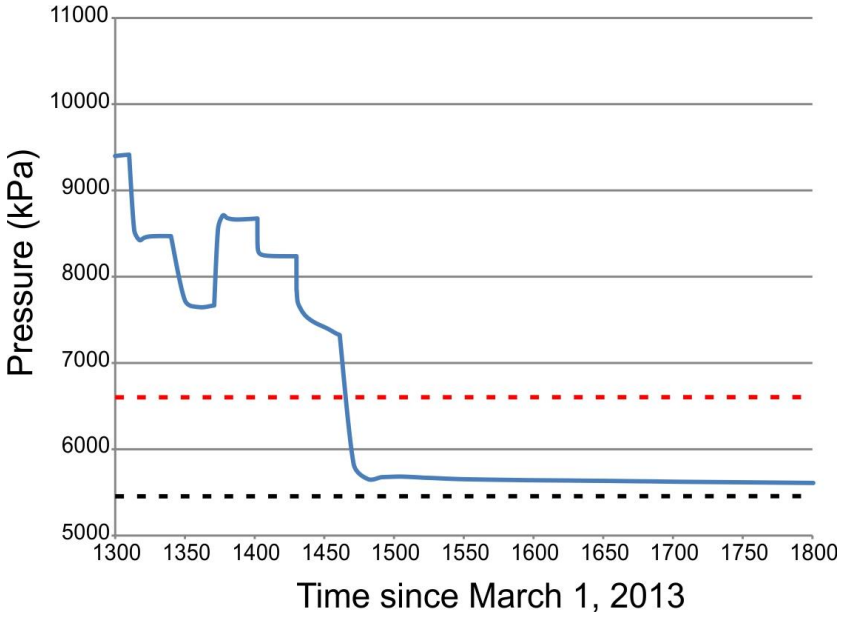

Figure 4.9. Modelled pressures in WA 19319 over the time period it was shut down for exceeding the 120% IVRP pressure limit (March 2017, Day 1461). Black dashed line shows the modelled IVRP and red dashed line shows 120% IVRP for WA 19319 calculated based on intial modelled pressure in the well.

4.2.1. Plume Extent and Shape

The simulated extents and shapes of the wastewater plumes for each disposal well are shown in Figure 4.10. The major factors originally thought capable of influencing the extent and shape of a plume were 1) the regional hydraulic gradient (towards the east), 2) formation slope (towards the south), and 3) differences in the formation pressure regime due to nearby source/disposal well operation (acting in variable directions - see Figure 2.2 for the relative positions of all wells in the model). The regional hydraulic gradient in the model is induced by assigning constant head boundaries to the model edges. This causes groundwater to flow from areas of high head (the north, west, and south boundaries) to areas of low head (the mid-center of the eastern boundary). In the study area, this means that groundwater flow is from west to east, and so wastewater plumes are hypothesized to elongate in this direction as they are advected. Additionally, the Paddy-Cadotte dips towards the south, and so as the dense wastewater sinks towards the bottom of the formation the plume is expected to elongate towards the south as well. Overall, formation slope and hydraulic gradient were not observed to have a significant impact on plume migration. However, it is noted that vertical discretization within hydrostratigraphic units is coarse, which may prevent buoyancy effects from manifesting, potentially obfuscating the influence of the slope of the formation.

The observed principal influence(s) on each plume's extent and shape is discussed below. For this purpose, the asymmetry of each plume was quantified using Equation 4.1:

$$P_A = \frac{A_{Max} - A_{Min}}{A_{Min}} \quad (4.1)$$

where P_A is the plume's asymmetry coefficient, A_{Max} is the plume's longest axis measured from the disposal well outwards, and A_{Min} is the plume's shortest axis measured from the disposal well outwards. A_{Max} and A_{Min} are not necessarily perpendicular to one another, but both are measured in the X-Y plane. Using this convention, a perfectly symmetric plume would have a P_A of 0. Symmetry coefficients were calculated for each plume using the extent of the 10 g/L concentration contour and are shown in Table 4.3.

Table 4.3. Data used to calculate plume asymmetry coefficient (P_A) for the wastewater plume surrounding each disposal well.

Well	10677	19319	24139	26366	27024
A_{Max}	908	372	552	522	240
A_{Min}	859	295	510	440	197
P_A	0.06	0.26	0.08	0.19	0.22

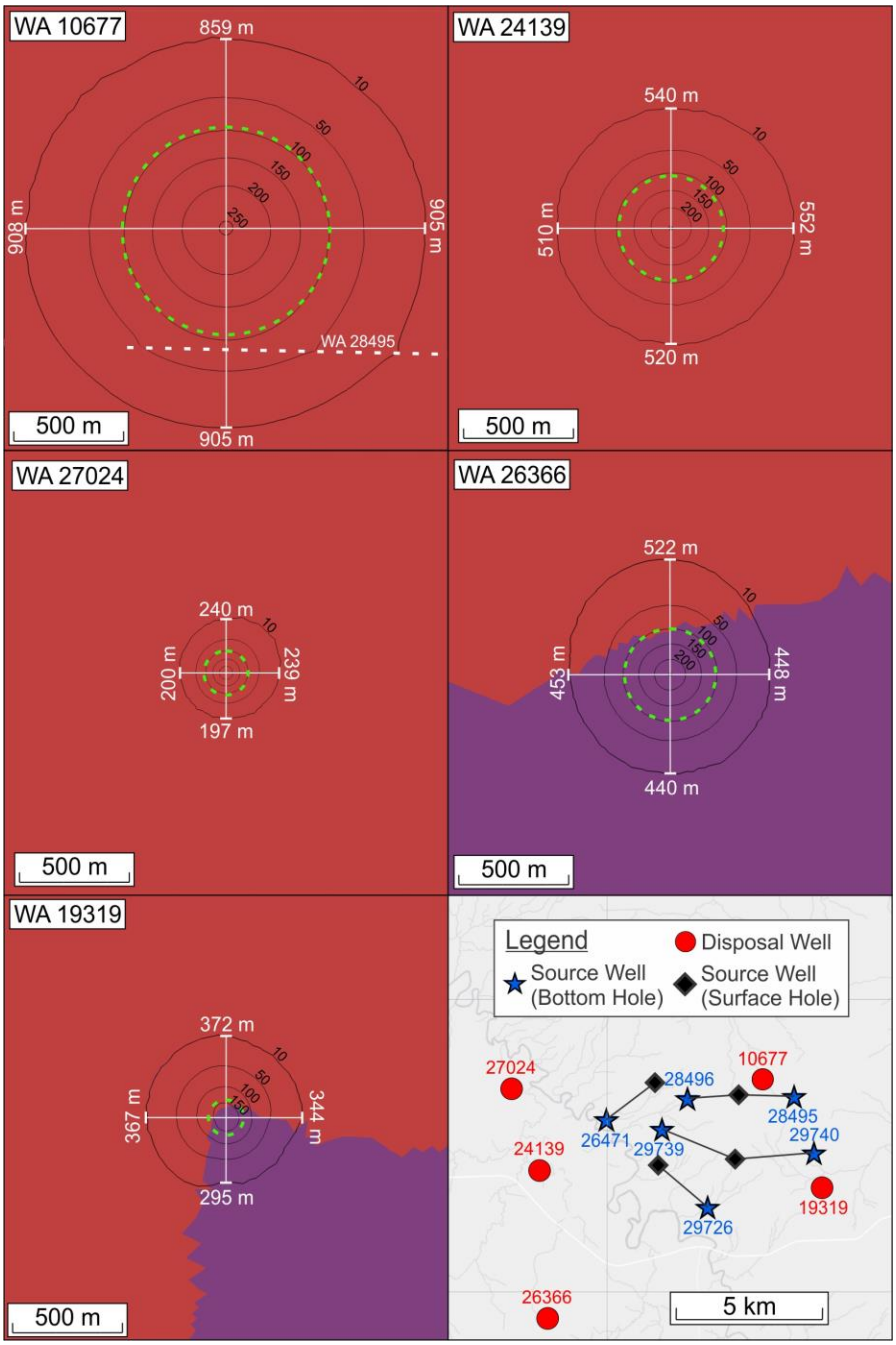

Figure 4.10. TDS concentration contours in g/L for modeled disposal wells (T = 14.75 years). Furthest extent of wastewater plumes is defined by 10g/L contour. All wells except WA 19319 show TDS concentrations of up to 250 g/L, but may not be labelled for the purpose of figure clarity. Green circles show the extent of the wastewater determined using the volumetric calculation. Red indicates the presence of HSU 2 (K = 1.5×10^{-6} m/s), while purple shows where it pinches out (K = 1.5×10^{-7} m/s). The location of source well WA 28495 is indicated by the white dashed line close to disposal well WA 10677. Scale is constant between sub-figures. Relative well locations are shown in bottom-right. Contours are taken on Slice 9 (base of HSU 2).

WA 27024

This plume shows a high degree of asymmetry (P_A=0.22). WA 27024 operates at the lowest rate of the five disposal wells, and thus produces the smallest wastewater plume. It extends 200 m from the well to the south and west, and 240 m to the east and north. The shape of this plume is thought to be influenced by the surrounding wells: WA 24139 which is injecting to the south, and the group of source wells to the east, resulting in an overall plume elongation towards the northeast. This is demonstrated in Figure 4.11, which shows that the plume created at WA 27024 travels to the northeast along the hydraulic head gradient.

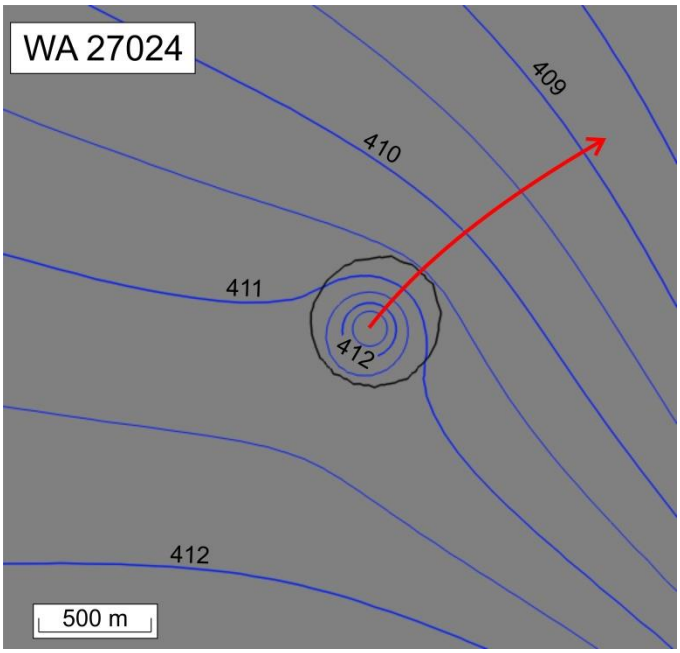

Figure 4.11. Comparison of the wastewater plume around WA 27024 (defined by the 10 g/L concentration contour shown in black) with surrounding equivalent freshwater hydraulic head contours (blue). Head contour interval is 0.5 m. A representative flow line is shown in red.

WA 24139

One of the most symmetric plumes is that of WA 24139, with an asymmetry coefficient of 0.08 (Figure 4.10). This plume extends further to the northeast than the southwest, with a long axis that is 42 m longer than its short axis. This is interpreted to be a result of WA 26366 creating a high pressure zone towards the south, and source well WA 26471 (and other source wells somewhat further away to the east) creating a low pressure zone to the northeast. Both of these factors may cause the plume for WA 24139 plume to extend

further in the northeast direction. WA 27024 is injecting to the north of WA 24139, and so has the potential to create a high pressure zone that affects plume movement, but the injection rate is so low that it appears to have a negligible effect.

WA 26366

WA 26366 is interesting in that, according to the way the hydrostratigraphy was interpreted for this model, it injects into the low permeability HSU 1 in an area where HSU 2 has pinched out. This plume has roughly equal axis lengths to the west, south, and east, but elongates to the north, resulting in an asymmetric plume (P_A=0.19). This plume shape/extent is interpreted to be affected by the high permeability of HSU 2, which exists roughly 200 m to the north.

WA 19319

Injection at WA 19319 occurs in the low permeability HSU 1, but HSU 2 is located nearby and so the plume elongates once it enters this unit (towards the west, north, and east). The plume is significantly shorter towards the south and southwest, producing the largest asymmetry coefficient for any well in the model (P_A=0.26). This large asymmetry could be due to the fact that, after March 2017, WA 19319 no longer injected any wastewater as it had exceeded the 120% IVRP limit. This means that any growth of this plume is a result of the wastewater sinking and spreading out, which, as shown in Section 3.3.2, occurs more strongly in high permeability materials. The concentration of the wastewater around this well is lower than that around the other wells, because without a continuous source of solute the plume becomes diluted, resulting in lower concentrations.

WA 10677

The largest plume, with a radius of nearly 1 km, is that surrounding WA 10677. This plume is the most symmetric, with axes to the west, south, and east being essentially equivalent. The largest influence on the shape of this plume is likely source well WA 28495, located 500 m to the south. This source well causes the plume to spread less far to the north, as observed in the concentration contours of the plume (Figure 4.10). The absolute difference between the longest and shortest axes for this plume is on the same order as observed in other wells, but is smaller relative to the overall size of the plume, leading to the low asymmetry coefficient (P_A=0.06). The mean concentration of the water

extracted by source well WA 28495 is plotted in Figure 4.12. The concentration steadily increases as the plume migrates southwards. The salinity begins to increase around the end of the historical injection period, and so, theoretically, wastewater from WA 10677 may already be getting intercepted by WA 28495, though no known concentration data for this well exists with which the results of the model can be compared.

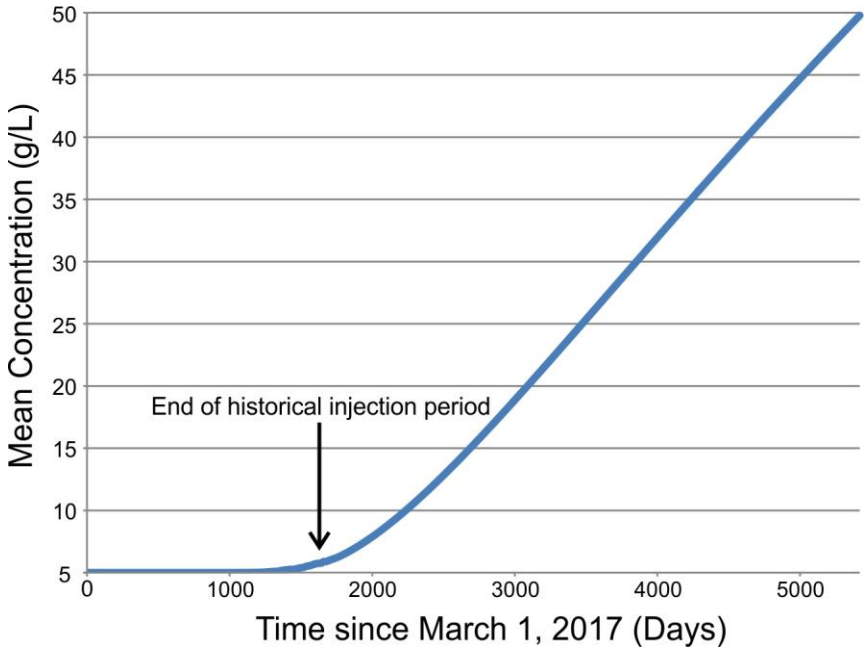

Figure 4.12. Modelled mean concentration of water extracted by source well WA 28495. Background formation water salinity is modelled at 5 g/L. No increases in mean concentration were observed at any other source well.

The contaminant plume for WA 10677 is also shown in cross-section in Figure 4.13, where wastewater is modeled to travel furthest in HSU 2. Wastewater travels farther in HSU 3 than HSU 1 despite the lower permeability in this bottom unit. This is interpreted to be a result of the density of the wastewater causing it to sink to the bottom of the Paddy-Cadotte. The axisymmetric cross-section shown in Figure 3.24 represents a case that initially looks similar to that shown in Figure 4.13, but a number of differences between the two models (including higher injection rate, greater wastewater concentration, coarser discretization, decreased permeability of HSU 3, and higher dispersivity in the study area model) preclude a meaningful comparison between the two models.

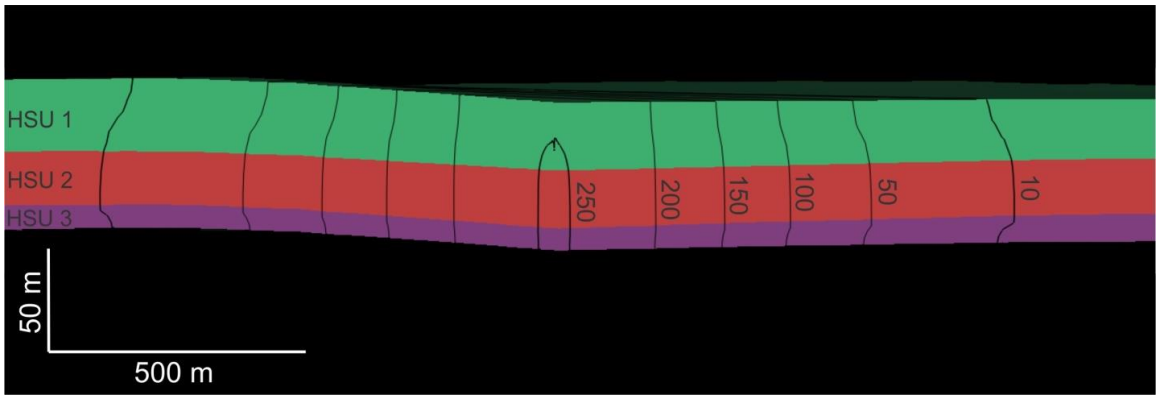

Figure 4.13. Cross-section of the wastewater plume surrounding disposal well WA 10677. Contour lines show concentration (g/L) and are at irregular intervals. HSUs are differentiated based on color. View is facing north and vertical exaggeration is 4x.

Comparison of Modeling Approach to Volumetric Approach

The estimated plume extent based on the volumetric calculation (Equation 1.1) is marked by the green dashed circle centered on each well in Figure 4.10. To determine these calculated extents, the following parameters were used: 1) the length of the perforated section of each well, 2) the porosity of the zone into which the well injects, and 3) the total volume of wastewater injected over the entire simulation. For most wells, the volumetric extent aligns with the 100 g/L contour, which was expected based on the results in Chapter 3. The box model results for a disposal well perforated over the entire hydrostratigraphic unit (as in the Base Case) indicated the volumetric approach aligned with the advective front, which in that case was half of the concentration of the injected wastewater. In this case, with an injected wastewater salinity of 260 g/L, the volumetric extent could be expected to align with the 130 g/L contour, which is close to 100 g/l contour. This difference is interpreted to be due to the wastewater spreading into the parts of the Paddy-Cadotte above and below each disposal well's perforated interval. The loss of mass causes the plume to not spread as far as it would if the wells were perforated over the entire length of the formation. The only plume for which the 100 g/L concentration contour does not align with the volumetrically calculated extent is WA 19319, which was not actively injecting throughout the entire simulation. Therefore, as shown in Figure 3.2, a greater disparity exists between the volumetrically calculated extent and simulated extent than it does for other plumes. In Figure 3.2, as well as for the plume created around disposal well WA 19319, once injection stops the volumetrically calculated extent does not change since no additional wastewater is being

injected, but the previously injected wastewater continues to sink and extend further along the base of the disposal formation.

4.2.2. Inter-Well Communication

The results from the previous sections show that communication occurs between the wells in the Paddy-Cadotte. This is manifested 1) in the pressure drop in WA 10677 prior to it beginning injection (Figure 4.8b), and 2) as elongation of wastewater plumes away from or towards other disposal or source wells (Figure 4.10). To further investigate inter-well communication, the simulation was run a second time with no source wells operating. The pressure results obtained for WA 10677 are compared to the results from the original simulation and are shown in Figure 4.14. Throughout the simulation, pressures in the well are consistently 100-150 kPa lower in the case with source wells turned on. The pressure differences were also examined in the other disposal wells, but are not plotted here because the differences are difficult to resolve at the scale chosen for the figure. Pressures were reduced by 60 kPa in WA 19319, 30 kPa in WA 24139, 15 kPa in WA 27024, and 10 kPa in WA 26366, which are listed in order of increasing distance from the group of source wells. WA 10677 is very close to the source wells, so it has the greatest reduction in pressure, while WA 26366 is the furthest, and so has the smallest pressure reduction.

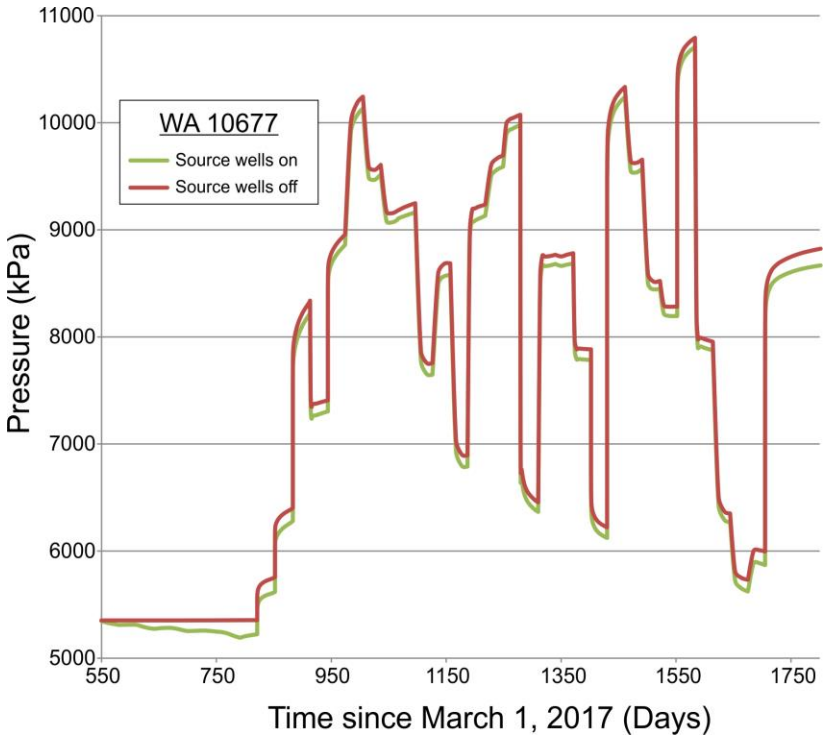

Figure 4.14. Comparison of pressures measured in WA 10677 over the historical period when source wells were turned on (green) and off (red).

Variations in plume shape are also compared between the two model runs (source wells on and off) and most of the plumes behave as expected (Figure 4.15). Without source wells operating, the only influence is due to the other disposal wells. In this case, the plumes tend to move in directions opposite to those seen in Figure 4.10. The largest change in plume shape relative to its size occurs for WA 27024, which is deflected towards the northwest, but similar shifts are observed in WA 10677 and WA 24139. WA 26366 is the furthest from the source well group and experiences the least changes in pressure between model runs (10 kPa, as mentioned above). As a result, its shape does not vary significantly. WA 19319 behaves unexpectedly in that when the source wells are turned off, the plume extends towards them despite the fact that the high pressures created by WA 10677 should push it further to the south in the absence of the mitigating lower pressures from the source wells that act to counter this influence. It is unclear why the WA 19319 plume is behaving in this manner.

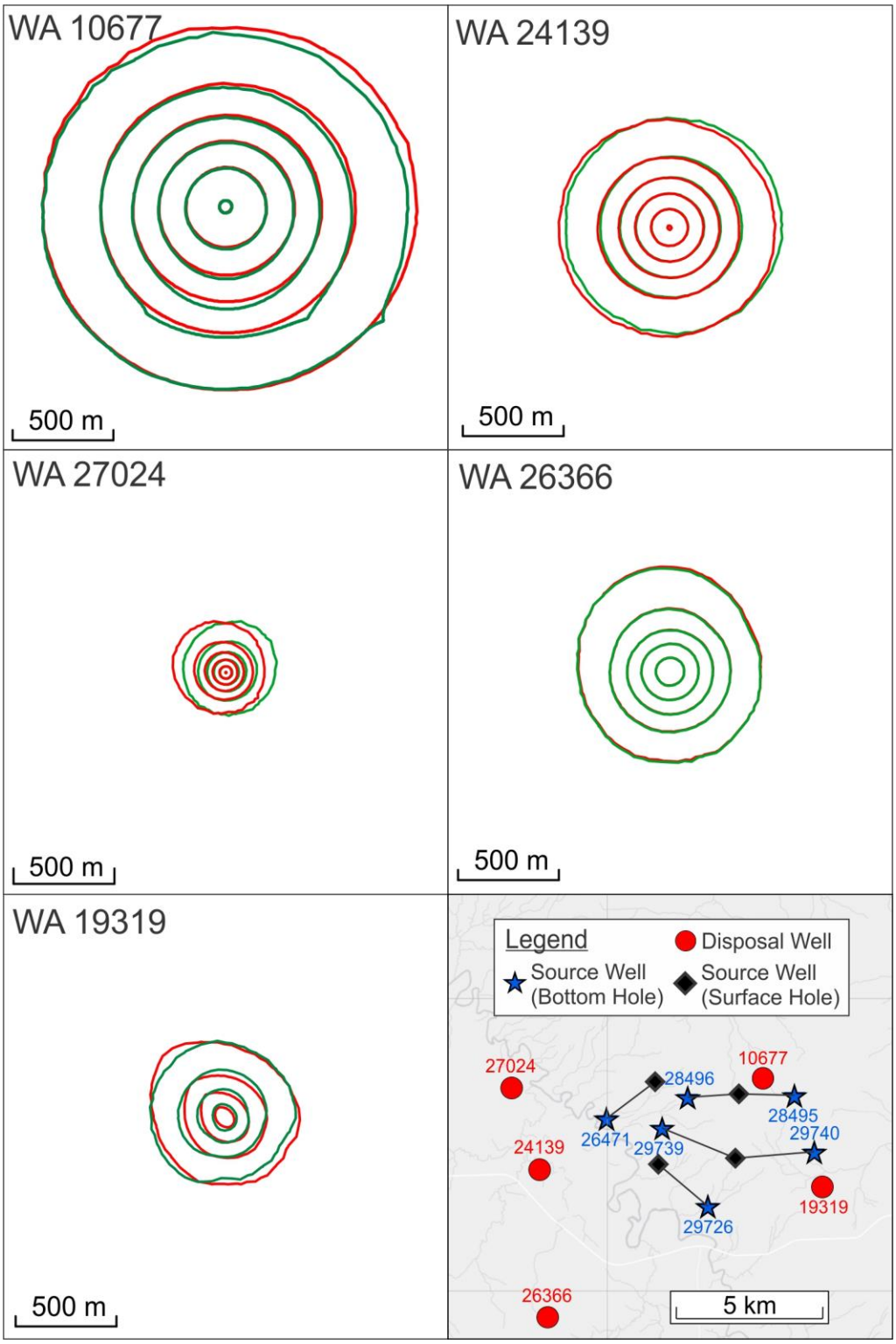

Figure 4.15. Comparison of plume shape when source wells are active (green) and inactive (red). Contour intervals are the same as in Figure 4.10, but are not labelled to increase clarity. Relative well locations are shown in bottom-right. Contours are taken from Slice 9 (base of HSU 2).

4.3. Discussion

4.3.1. Pressure and Chemistry

Initially, based on the proximity of the disposal and source wells to one another (Figure 2.2) it was hypothesized that there was high potential for wastewater to migrate to the source wells, potentially affecting the chemistry of the water extracted from the source wells in the Paddy-Cadotte. However, simulations of plume transport revealed that this only occurs in cases where a disposal well and source well are in very close proximity (i.e. disposal well WA 10677 and source well WA 28495), and even then, the change in water chemistry is only on the order of a 45 g/L increase after 10 years of injection (Figure 4.12). Discussion with Encana (James Armstrong, personal communication) revealed that a change to extracted water chemistry would not significantly impact its ability to be used for hydraulic fracturing purposes. The cluster of source wells serves to reduce pressure in the formation, allowing disposal wells to inject longer and/or at a higher rate before exceeding any pressure limitations imposed on disposal. More source water wells are anticipated to be installed in the Paddy-Cadotte in coming years, which would further reduce pressures at nearby disposal wells (Encana Corporation, 2014).

The pressures simulated in the study area model represent ideal conditions, affected by the setup of the boundary value problem and pertain to the regional context. Factors such as wellbore inefficiencies or changes to formation permeability due to the mobilization of fines or scale buildup are not incorporated into the model. Simulated pressure results from the model do not replace in-situ annual pressure testing or wellhead pressure monitoring. This is exemplified by the pressure fall-off in WA 19319 after it was shut down in March 2017. Had the modelled pressures been accurate, they should have remained above 120% IVRP for at least 60 days, in accordance with real pressure test data (Petro Management Group Ltd. 2017), but they do not. This could be a result of inaccurate model parameterization (discussed below), but these differences likely reflect the differences in specific fall-off pressure testing methodologies that are employed under specific regulatory protocols (BCOGC, 2016c) illustrating that these simulations do not replace real world testing for formation pressures.

4.3.2. Plume Extent and Shape

It was hypothesized that the major factors influencing plume extent would be the regional hydraulic gradient, direction of formation dip, and interference from other nearby wells. As discussed in Section 4.1.1, interference at one well from surrounding wells modelled in the Paddy-Cadotte was found to be the only factor of the three that had a significant effect on plume extent; i.e. wastewater was shown to be drawn towards source wells and/or pushed away from disposal wells. Neither the regional hydraulic gradient nor the dip of the Paddy-Cadotte were found to have a discernible impact - if they affected the shape of the wastewater plume at all it was masked by the influence from other wells. This is not to imply that these factors do not have the potential to impact the distribution of wastewater in the subsurface, but rather it is likely that the hydraulic gradient (roughly 0.002 m/m through the study area at the beginning of the simulation) and formation dip (0.013 m/m) are too small to be significant factors.

Another factor found to be important in controlling the shape of wastewater plumes was variation in formation permeability, as observed for WA 26366 and 19319, both of which target HSU 1 but are located close to HSU 2. Plumes from both of these wells extend further in the higher permeability unit than in the lower permeability unit. This demonstrates the importance of properly mapping and understanding the hydrostratigraphy surrounding a disposal well to support predictions of plume extent and shape by numerical modeling. Unfortunately, gathering data in these deep formations to model the hydrostratigraphy is extremely difficult and expensive.

As in Chapter 3, the volumetric calculation used to estimate the extent of a wastewater plume (marked by the abrupt transition from full concentration wastewater (260 g/L) to the background formation water concentration (5 g/L)) was found to be capable of predicting the location of the advective front approximately marked by the 50% original wastewater modelled concentration contour (130 g/L in this case). Dispersion causes the plume to travel further than the volumetric equation would predict. The difference between the model approach for plume delineation and volumetric approach becomes evident once a well stops injecting, as in the case of WA 19319. For WA 19319, the plume continues to spread away from the well after disposal stops due to the negative buoyancy of the dense wastewater, leading to the volumetric extent being less than the extent defined by the 10 g/L salinity/TDS contour. The significance of this difference is

dependent on the regional multi-well scenario and associated subsurface rights. With respect to the significance is the potential for wastewater to spread into an adjacent tenure of another party also interested in accessing the Paddy-Cadotte for disposal or source water purposes.

The longitudinal dispersivity value (400 m) applied to this model was suggested by FEFLOW support staff to increase model stability, but is arguably high. Most measurements of this parameter place it in the 1-100 m range (Gelhar et al., 1992; Schulze-Makuch, 2005), though the majority of these are for smaller scale models. A 60 km^2 model by Kennedy and Woodbury (2005), similar in size to the roughly 10 km^2 model presented in this chapter, uses a calibrated value for dispersivity of 15,000 m for a sandstone aquifer. Ultimately, the dispersivity value used in this model is uncertain and would ideally be investigated in a sensitivity analysis (see Section 4.3.4).

4.3.3. Sources of Uncertainty

The calibrated steady-state head distribution was not optimal. A good NRMS error is considered to be between 5-10%, whereas the lowest value achieved during calibration was 18.4%. This high degree of error stems from the low resolution of data for such a large area. Permeability measurements are inferred from a single core and boundary conditions are estimated from relatively few DSTs (n = 44). While it is felt that the model was calibrated as well as possible given the information available, potential inaccuracy is acknowledged. As discussed above, permeability exerts some control on plume shape and disposal pressures, and so any unmapped high/low permeability units or variations within units have the potential to affect the results of the model discussed in this chapter. Moreover, values for specific storage were calculated using the density of freshwater and assigned as constant values according to their respective HSU, when in reality the density of the water in formation changes as disposal progresses. This would result in a higher specific storage value which, as shown in Figure 3.23, would result in a more gradual pressure response curve. Ideally, specific storage in the model would vary as a function of the mean fluid density within an element, but this could not be implemented in the code used. This constant specific storage value may be one of the contributing factors as to why the pressure fall-off observed in WA 19319 after injection stopped did not remain above 120% IVRP. Fluid around the disposal well at the time of well shut-off would be of high salinity and density, and thus impart a higher specific storage. This

could potentially result in a slower simulated pressure response in the well, which might be more in line with actual observations. Further investigation of the role of changes in specific storage due to salinity and density differences is warranted.

An assumption made for this model was that all wastewater disposal occurred at an even rate throughout each month. This was done because disposal volumes are only available on a month by month basis. In reality, disposal operations in one month could be as variable (in terms of injection rate) as over the entire historical disposal period. Both wellhead and reservoir pressures will most likely spike higher than modelled if large quantities of wastewater are injected over short periods of time. Maximum wellhead injection pressures for each month for each well are available through the BCOGC data downloads portal, and the original intention was to translate these pressures to downhole pressures so that they could be compared to the modelled results. However, this would not produce any meaningful results, since the modelled disposal is evenly distributed throughout the month, resulting in lower pressures, while the actual disposal could potentially be variable and intermittently spike higher than the model calculates.

It is known that the reservoir immediately surrounding the perforated interval of the disposal wells in the Paddy-Cadotte has been stimulated, i.e. hydraulically fractured, in order to increase the formation's permeability (see Section 2.1.1). FEFLOW simulates fractures using DFEs inserted along element edges, which can be assigned parameter values that are different from the surrounding elements. Simulating these fractures accurately would necessitate vertical discretization on the order of one slice every metre, which would more than triple the number of elements in the model and produce prohibitively long run times on the order of 4-7 days. For this reason, fractures were not incorporated into the study area model. Simulation of the effect of fractures on wastewater migration and disposal pressures would be better suited to smaller, single-well models, potentially similar to the axisymmetric models presented in Chapter 3.

4.3.4. Potential Model Improvements Related to Numerical Accuracy

The problems observed during the simulation, including negative concentration values and other errors in the simulation log, all stemmed from discretization not being fine enough. Increasing the discretization, particularly vertically, would likely have improved

model stability, but at the expense of longer run times. If discretization were to be increased (i.e. the spacing between nodes decreased), the layers in HSU 1 should be targeted first as they were the ones in which negative concentrations were observed. Layers in this unit are on the order of 10 m and, as a first pass, should be reduced to at least 5 m in order to assess whether negative concentrations are eliminated. If not, layer thickness should be reduced further. Similarly, temporal resolution, i.e. the maximum allowable time step, should also be halved from 10 days to 5 days and pressure results re-evaluated. Upon closer inspection of the pressure results (Figure 4.8b), there are certain instances where large pressure drops occur over this maximum time step length of 10 days. Temporal resolution is likely too coarse in these cases.

To properly explore and understand the results from this model, a sensitivity analysis should be performed, though long run times precluded this from being included in this thesis. Of particular interest is solute dispersivity as this parameter was shown in Chapter 3 to exert a strong control on plume extent. In the study area model, only a single value was used (400 m), and this value is poorly constrained due to a lack of data. Ideally, a monitoring well could be installed in the Paddy-Cadotte from which solute transport data could be monitored in order to determine a more accurate value for dispersivity.

The main limiting factor discussed above is the long run times inherent in detailed density-dependent heat and mass transport models. The domain chosen for the study area model was overly large so as to minimize boundary effects. The changes to the hydraulic head contour lines in Figure 4.7 show that the pressure influence from the disposal wells reaches roughly 20 km from the well field, and so the model domain could likely be reduced to a 40 km x 40 km square area centered on the well field. Doing so would allow for vertical and horizontal discretization to be increased without producing drastically longer simulation run times.

Chapter 5.

Conclusions

The goal of this thesis was to characterize the potential migration of saline wastewater in deep disposal formations. A wide range of potential subsurface conditions exist, and so the results from this thesis represent just one of many such cases. The Paddy-Cadotte of NEBC was selected for this study, as it has only recently begun to be used for wastewater disposal and so has a less complex disposal history than other formations in the area that may have been used for decades. The formation is also used conjunctively for disposal and deep water source extraction.

Two different modeling approaches were used to understand the migration of wastewater in the Paddy-Cadotte. The first was a series of axisymmetric box models used to carry out a sensitivity analysis for simplified, ideal disposal conditions for a single disposal well. The second is a study area model of the Paddy-Cadotte that incorporates multiple disposal and water source wells. In both cases, simulated plume extents are compared to those determined using a volumetric calculation (Equation 1.1), which is commonly employed by industry to estimate the distance that wastewater will travel. Additionally, the potential for disposal-source well interference is explored using the model. The major findings and insights gained using each modeling approach are summarized below.

5.1. Axisymmetric Box Models

In the Base Case model, single well wastewater disposal was simulated. A combination of mass transport processes (dominantly dispersion) and buoyancy effects related to the density difference between the wastewater and formation water were observed to cause the wastewater to sink towards the bottom of the disposal formation and extend further than otherwise predicted using the volumetric calculation alone. This disparity was evident during active disposal, but became even more pronounced once disposal stopped and the wastewater began to settle to the bottom of the formation. During injection, the modeled extent of the plume (defined by the location of the 1 g/L concentration contour) was found to extend roughly 90% further than the volumetrically

estimated extent. During the post-injection period, this difference increased to 300%. For the scenario tested, the extent of the plume predicted using the volumetric calculation was found to align with the approximate location of the 100 g/L concentration contour (half of the initial concentration of 200 g/L), within which the most concentrated wastewater was located, though this was only true during injection and not the post-injection period.

The Base Case model was subjected to a sensitivity analysis in which a range of possible values for various parameters related to wastewater disposal in the Paddy-Cadotte were investigated. The dominant controls on plume extent were found to be, in roughly decreasing order of significance, injection rate, dispersivity, formation permeability, permeability anisotropy, formation thickness, and salinity contrast. The effects of injection rate and formation thickness are obvious; an increase in the amount of wastewater being disposed of or a reduction of the available space into which the wastewater is injected will result in the wastewater plume migrating further downgradient. Permeability and permeability anisotropy are closely linked in their effect on plume extent. As the model set up in FEFLOW requires relating K_z to K_x using a ratio, a general increase in formation permeability (K_x) will also result in an increase in K_z, allowing the dense wastewater to sink more readily and travel further along the bottom of the disposal formation relative to the top. Dispersivity plays a strong role in the migration of wastewater during disposal; higher dispersivity causes the plume to extend further, but also to become more dilute. Salinity contrast (as opposed to temperature difference) is the main factor behind the density dependence of flow in these models, with a greater contrast in salinity producing a correspondingly greater density difference. This results in a stronger negative buoyancy force, increasing the degree to which the disposed wastewater will sink to the bottom of the formation. The effect of varying porosity was not expressly investigated as it was felt that the result was obvious; an increase in porosity would result in a greater available volume for wastewater to fill, resulting in the plume travelling less far.

During this sensitivity analysis, the outflow boundary condition was also modified and found to influence the pressures observed at the disposal well. For this reason, and because other real-world disposal influences (such as well inefficiency or formation permeability reduction due to the mobilization of fines) could not be integrated into the model, the modeling procedure employed here should not be used to inform disposal

practices at any particular well. Additionally, this model was not calibrated to site-specific conditions, and so only serves as an indicator of potential conditions.

5.2. Study Area Model

In the study area model, historical pumping and injection were simulated in the Paddy-Cadotte to provide insights regarding the controls on wastewater migration to date and where it may migrate 10 years into the future under similar injection scenarios. This model allowed for the effect of formation dip, regional hydraulic gradient, and influence of well interference on a wastewater plume to be investigated, none of which could be simulated using the box models previously discussed. Of these three factors, the influence from nearby wells was found to have the greatest impact on overall plume extent. Plumes were observed to migrate away from nearby disposal wells, towards nearby source water wells, or a combination of the two. Formation dip and regional hydraulic gradient had no discernible effect, though both of these are relatively small in the Paddy-Cadotte and may play more significant roles in more steeply dipping formations or formations with higher regional gradients. Spatial variability in formation permeability was also observed to impact plume behaviour, as two wells targeting lower permeability parts of the Paddy-Cadotte were observed to produce plumes that elongated towards a higher permeability part of the formation. This illustrates the importance of understanding permeability heterogeneity in a disposal formation to predict plume migration, though this is often difficult in such deep and data-sparse units.

Simulation results show the potential for pressure communication to occur between wells, most notably as lower pressures in disposal wells when nearby source wells were pumping. Wastewater migration from a disposal well (WA 10677) to a source well (WA 28495) was modeled, resulting in an increase in the salinity of the water pumped by the source well. However, in this case (compared to other well relationships within the study area) the wells were very close to one another (~500 m) and wastewater was injected at a high rate (>1000 m^3/day). For the remaining disposal wells, plumes did not come close to reaching source wells.

Plume extent was also compared to the volumetrically calculated estimate and found to agree with the results from Chapter 3. Depending on the well, modeled plume extent was found to be 90-365% greater than otherwise predicted using the volumetric

approach. However, this difference is strongly influenced by the longitudinal and transverse dispersivity value assigned to the model, which were poorly constrained due to a lack of contaminant transport data within the Paddy-Cadotte. This parameter could be further investigated in a sensitivity analysis of the study area model (see below). For the situation modeled and with the current well spacing and configuration, the consequences of underestimating wastewater plume extent using the volumetric estimate are minimal. However, should demands on this reservoir increase resulting in greater well density and closer proximity of wells in the future, the uncertainty created by a reliance on the volumetric approach becomes potentially more significant with respect to management of reservoir use.

5.3. Recommendations for Future Work

The box models provide a useful method for scenario testing at the individual well scale. In regards to the box models, the outflow boundary condition was observed to influence pressure results at the disposal well. In order to further explore this boundary condition it is recommended that the model domain be extended. Results from the study area model show that pressure increases in the disposal formation are felt up to 20 km away, and so a 20 km model size is recommended. Additionally, the effect of induced fractures immediately surrounding a disposal well should be investigated using the box models. The disposal wells in the Paddy-Cadotte have all been stimulated (i.e. hydraulically fractured), but this characteristic could not be included in the study area model as they would require a degree of vertical discretization not realistic for a large-scale model. It is felt that the higher permeability proximal to the well due to these fractures will not significantly change the model results, but should be investigated nonetheless to confirm this.

Time constraints prevented a sensitivity analysis from being performed on the study area model. This was anticipated, and so the sensitivity analysis performed on the axisymmetric box models is meant to serve as a substitute. However, certain factors only present in the study area model (such as formation dip and regional hydraulic gradient) were not investigated, and so it could prove useful to simulate a range of possible values for these factors in order to assess their influence on the results, though this would require a significant time investment. Further, vertical discretization in the study area model was shown to be too coarse, as evidenced by numerical oscillations

and negative concentration values. Discretization should be increased, particularly in HSU 1 where some layers are 10 m thick.

The study area model provided useful insights regarding current use of the Paddy-Cadotte for disposal and water sourcing. As unconventional gas development activity increases over time in this region, it is possible that additional disposal or source wells may be drilled. If this model is to be used again, it should be updated to reflect any new wells that may have been drilled. For vertical wells this is straight-forward, as it would only require increasing the horizontal discretization in the area immediately around the new well. Updating the model to include new horizontal wells would be more difficult, however, as it would require remeshing the entire domain and manually correcting slice geometry to properly reflect actual well elevations and reduce the irregularity of elements surrounding them.

The Paddy-Cadotte was selected for this study in part because it is a relatively new host for wastewater disposal and it was felt that this would make it more straightforward to model in terms of disposal history. However, because the formation became economically interesting only recently, there are few data available, specifically core logs with permeability measurements. Because of this, homogeneous permeability values had to be assigned to the three HSUs identified in the Paddy-Cadotte, which was potentially the root of the poor calibration results achieved in Chapter 4. This research suggests that the understanding of subsurface behaviour of disposed wastewater would benefit from future data collection opportunities to inform hydrogeological properties of deep formations.

It would be interesting to perform formation-scale wastewater disposal simulations in another formation that has been used for a longer period of time and for which more data may be available. Potential candidates include the Halfway, which has been host to disposal since at least the mid-1970s, and the Cadomin, which has been used for disposal since the early 1990s.

References

AER, 1994. Directive 51: Injection and Disposal Wells – Well Classifications, Completions, Logging, and Testing Requirements. https://www.aer.ca/rules-and-regulations/directives/directive-051 (accessed July 13, 2016).

AER, 2016. Energy Fact Book 2015-2016. https://www.nrcan.gc.ca/sites/www.nrcan.gc.ca/files/energy/files/pdf/EnergyFactBook2015-Eng_Web.pdf (accessed July 10, 2017).

Alberty, M.W., 1992, Part 4, wireline methods basic openhole and cased-hole tools, in Morton-Thompson, D., and Woods, A.M., eds., Development geology reference manual: AAPG Methods in Exploration Series, No. 10, pp. 143-153.

Alessi, D.S., Zolfaghari, A., Kletke, S., Gehman, J., Allen, D.M. and Goss, G.G., 2017. Comparative analysis of hydraulic fracturing wastewater practices in unconventional shale development: Water sourcing, treatment and disposal practices. *Canadian Water Resources Journal/Revue canadienne des ressources hydriques*, *42*(2), pp.105-121.

Alley, W.M., Wireman, M., and Musick, M., 2014. Characterization of Deep Groundwater: A Conference Report. Report presented at 2014 Groundwater Protection Council Annual Forum, Seattle, WA.

Alley, W.M., E. Scott Bair, and M. Wireman. 2013. “Deep” groundwater. *Groundwater,* 51, pp.653–654.

Anderson, M.P., Woessner, W.W. and Hunt, R.J., 2015. Applied groundwater modeling: simulation of flow and advective transport. Academic press.

Bachu, S., and Burwash, R. A., 1994. Geological history of the Peace River Arch; in Geological Atlas of the Western Canada Sedimentary Basin, G.D. Mossop and I. Shetsen (comp.), Canadian Society of Petroleum Geologists and Alberta Research Council, URL http://www.ags.gov.ab.ca/publications/wcsb_atlas/atlas.html, (accessed July 23, 2016).

Bachu, S., 1995. Flow of variable-density formation water in deep sloping aquifers: review of methods of representation with case studies. *Journal of Hydrology*, *164*(1-4), pp.19-38.

Bachu, S., 1988. Analysis of heat transfer processes and geothermal pattern in the Alberta Basin, Canada. *Journal of Geophysical Research*, *93*(B7), pp.7767-7781.

Bachu, S. and Underschultz, J.R., 1993. Hydrogeology of formation waters, northeastern Alberta basin. *AAPG Bulletin*, *77*(10), pp.1745-1768.

Bachu, S. and Michael, K., 2002. Flow of variable-density formation water in deep sloping aquifers: minimizing the error in representation and analysis when using hydraulic-head distributions. *Journal of Hydrology*, *259*(1-4), pp.49-65.

BCOGC, 2011. Oil and Gas Commission Fact Sheet: Hydraulic Fracturing and Disposal of Fluids. https://www.bcogc.ca/public-zone/fact-sheets (accessed July 12, 2016).

BCOGC, 2012. Montney Formation Play Atlas NEBC. https://www.bcogc.ca/node/8131/download (accessed October 12, 2017).

BCOGC, 2012a. Hydrocarbon and By-Product Reserves in British Columbia. http://www.bcogc.ca/node/11111/download (accessed July 18, 2016).

BCOGC, 2014. Hydrocarbon and By-Product Reserves in British Columbia. https://www.bcogc.ca/node/12952/download (accessed July 10, 2017).

BCOGC, 2015. 2015 Annual report on water management for oil and gas activity. https://www.bcogc.ca/node/13261/download (accessed July 26, 2017).

BCOGC, 2016a. Application Guideline for: Deep Well Disposal of Produced Water. https://www.bcogc.ca/node/8206/download (accessed July 13, 2016).

BCOGC, 2016b. Water Management for Oil and Gas Activity: 2015 Annual Report. https://www.bcogc.ca/node/13261/download (accessed October 5, 2016).

BCOGC, 2016c. Water Service Wells Summary Information. www.bcogc.ca/node/5997/download (accessed July 13, 2016).

BCOGC, 2016d. Industry Bulletin: Technical Guidance for Determining the “Base of Usable Groundwater”. http://www.bcogc.ca/node/13074/download (accessed August 14, 2017).

BCOGC, 2017a. Online Services: Data Downloads. https://www.bcogc.ca/online-services (accessed July 12, 2017).

BCOGC, 2017b. Abandonment Report for WA 19319. https://www.bcogc.ca/elibrary (accessed March 13, 2018).

Bear, J., 1972. Dynamics of Fluids in Porous Media. Elsevier Scientific, New York, pp.764.

Buckley, R.A. and Plint, A.G., 2011. Stratigraphy, Sedimentology and Paleogeography of the Middle to Upper Albian Peace River Formation, NW Alberta and NE British Columbia. Presented at 2011 CSPG/CSEG/CWLS GeoConvention, Recovery: Energy Environment Economy, Calgary, Alberta, Canada, May 9-11.

Buckley, R.A. and Plint, A.G., 2013. Allostratigraphy of the Peace River Formation (Albian) in north-western Alberta and adjacent British Columbia. *Bulletin of Canadian Petroleum Geology*, *61*(4), pp.295-330.

Burnett, D.B., 2004. Potential for Beneficial Use of Oil and Gas Produced Water. Texas Water Resources Institute, Global Petroleum Institute, Texas A&M University, College Station, TX, pp.1–11.

Clark, C.E. and Veil, J.A., 2009. Produced water volumes and management practices in the United States (No. ANL/EVS/R-09-1). Argonne National Laboratory (ANL).

Croucher, A. E., and M. J. O'Sullivan, 1995. The Henry problem for saltwater intrusion, *Water Resources Research*, 31,1809–1814.

Dahlberg, E.C., 1994. Applied hydrodynamics in petroleum exploration. SpringVerlag, p. 295.

Diersch H.-JG. 2002. Interactive, Graphics Based Finite Element Simulation System FEFLOW for Modelling Groundwater Flow, Contaminant Mass and Heat Transport Processes. WASY Ltd: Berlin.

Diersch, H.J. and Kolditz, O., 1998. Coupled groundwater flow and transport: 2. Thermohaline and 3D convection systems. *Advances in Water Resources*, *21*(5), pp. 401-425.

Diersch, H.J. G., 2005a. FEFLOW: Finite Element Subsurface Flow & Transport Simulations System. WASY GmbH Institute for Water Resources Planning and Systems Research.

Diersch, H.J.G. 2005b. About the difference between the convective form and the divergence form of the transport equation. In: FEFLOW White Papers Vol. I.

Diersch, H.J.G. and Kolditz, O., 1996. On finite-element analysis of spatio-temporal buoyancy-driven convection processes in porous media. *IAHS Publications-Series of Proceedings and Reports-Intern Assoc Hydrological Sciences*, *237*, pp.407-416.

Diersch, H.J.G. and Kolditz, O., 2002. Variable-density flow and transport in porous media: approaches and challenges. In: FEFLOW White Papers Vol. II.

Diersch, H.J.G., 2013. FEFLOW: finite element modeling of flow, mass and heat transport in porous and fractured media. Springer Science & Business Media.

Diersch, H.J.G., 2013. FEFLOW: finite element modeling of flow, mass and heat transport in porous and fractured media. Springer Science & Business Media.

Driesner T., and Heinrich C.A., 2007. The System H2O-NaCl. I. Correlation Formulae for Phase Relations in Temperature-Pressure-Composition Space from 0 to 1000°C, 0 to 5000 bar, and 0 to 1 XNaCl. Geochimica et Cosmochimica Acta 71, 4880-4901.

Encana Corporation, 2014. Application for Dual Water Source and Water Disposal Wells: ECA CRP Sunrise 14-35-78-17W6 (10677), ECA CRP Hz Sunrise A13-33-78-17W6 (26471), ECA CRP Hz Sunrise 09-34-78-17W6 (28495), ECA CRP Hz Sunrise A09-34-78-17W6 (28496).

Eppelbaum, L., Kutasov, I. and Pilchin, A., 2014. Thermal properties of rocks and density of fluids. In *Applied Geothermics* (pp. 99-149). Springer Berlin Heidelberg.

Evans, D.G. and Raffensperger, J.P., 1992. On the stream function for variable-density groundwater flow. *Water Resources Research*, *28*(8), pp.2141-2145.

Fakhru'l-Razi, A., Pendashteh, A., Abdullah, L.C., Biak, D.R.A., Madaeni, S.S. and Abidin, Z.Z., 2009. Review of technologies for oil and gas produced water treatment. *Journal of Hazardous Materials*, *170*(2), pp.530-551.

Ferguson, G., 2015. Deep injection of waste water in the western Canada sedimentary basin. *Groundwater*, 53(2), pp.187-194.

Francke, H. and Thorade, M., 2010. Density and viscosity of brine: An overview from a process engineers perspective. Chemie der Erde-Geochemistry, 70, pp.23-32.

Gelhar, L.W., Welty, C. and Rehfeldt, K.R., 1992. A critical review of data on field-scale dispersion in aquifers. *Water Resources Research*, *28*(7), pp.1955-1974.

Goss, G., Alessi, D., Allen, D., Gehman, J., Brisbois, J., Kletke, S., Zolfaghari, A., Notte, C., Thompson, Y., Hong, K. and Covalski, V., 2015. Unconventional wastewater management: a comparative review and analysis of hydraulic fracturing wastewater management practices across four North American basins.

Gregory, K.B., Vidic, R.D. and Dzombak, D.A., 2011. Water management challenges associated with the production of shale gas by hydraulic fracturing. Elements, 7(3), pp.181-186.

Hallock, J.K., Roell, R.L., Eichelberger, P.B., Qiu, X.V., Anderson, C.C. and Ferguson, M.L., 2013. Innovative friction reducer provides improved performance and greater flexibility in recycling highly mineralized produced brines. In *SPE Unconventional Resources Conference-USA*. Society of Petroleum Engineers.

Hanor, J.S., 1994. Origin of saline fluids in sedimentary basins. *Geological Society, London, Special Publications*, *78*(1), pp.151-174.

Hayes, B.J.R. 1988. Incision of a Cadotte Member paleovalley-system at Noel, British Columbia - evidence of a Late Albian sea level fall. *In*: Sequences, Stratigraphy, Sedimentology: Surface and Subsurface, D. James and D.A. Leckie (eds.). *Canadian Society of Petroleum Geologists*, Memoir 15, p. 431-438.

Hayes, T., 2009. Sampling and Analysis of Water Streams Associated with the Development of Marcellus Shale Gas. Available as Attachment A at http://catskillcitizens.org/learnmore/20100916IOGAResponsetoDECChesapeake_IOGAResponsetoDEC.pdf (accessed April 30, 2018).

Henderson, C., Acharya, H., Matis, H., Kommepalli, H., Moore, B. and Wang, H., 2011. Cost Effective Recovery of Low-TDS Frac Flowback Water for Re-use. General Electric Company.

Hubbert, M. K., and Willis, D. G., 1957. Mechanics of Hydraulic Fracturing, *Transaction of Society of Petroleum Engineers of AIME*, 210, pp.153-168.

Hyde, R.S. and Leckie, D.A., 1994. Provenance of the Lower Cretaceous Paddy Member (Peace River Formation), northwestern Alberta. *Bulletin of Canadian Petroleum Geology*, *42*(4), pp.482-498.

IHS Energy, 2016. IHS AccuMap®, version 26.06; IHS Energy, mapping, data management and analysis software, URL <https://www.ihs.com/products/oil-gas-toolsaccumap.html> [January 2016].

Johnson, E.G. and Johnson, L.A., 2012. Hydraulic fracture water usage in northeast British Columbia: locations, volumes and trends; in Geoscience Reports 2012, British Columbia Ministry of Energy and Mines, pp.41-63.

Kennedy, P.L. and Woodbury, A.D., 2005. Sustainability of the bedrock aquifer systems in south-central Manitoba: implications for large-scale modelling. *Canadian Water Resources Journal*, *30*(4), pp.281-296.

Kirste, D., 2000, Compositional variation in formation fluids and their relation to fluid flow and water-rock interaction in Devonian to Lower Cretaceous sedimentary rocks of southern Alberta. Ph.D. thesis, Alberta, Canada, University of Calgary. 219p.

Kirste, D., Desrocher, S., Spence, B., Hoyne, B., Tsang, B. and Hutcheon, I., 1997. Fluid flow, water chemistry, gas chemistry and diagenesis in the subsurface Triassic in Alberta and British Columbia. *Bulletin of Canadian Petroleum Geology*, *45*(4), pp.742-764.

Kondash, A.J., Albright, E. and Vengosh, A., 2017. Quantity of flowback and produced waters from unconventional oil and gas exploration. *Science of the Total Environment*, *574*, pp.314-321.

Leckie, D.A. and Reinson, G.E., 1993. Effects of Middle to Late Albian sea level fluctuations in the Cretaceous interior seaway, Western Canada. In: Evolution of the Western Interior Basin (Eds W.G.E. Caldwelll and E.G. Kauffman), *Geological Association of Canada Special Paper*, 39, pp.151-176.

Leckie, D.A., Staniland, M.R. and Hayes, B.J., 1990. Regional maps of the Albian Peace River and lower Shaftesbury formations on the Peace River Arch, northwestern Alberta and northeastern British Columbia. *Bulletin of Canadian Petroleum Geology*, *38*(1), pp.176-189.

Lee, K., Neff, J., & DeBlois, E., 2011. Produced water: Environmental risks and advances in mitigation technologies. New York, NY: Springer Science Business Media, LLC.

Mississippi Oil and Gas Board, 2012. Form 14 - Monthly Report on Fluids Injected. http://www.ogb.state.ms.us/forms.php (accessed July 13, 2016)

Oklahoma Corporation Commission, 2014. Application for Administrative Approval to Dispose of or Inject Water into Wells. http://www.occeweb.com/og/ogforms.html (accessed July 13, 2016).

Ontario Oil, Gas and Salt Resources, 2002. Oil, Gas and Salt Resources of Ontario: Provincial Operating Standards. http://www.ogsrlibrary.com/documents/Provincial_Operating_Standards_v2_Jan_24_2002.pdf (accessed July 13, 2016)

Petrel Robertson Consulting Ltd. and Canadian Discovery Ltd. 2011. Deep Subsurface Aquifer Characterization in support of Montney Tight Gas Development: Geological Report; Geoscience BC, Report 2011-11, 386 p.

Petro Management Group Ltd., 2017. Injectivity Fall-Off Test Report for WA 19319. https://www.bcogc.ca/elibrary (accessed March 13, 2018).

Plint, A.G., Tyagi, A., McCausland, P.J., Krawetz, J.R., Zhang, H., Roca, X., Varban, B.L., Hu, Y.G., Kreitner, M.A. and Hay, M.J., 2012. Dynamic Relationship between Subsidence, Sedimentation, and Unconformities in Mid-Cretaceous, Shallow-Marine Strata of the Western Canada Foreland Basin: Links to Cordilleran Tectonics. *Tectonics of Sedimentary Basins: Recent Advances*, pp.480-507.

Precht, P., Dempster, D., 2012. Jurisdictional Review of Hydraulic Fracturing Regulation. Final report for Nova Scotia Hydraulic Fracturing Review Committee. Nova Scotia Department of Energy and Nova Scotia Environment http://www.gov.ns.ca/nse/pollutionprevention/docs/Consultation.Hydraulic.Fracturing-Jurisdictional.Review.pdf (accessed July 12, 2016).

Riddell, J., 2012. Potential for freshwater bedrock aquifers in northeast British Columbia: regional distribution and lithology of surface and shallow subsurface bedrock units (NTS 093I, O, P; 094A, B, G, H, I, J, N, O, P); *in* Geoscience Reports 2012, *British Columbia Ministry of Energy and Mines*, pp.65-78.

Rivard, C., Lavoie, D., Lefebvre, R., Séjourné, S., Lamontagne, C. and Duchesne, M., 2014. An overview of Canadian shale gas production and environmental concerns. *International Journal of Coal Geology*, *126*, pp.64-76.

Schulze-Makuch, D., 2005. Longitudinal dispersivity data and implications for scaling behavior. *Groundwater*, *43*(3), pp.443-456.

Simons, M., Allen, D.M., Kirste, D., and Welch, L.A., 2017. Numerical modelling of highly saline wastewater disposal in Northeast British Columbia. Paper presented at GeoOttawa 2017, Ottawa, ON.

Wang, Q., Chen, X., Jha, A.N. and Rogers, H., 2014. Natural gas from shale formation–the evolution, evidences and challenges of shale gas revolution in United States. *Renewable and Sustainable Energy Reviews*, *30*, pp.1-28.

Warner, D.L., Davis, S.N., and Syed, T., 1986. Evaluation of confining layers for containment of injected wastewater: Proceedings of the International Symposium on Subsurface Injection of Liquid Wastes, New Orleans, LA, National Water Well Assoc., Dublin, Ohio, pp.417-446.

Williams, G. D., and Stelck, C. R., 1975. Speculations on the Cretaceous paleogeography of North America. *In:* Caldwell, W. G. E., ed., The Cretaceous System in the Western Interior of North America: Geological Association of Canada, Special Paper 13, pp.1-20

Appendix A.

Disposal and Source Well Info and Volumes

Table A1. Production histories for the source wells and disposal wells in the study area. Cells with a dash show months prior to any production occurring in a well. Cells marked with NA had no value entered in either the BCOGC database or Accumap, but are assumed to be 0 m^3.

		Disposal Wells (WA)					Source Wells (WA)					
Year	Month	19319	26366	24139	27024	10677	29740	28495	29739	26471	28496	29726
2013	4	-	-	-	-	-	-	-	-	-	5059.2	-
	5	-	-	-	-	-	-	-	-	-	5571.2	-
	6	-	-	-	-	-	-	-	-	-	NA	-
	7	-	-	-	-	-	-	-	-	-	NA	-
	8	-	-	-	-	-	-	-	-	-	NA	-
	9	-	-	-	-	-	-	-	-	-	NA	-
	10	-	-	-	-	-	-	-	-	-	NA	-
	11	-	-	-	-	-	-	-	-	-	NA	-
	12	-	-	-	-	-	-	-	-	-	NA	-
2014	1	-	-	-	-	-	-	-	-	-	NA	-
	2	-	-	-	-	-	-	-	-	-	NA	-
	3	-	-	-	-	-	-	-	-	-	NA	-
	4	-	-	-	-	-	-	-	-	-	NA	-
	5	-	-	-	-	-	-	-	-	-	NA	-
	6	-	-	-	-	-	-	-	-	-	NA	-
	7	-	-	-	-	-	-	-	-	-	NA	-
	8	-	-	-	-	-	-	-	-	-	NA	-
	9	-	-	-	-	-	-	9982.8	-	-	10065.4	-
	10	2103.5	-	-	-	-	-	3409	-	-	2389.2	-
	11	5101.5	-	-	-	-	9509.4	11762.2	12637	-	12333.1	-
	12	5452	-	-	-	-	4071.3	3279.8	3400.7	-	2760	-

		Disposal Wells (WA)					Source Wells (WA)					
Year	Month	19319	26366	24139	27024	10677	29740	28495	29739	26471	28496	29726
2015	1	5830	-	-	-	-	9266.9	10277.7	11055.1	-	9175.1	6600.4
	2	5529.8	-	-	-	-	3055.6	3949.4	4054.7	-	4215.2	3591.9
	3	5409.6	-	-	-	-	5558.6	6627.1	7159.3	-	7360.3	5624.7
	4	5976.2	-	-	-	-	7155.6	15638.2	9444	7470.1	14221.7	11205.5
	5	NA	-	-	-	-	NA	NA	NA	NA	250.5	2.4
	6	6960.4	-	-	-	6040.5	2908.5	5682.6	3947.6	3572	5125	3045.5
	7	6573.4	-	-	281.2	14923.2	334.4	538.4	274.8	148.4	466.3	328.6
	8	5971.9	-	8244.9	1499.1	39926.1	NA	NA	NA	NA	NA	NA
	9	6619.6	-	7270	177.3	24788.5	NA	NA	NA	NA	NA	NA
	10	NA	1851.3	4741.1	938.9	44768.2	28.8	28.8	28.8	28.8	53.6	28.8
	11	6418.5	3212.5	2520.9	534.7	56516	NA	NA	NA	751.8	NA	NA
	12	6841.2	4569.4	3198.7	109.4	49107.1	28.8	28.8	28.8	28.8	53.6	28.8
2016	1	7270	4506.4	4502.1	2.5	42932	NA	NA	NA	NA	NA	NA
	2	7835	4271.4	3943.7	41	40243.9	NA	NA	NA	NA	NA	NA
	3	7887	3736	3031.7	859.1	25065.8	8285.8	7596.1	9111.9	9326.7	5268.9	4358.2
	4	5239	3355.8	3084	345.9	34549.2	51	NA	NA	NA	NA	NA
	5	6114.8	3622.1	2694.4	1044.6	14715.8	3586.7	4032.2	4102.6	3488.7	2549	NA
	6	5692	2880.3	11120.4	9.3	40860.3	NA	NA	NA	NA	NA	NA
	7	6936.4	7607.8	11092.4	9	46436.6	NA	NA	NA	NA	NA	NA
	8	3106	5951.7	10720.3	0	50108.4	NA	NA	NA	NA	NA	NA
	9	6332.8	2634.8	4700	0	7448.9	NA	NA	NA	NA	NA	NA
	10	4824.2	4688.8	6921.1	0	35199.3	NA	NA	NA	NA	NA	NA
	11	3327.4	4275.2	6842.6	NA	33680.1	2730.1	3081.5	2463.3	3469.6	2215.4	1221.8
	12	5194	NA	6854.2	0	24311.3	1910.8	3149.8	1977.8	4201.9	1769.3	2020.4
2017	1	4393.7	5556.1	5627.2	5	5331	1896.9	1957.6	1941.2	2205	2129.6	1125.4
	2	3207	3860.5	2800.8	956.5	47619.9	4	3.4	457.3	3.4	3.2	1.4
	3	0	4152.7	3824.9	290.8	43861.6	22.1	10.4	6.6	46.5	2.1	30.4
	4	0	3662.7	4404.9	26.5	29844.6	NA	2	0.1	0.1	NA	NA
	5	0	3514.8	4230.3	0	28030.3	1766.3	1825.1	2085.4	1621.1	1512.4	1092.6
	6	0	6020.5	4267.8	859.7	54194.1	10.1	280.9	11.1	70	59.3	275.7

		Disposal Wells (WA)					Source Wells (WA)					
Year	**Month**	**19319**	**26366**	**24139**	**27024**	**10677**	**29740**	**28495**	**29739**	**26471**	**28496**	**29726**
2017	7	0	5548.1	8404	41.3	23459.9	7.2	35.4	19.5	2.6	49.3	86.9
	8	0	5370.7	5664.4	91.6	6461.2	6891.2	14	10038	9724.3	7203.2	5196.6
	9	0	5340.5	7373	0	41.4	7429.2	5106	8226	6903.1	7058.8	5095.2
	10	0	5355.5	5635.2	0	3367.6	4255.5	6022.5	4797.9	3338.1	5320.6	3892
Cumulative		152147	105545	153715	8123	873833	80765	104322	97270	56401	103610	54853

Table A2 General information concerning the disposal wells targeting the Paddy-Cadotte. Cumulative disposed water volumes are current up to May 2017.

Authorization Number	**019319**	**010677**	**026366**	**024139**	**027024**
UWI	100/10-24-078-17W6/0	100/14-35-078-17W6/4	102/16-01-078-18W6/0	100/02-25-078-18W6/0	100/13-36-078-18W6/2
Surface Hole Latitude	55.774110	55.808124	55.736919	55.782375	55.807838
Surface Hole Longitude	-120.491100	-120.521491	-120.643414	-120.645101	-120.659035
Surface Hole UTM Easting (m)	657373.33	655331.99	647962.08	647684.25	646714.79
Surface Hole UTM Northing (m)	6183574.47	6187290.12	6179101.06	6184154.89	6186958.30
Surface Hole UTM Zone	10	10	10	10	10
Bottom Hole Latitude	55.774110	55.808124	55.736959	55.782497	55.807907
Bottom Hole Longitude	-120.491100	-120.521491	-120.643421	-120.644935	-120.658978
Bottom Hole UTM Easting (m)	657373.33	655331.99	647961.49	647694.20	646718.11
Bottom Hole UTM Northing (m)	6183574.47	6187290.12	6179105.50	6184168.82	6186966.10
Bottom Hole UTM Zone	10	10	10	10	10
Authorization Date	3/2/2005	9/2/1997	5/12/2010	5/22/2008	2/10/2011
Spud Date	3/20/2005	9/23/1997	5/18/2010	7/21/2008	3/24/2011
True Vertical Depth (m)	1029.0	2720.0	1144.9	2708.6	2811.8
Cum. Disposed Water (m^3)	152146.9	786308.6	77910.3	122370.6	7130.8

Licensee	Aqua Terra	Encana	Murphy Oil	Arc Resources	Arc Resources

Table A3 General information for the source wells targeting the Paddy-Cadotte. Cumulative extracted water volumes are current up to May 2017.

Well Authorization Number	**29726**	**29740**	**29739**	**26471**	**28496**	**28495**
UWI	100/04-22-078-17W6/0	100/03-25-078-17W6/2	100/14-28-078-17W6/0	100/04-32-078-17W6/0	100/08-33-078-17W6/0	100/05-36-078-17W6/0
Surface Hole Latitude	55.782532	55.784962	55.784962	55.80884	55.803663	55.803663
Surface Hole Longitude	-120.58122	-120.5371	-120.53721	-120.5809	-120.53535	-120.53521
Surface Hole UTM Easting (m)	651688.92	654448.59	654438.62	651605.9	654481.3	654490.32
Surface Hole UTM Northing (m)	6184310.4	6184678.4	6184678	6187238.1	6186762.8	6186763.1
Surface Hole UTM Zone	10	10	10	10	10	10
Bottom Hole Latitude	55.769264	55.784892	55.793866	55.797379	55.802951	55.802496
Bottom Hole Longitude	-120.55399	-120.4949	-120.5774	-120.6075	-120.56278	-120.50455
Bottom Hole UTM Easting (m)	653448.29	657094.14	651884.25	649983.73	652765.25	656416.23
Bottom Hole UTM Northing (m)	6182894.2	6184765.5	6185579.8	6185905	6186622.7	6186702.1
Bottom Hole UTM Zone	10	10	10	10	10	10
Authorization Date	1/25/2014	1/14/2014	1/14/2014	6/9/2010	10/1/2012	9/19/2012
Spud Date	5/5/2014	3/29/2014	4/19/2014	7/16/2013	12/13/2012	11/28/2012
True Vertical Depth (m)	952.4	1012.5	1005.7	914.3	1016.7	997.4
Cum. Extracted Water (m3)	40306.8	62171.6	74177	36362.9	94549.3	92862.9
Horizontal Perforated Length (m)	1899	2085	2151	1717	1300	1514

Appendix B.

Disposal Well Approval Letters

Description:

The accompanying PDF contains the approval letters from the BCOGC for disposal wells WA 19319, WA 27024, WA 24139, WA 26366, and WA 10677. Each letter states the maximum allowable injection wellhead pressure and formation pressure for each well.

File Name:

Disposal-Well-Approval-Letters.pdf

Appendix C.

Encana Wastewater Analysis

Core Lab

WATER ANALYSIS

362 - 2			52137-2016-2916
CONTAINER IDENTITY	METER ID	WELL LICENSE NUMBER	LABORATORY FILE NUMBER
EnCana Corporation			2
OPERATOR			PAGE
16-36-078-17W6	ECA Dawson Creek 16-36 Facility		KB ELEV (m) / GR ELEV (m)
LOCATION (UWI)	WELL NAME		
Dawson Creek		Core Lab - FSJ	
FIELD OR AREA	POOL OR ZONE	SAMPLER	
TEST TYPE AND NO.	TEST RECOVERY		
Frac Water Supply			
POINT OF SAMPLE		SAMPLE POINT ID	
PUMPING	FLOWING	GAS LIFT	SWAB
WATER m³/d	OIL m³/d	GAS m³/d	
TEST INTERVAL or PERFS (meters)			
SEPARATOR / RESERVOIR / OTHER / @ °C CONTAINER WHEN SAMPLED / @ °C CONTAINER WHEN RECEIVED		SEPARATOR / OTHER	
Pressures, kPa (gauge)		Temperatures, °C	
2016 11 02	2016 11 04	2016 11 16	SR
DATE SAMPLED (Y/M/D)	DATE RECEIVED (Y/M/D)	DATE ANALYZED (Y/M/D)	ANALYST

AMT. AND TYPE CUSHION

@ °C MUD RESISTIVITY

CATIONS

ION	mg/L	mg Fraction	meq/L
Na	65,300	0.2728	2,840.4
K	2,540	0.0106	65.0
Ca	18,310	0.0765	913.7
Mg	1,930	0.0081	158.8
Ba	65	0.0003	0.9
Sr	1,790	0.0075	40.9
Fe	25	0.0001	0.9
Mn	4.0	0.0000	0.1

ANIONS

ION	mg/L	mg Fraction	meq/L
Cl	149,330	0.6239	4,212.0
Br			
I			
HCO_3	41	0.0002	0.7
SO_4	4.6	0.0000	0.1
CO_3	0.00	0.0000	0.0
OH	0.00	0.0000	0.0
H_2S	N.D.		

Total Dissolved Solids (mg/L)

285821 By Evaporation @ 110 °C	258984 By Evaporation @ 180 °C
	239340 Calculated
1.1639 @ 15.6 °C Specific Gravity	1.3740 @ 24 °C Refractive Index (n_D)
5.7 @ 25.0 °C pH	0.045 @ 25 °C Resistivity (Ohm-Meters)

LOGARITHMIC PATTERNS OF DISSOLVED IONS

meq/L

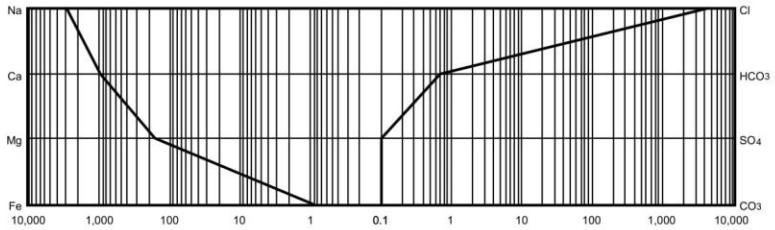

REMARKS: N.D.- Not Detected. Total Alkalinity as CaCO3 (mg/L) = 33.5; Total Hardness as CaCO3 (mg/L) = 53668; Total Suspended Solids (mg/L) = 1742; EC @ 25°C (mS/cm) = 219.8; Total Fe (mg/L) = 69; Total Mn (mg/L) = 4.1

Appendix D.

Box Model Supplemental Figures

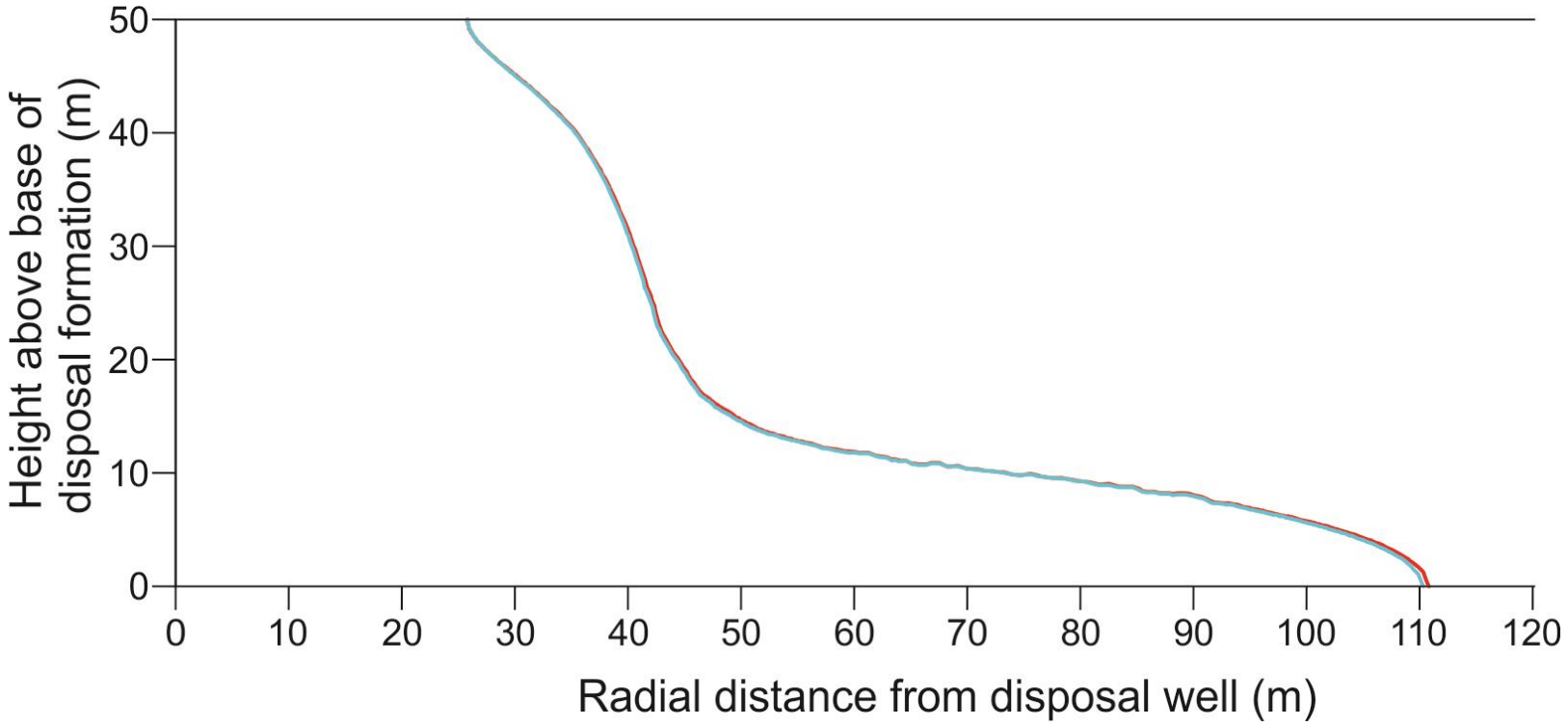

Appendix D1. Comparison of effect of Boussinesq approximation (red) and no Boussinesq approximation (blue) on extent of 10 g/L concentration contour for the Base Case model after full injection and post-injection periods .

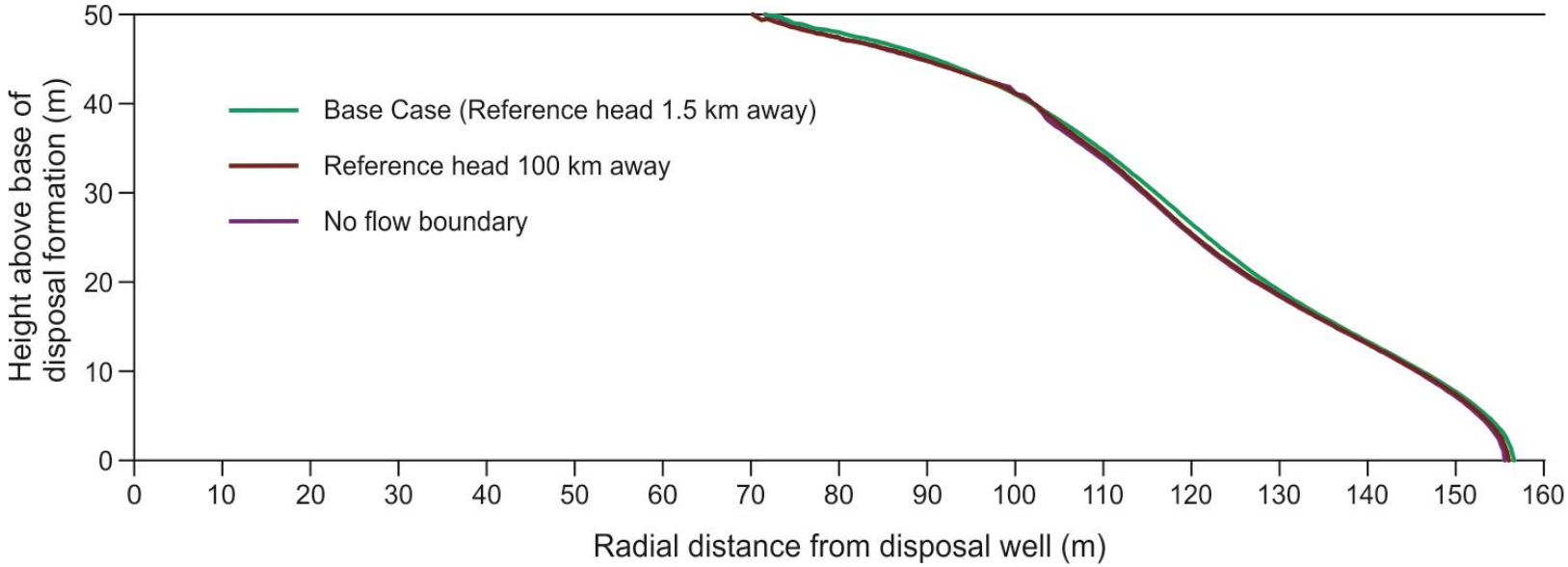

Appendix D2. Extent of 10 g/L isohaline after ten years of disposal for different outflow boundary conditions.

Appendix E.

HSU 2 Files (E1-E3)

E1 Description:

This PDF contains the geophysical neutron and density porosity logs for wells targeting the Paddy-Cadotte in which the high permeability HSU 2 is present.

E1 Filename:

Geophysical-Logs-HSU-2-Present.pdf

E2 Description:

This PDF contains the geophysical neutron and density porosity logs for wells targeting the Paddy-Cadotte in which the high permeability HSU 2 is absent.

E2 Filename:

Geophysical-Logs-HSU-2-Absent.pdf

E3 Description:

This Excel spreadsheet relates the geometry of HSU 2 determined from the above PDF documents to the geographic UTM coordinates of each measurement, allowing it to be imported into FEFLOW and used to define layer geometry.

E3 Filename:

HSU-2-Geometry-Data.xlsx